Accelerating Solid Form Discovery for Pharmaceuticals

by

Laura Yvonne Pfund

A dissertation submitted in partial fulfillment
of the requirements for the degree of
Doctor of Philosophy
(Chemistry)
in The University of Michigan
2015

Doctoral Committee:

Professor Adam J. Matzger, Chair
Professor Charles L. Brooks III
Professor Zhan Chen
Associate Professor Kenichi Kuroda

For my parents

Sharon and Jimmy Pfund

Acknowledgements

Thank you to Professor Matzger who has been a constant source of support throughout my graduate career. I could never fully express my appreciation for all that he has taught me. He has always encouraged me to push myself and strive for excellence. I have always admired his honesty, forthrightness and his sense of humor, even if it was often at the expense of the great state of New Jersey. His vast knowledge and keen insight truly furthered the research endeavors of everyone in the group and allowed us all to succeed as scientists. Professor Matzger truly makes his lab environment an incredibly fun and welcoming place to work.

I am also very thankful for my committee members: Professor Charles Brooks III, Professor Zhan Chen, and Professor Kenichi Kuroda. I am very appreciative of their guidance and support as I started my thesis work on and have benefited from their insight. Thank you also to Professor Melanie Sanford who worked with me on the MOF catalysis project. She has always been a source of support and encouragement.

I would like to thank all of the members of the Matzger lab, both past and present: Ping, Jake, Jon, Raj, Li Zi, Kortney, Amanda, Ananya, Ly, Jialiu, and Kyle. You have all supported me in every way possible throughout my time in lab. Thank you to Antek, his expertise with all the lab equipment and willingness to help truly keeps the Matzger lab going. I am very thankful for his kindness and his continual willingness to help and provide whatever suggestions he can for all of the problems and questions I have proposed over the years. Thank you for being a constant source of hilarious comments and always making me laugh even in the most stressful situations. Thank you to the former lab members Kira, Roy, and Leila, you were all so kind to me when I first started in the lab and truly paved the way for the start of my graduate career. Thank you all for training me on all of the instrumentation. Thank you to Onas whose expertise in crystallization and materials science helped me to excel in my own research. Thank you to Jeremy, who has always been so kind to me since the moment I met him, I truly value our friendship. Thank you to Dr. Chris Price, although we have not met in person, he has been extremely kind and helpful to me. Thank you to Brianna, you were an incredibly talented student

and it was a lot of fun working with you. Thank you to Jessica, without you I would not have been able to complete the additive project. You are a wonderful and meticulous scientist, I am so grateful I was given the opportunity to mentor you. Thank you to Doug, who although not a member of the lab per se, was a constant fixture in the lab for many years. Thank you for being a wonderful collaborator and friend. Thank you to Ping, who has been such a wonderful partner in crime during my time here. Thank you for helping me relax and enjoy life, you always can find joy and adventure in everything you do. Thank you to Jon who, whether he likes it or not, is inheriting most of the lab instruments from me. I truly appreciate and cherish our friendship; you can always turn my day around when I am stressed. Thank you for teaching me so much about New Hampshire even if I have been very reluctant to learn. Thank you to Ly who is always a bright ray of sunshine. Thank you for always sharing your expertise in organic chemistry with me and with all of the members of the lab. Thank you to Ananya for always being a kind friend for me to talk to.

I would not be here today if it were not for the love and support of my family. I dedicate my thesis to my mom and dad, who have always put me and my siblings above everything. Thank you to mom, dad, Stephen, and Katie, I love you all so much. I would not be the person I am today without you. Thank you to my amazing husband Brian, I am so happy to have shared this journey with you. Thank you for your constant love and support, it has truly helped me get through the toughest of times. Thank you my closest friends: Casey, Colleen, and Wendi. Thank you for always getting me to go out and have fun, you have all been such wonderful friends to me.

Table of Contents

List of Figures

List of Tables

Abstract

Polymorphism is the ability of a molecule to exist in multiple crystalline phases, each with a different arrangement or conformation of molecules within the solid state. The focus of this thesis is both the use of polymer-based approaches to crystallization control to explore the role of solid form diversity in pharmaceuticals and also developing methods based on these approaches to accelerate solid form discovery. Polymer-induced heteronucleation (PIHn), a powerful crystalline polymorph discovery method, has revealed two novel polymorphs of piperine exhibiting enhanced solubility as compared to the known polymorph. These unique forms may now be able to improve the efficacy of piperine as a bioenhancer.

As demonstrated by the discovery of these new piperine forms, it is imperative to determine the potential polymorphism of a compound, especially at an early stage in the pharmaceutical development process, due to the unique physiochemical properties of each distinct form. However, methods capable of exhaustively screening for crystal polymorphism remain an elusive goal in solid-state chemistry due to large sample requirements and long analysis times. PIHn has now been redeployed in a high density format in which 288 distinct polymers, each acting as a heteronucleant, are arrayed on one substrate. This format allows determining the outcome of thousands of crystallizations in an automated fashion with only a few milligrams of sample. This technology enables the study of a broader range of targets, including preclinical candidates, facilitating determination of polymorphism propensity much earlier in the drug

development process. The efficacy of this approach has now been demonstrated using four pharmaceutically relevant compounds: acetaminophen, tolfenamic acid, ROY, and curcumin.

A further problem explored in this thesis relates to compounds which are very slow or even resistant to crystallization. This behavior can severely hinder the development and formulation of a target pharmaceutical. In order to combat this issue, inspiration was drawn from the extensive work on soluble tailor-made additives, which can affect crystal morphology by selectively binding to the faces of a growing crystal. If these strong interactions between a tailor-made additive and a target compound could instead be applied at the surface of an insoluble polymer, it was hypothesized that the additive would instead act as crystallization promoter. To investigate this hypothesis, additives were synthesized that mimic the pharmaceuticals acetaminophen or mefenamic acid and also possess polymerizable functionality. It was found that, in solution, these additives face-selectively inhibit crystal growth and lead to overall slower crystal appearance. In contrast, when the tailor-made additives were incorporated into an insoluble polymer, the induction time for the onset of crystal formation for both pharmaceuticals was substantially decreased. This approach now allows for the synthesis of tailor-made polymers that decrease the induction time for crystal appearance and may find application with compounds that are resistant to crystallization or in improving the fidelity of heteronucleation approaches to solid form discovery.

Chapter 1 Introduction

1.1 Pharmaceutical Polymorphism

Solid forms of active pharmaceutical ingredients (APIs) are the most prevalent dosage forms due to the significant advantages in their stability and convenience of administration. In the vast majority of these solid formulations, the API is crystalline. However, it is well known that most APIs exhibit multiple solid forms including polymorphs. Polymorphism is the ability of a molecule to exist in multiple crystalline phases, each exhibiting a different arrangement or conformation of molecules within the solid state.[1, 4] Determining the potential polymorphism of a newly synthesized compound is extremely important due to variations in the solubility and bioavailability of different polymorphic forms. However, pre-formulation, where issues of polymorphism are addressed in detail, occurs as a late stage consideration in drug development despite its central role in the creation of a viable pharmaceutical product. Additionally, the process by which a solid form is chosen is rather inefficient and prone to missing potential solid form diversity. Failure to properly formulate a drug can, and indeed does, derail the introduction of new therapeutics to market. Furthermore, if unknown polymorphic transitions occur after the drug has gone on the market, it can be detrimental for the dosage and administration of the compound. This is most apparent in the case of ritonavir, an anti-HIV compound. During the discovery process, only one form of the compound was identified.[5, 6] The crystalline form was found to have limited bioavailability and, as a result, the compound was formulated as a water/ethanol solution, leading researchers to believe that the crystalline form would not be

important in the formulation process. However several years after ritonavir was put on the market, it was found that the capsules were not passing dissolution requirements, due to the presence of a new polymorph which had crystallized within the capsules.[5, 6] This new, more stable form had a significantly lower solubility as compared to the known polymorph, resulting in researchers reformulating the dosage so that this new form could be utilized.[5, 6] Thus, it is imperative that all polymorphs of a newly synthesized compound can be found and characterized in order to circumvent any potential issues caused by unknown form conversion.

1.2 Nucleation

Nucleation is typically considered the controlling step in the formation of different polymorphs. Nucleation can be classified as primary or secondary nucleation. Secondary nucleation occurs when nuclei form in the presence of crystals in a supersaturated solution.[1, 2] Primary nucleation occurs when no seeds of the crystallizing material are present in the supersaturated solution. There are two mechanisms, homogeneous or heterogeneous nucleation, by which primary nucleation can occur. Homogeneous nucleation involves the spontaneous formation of nuclei in the bulk of a supersaturated or supercooled system.[2, 3]

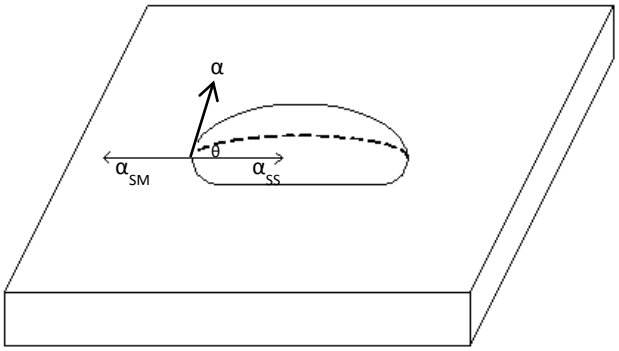

Figure 1.1. Shape of the crystallizing solution for the isotropic approximation of heterogeneous nucleation.[3]

Although homogeneous nucleation has been studied theoretically, it occurs quite rarely experimentally. More commonly, the mechanism for nucleation can be described as heterogeneous nucleation, in which a foreign surface is present that interacts with the crystallizing material in solution.[3] The classical mechanism for heterogeneous nucleation is an

isotropic approximation in which a liquid droplet, represented by a sphere, forms a wetting angle θ with a substrate (Figure 1.1.). The surface energy of this system can be defined as: $\alpha\cos\theta = \alpha_{sm}-\alpha_{ss}$ (where S is the substrate, α_{sm} is the substrate-medium droplet interface, and α_{ss} is the substrate-solid droplet interface). The free-energy change or potential barrier for heterogeneous nucleation is: $\Delta G_c^* = \frac{16\pi\Omega^2 \propto^2}{3\,(\Delta\mu)^2} \times \frac{(1-\cos\theta)^2\,(2+\cos\theta)}{4}$ where Ω is the molecular volume, $\Delta\mu$ $(= \mu_v - \mu_c)$ represents the difference between the chemical potentials of the initial vapor phase and the final condensed phase transformation, θ is the wetting angle, and α is the specific free energy of the surface formed. The second multiplier in the equation is the Volmer factor, having values from 0 (θ = 0°) to 1 (θ = 180°), which represents how well the crystallizing solution is able to interact with the substrate.[3] It is apparent that there are two potential extremes for this equation: the crystallizing solution could be interacting so strongly with the substrate that the wetting angle is zero or the crystallizing solution could be completely unable to interact with the substrate (i.e., completely non-wetting; rendered completely ineffective for heteronucleation) such that the wetting angle is 180°.[3] Typically, the wetting angle will be somewhere in between these two extremes, allowing the barrier for nucleation to be significantly lowered. For an anisotropic system, in which a drop with length *L* and height *h* is deposited onto a surface, the energy change of the system is $\Delta G = -(L^2h/\Omega)\,(\Delta\mu) + L^2\Delta\alpha + 4Lh\alpha$, where $\Delta\alpha$ $(= \alpha + \alpha_{ss}-\alpha_{sm})$ represents the strength of the interaction of the crystal with itself relative to the strength of the interaction between the forming crystal and the substrate, and the other symbols are defined identically to the isotropic system described above. If $\Delta\alpha < 0$, the forming crystal is interacting strongly with the surface, allowing for heteronucleation; however, if $\Delta\alpha > 0$, there is limited interaction between the molecules in solution and the surface, precluding heteronucleation.

1.3 Thermodynamic and Kinetic Contributions to the Nucleation of a Polymorph

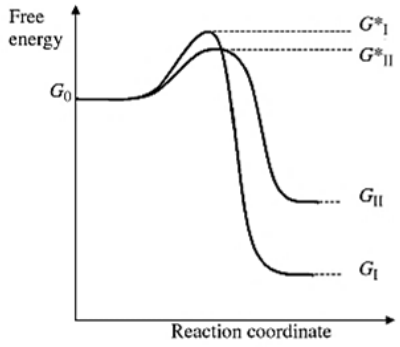

Figure 1.2. Schematic of the reaction coordinate for crystallization in a system with two polymorphs.[1]

To understand the mechanism by which one polymorph nucleates over another, the kinetics and thermodynamics of crystallization must be considered. A reaction coordinate for crystallization in a system with two polymorphs can be used to do this (Figure 1.2). Both forms have the same initial free energy (G_0), which represents the free energy per mole of the solute in a supersaturated fluid.[1] Once at this initial free energy, the molecules in solution can then crystallize into one of the two products, form I or II, in which form I is more stable polymorph with $G_{II} > G_I$. For both reaction pathways there is an associated transition state and an activation free energy which corresponds to the relative rates of formation for each form.[2, 3] Unlike a traditional reaction scheme, for crystallization there exists a phase boundary between the solid and liquid phase. A phase boundary is associated with an increase in the free energy of the system, which must be offset by an overall loss of free energy. As a result, the magnitudes of the activated barriers are dependent on the size of the crystal nucleus.[1] The critical radius, the minimum size of a crystal nucleus that must be formed for nucleation to occur, can be defined as $r_c = 2\Omega\alpha/\Delta\mu$, where Ω is the molecular volume, $\Delta\mu$ ($= \mu_v - \mu_c$) is the difference between the chemical potentials of the initial vapor phase and the final condensed phase transformation, and α is the specific free energy of the surface formed.[3] The higher the degree of supersaturation, the smaller the critical radius becomes. By examining Figure 1.2, it is apparent that the supersaturation with respect to form II ($G_0 - G_{II}$) is lower than that of form I ($G_0 - G_I$). If, for a

particular solution composition, the critical size is lower for form II, then the activation free energy for nucleation will be lower, and kinetics will favor the crystallization of form II. However, due to the thermodynamic stability of form I, form II will ultimately transform into form I. [1, 2]

The thermodynamic relationship between two different phases can be described by Gibbs' phase rule: P+F=C+2, where C is the number of components, P is the number of phases that exist in equilibrium, and F is the number of degrees of freedom or variance in the system.[7, 8] By examining the phase rule, it is apparent that, theoretically, only one phase can exist at any given temperature and pressure. The exception to this occurs at the transition temperature of at a defined pressure, in which case two phases can exist in equilibrium. It is possible for one polymorph to transform into another at a given pressure by changing the temperature. If the phase transition from one form to another is reversible, the polymorphs are said to be enantiotropically related, and the transition will be endothermic when heated.[7, 8] If the phase transition is irreversible, the two forms are monotropically related, and only one form is stable regardless of the temperature. For monotropes, the transformation from a metastable form to the stable form will be exothermic on heating.[7, 8] However, as stated previously, unstable polymorphs may exist for a time outside the region assigned by the phase diagram and the phase rule for a given compound due to kinetic reasons. [8]

1.4 Methods for Selecting and Discovering Polymorphs

Due to the differences in the kinetic and thermodynamic properties between different crystalline forms, determination of the potential polymorphism of a newly synthesized compound must occur as early as possible in the formulation process. The ideal technique should facilitate the formation and identification of all possible polymorphs of a molecule while

utilizing minimal amounts of the target compound via automated form identification. A typical polymorph screen can involve changing the degree of supersaturation, the temperature, and the solvent. Additionally, crystallization in the presence of various types of heteronucleants, including self-assembled monolayers,[9-12] crystalline substrates,[13-15] and amorphous polymers,[16-23] has been utilized to aid in the discovery and formation of novel polymorphs. Polymer-induced heteronucleation (PIHn) has proven to be an extremely powerful polymorph discovery platform, utilizing hundreds of insoluble, amorphous polymers as heteronucleants.[24-26] The polymer selectively promotes the growth of one form above others through a kinetic mechanism involving selective stabilization at the stage of nucleation.[27, 28] It has been found that the functional group interactions between the polymer surface and the growing crystal are responsible for promoting the formation of one polymorph over another.[27, 28]

Outline of the Thesis

1.5 Discovery of Two Novel Polymorphs of the Bioenhancer Piperine

The utility of discovering novel polymorphs was recently demonstrated for the nutraceutical piperine (Figure 1.3). Piperine has been found to act as a bioenhancer, a molecule which is able to increase the bioavailability of a compound for a variety of pharmaceuticals including propranolol, theophylline, ciprofloxacin, and tetracycline.[29-32] However, the efficacy of this compound as a bioenhancer is currently limited by its poor aqueous solubility (40 mg/L). When initially examining the known crystal structure of piperine it was found that the structure was completely devoid of any π-π interactions, despite the extended conjugation present in the molecule.[33] It was hypothesized that if alternative arrangements of piperine could be found, they would possess π-π interactions. Now,

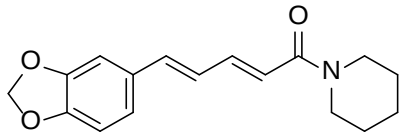

Figure 1.3. Structure of piperine.

as described in Chapter 2, two additional polymorphs of piperine have been discovered, both of which exhibit these interactions. Moreover, both newly discovered forms have an enhanced aqueous solubility as compared to the commercial form.

1.6 Towards Exhaustive and Automated High Throughput Screening for Crystalline Polymorphs[34]

As evidenced by the discovery of novel polymorphs of the bioenhancer piperine, PIHn is a very powerful method for discovering novel polymorphs. However, PIHn, along with many of the methods utilized for solid form screening, requires substantial sample quantity (roughly 1-5g). Therefore, it is not currently feasible to perform comprehensive solid form screening as an early stage selection criterion for choosing which bioactive compounds to advance in the pipeline. As described in Chapter 3, PIHn has now been reengineered into a novel high throughput system, termed µPIHn, in which hundreds of crystallizations can be conducted and studied in an automated fashion using only ~1 mg of material (Figure 1.4). This platform is created by contact printing solutions directly onto the µPIHn plate via custom fabricated pin tools (Figure 1.5). The efficacy of µPIHn was studied with four polymorphic pharmaceutically relevant compounds: acetaminophen, tolfenamic acid, ROY, and curcumin. For all of the compounds studied, polymorph selection was achieved while utilizing only ~1 mg of material. Additionally, all of the pharmaceutical polymorphs were successfully identified by automated analysis using Raman

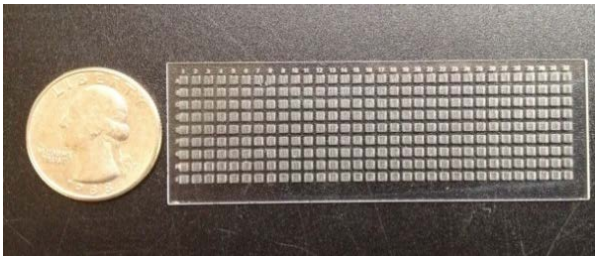

Figure 1.4. High throughput screening platform: µPIHn.

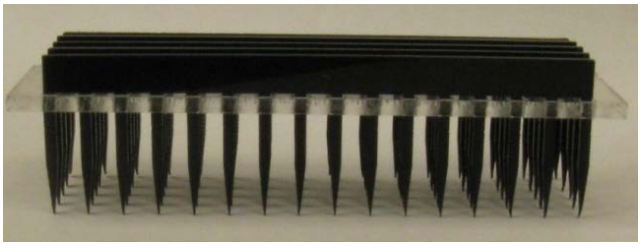

Figure 1.5. Custom pin tool used for the deposition of material onto the µPIHn plate.

microspectroscopy. μPIHn now offers a pathway to conduct more comprehensive phase space searches even with very limited quantities of material. This high throughput platform allows for rapid and reliable polymorph screening of a pharmaceutical, enabling more informed decisions about which forms are the most promising for further development.[34]

1.7 Controlling Pharmaceutical Crystallization with Designed Polymeric Heteronuclei[35]

Despite the success of PIHn in discovering novel polymorphs, it currently only utilizes commercial monomers to build the polymer libraries. By expanding the monomer scope to include monomers which are specifically tailored for a particular target compound one may be able to exude even more control over crystallization by taking advantage of the strong intermolecular interactions at the polymer crystal interface. This could be of particular importance for compounds that are resistant to crystallization.[36] This issue can greatly complicate the formulation process by preventing one from purifying a compound by

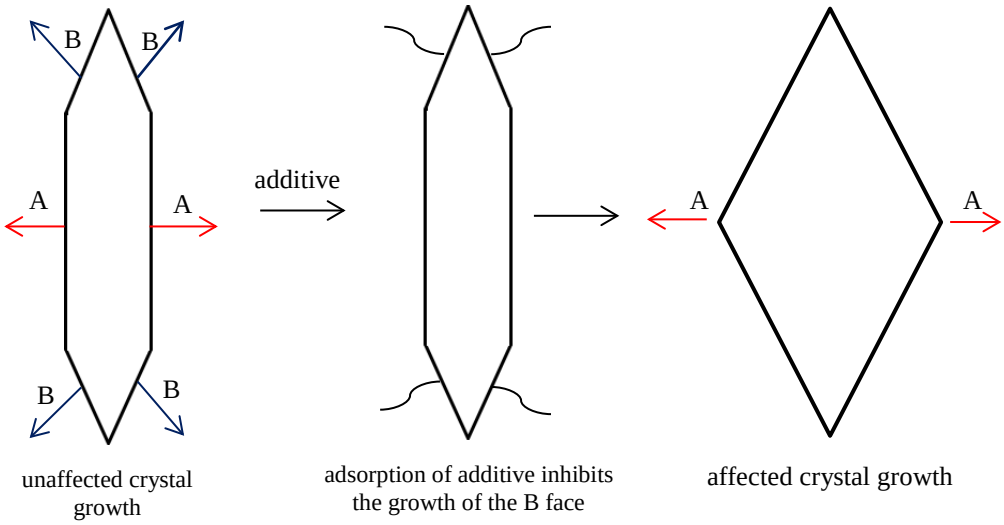

Figure 1.6. Diagram showing how a tailor-made additive selectively adsorbs onto to certain faces of a growing crystal resulting in a change in morphology.[2]

crystallization and determining the structure of the compound by crystallography. In order to circumvent this problem, inspiration was drawn from what is known about tailor-made soluble additives. These compounds can affect the morphology and polymorphism of a compound by

preferentially adsorbing to certain faces of a growing crystal (Figure 1.6).[37, 38] Because of the favorable interactions between an additive and its target compound, a soluble additive is able to

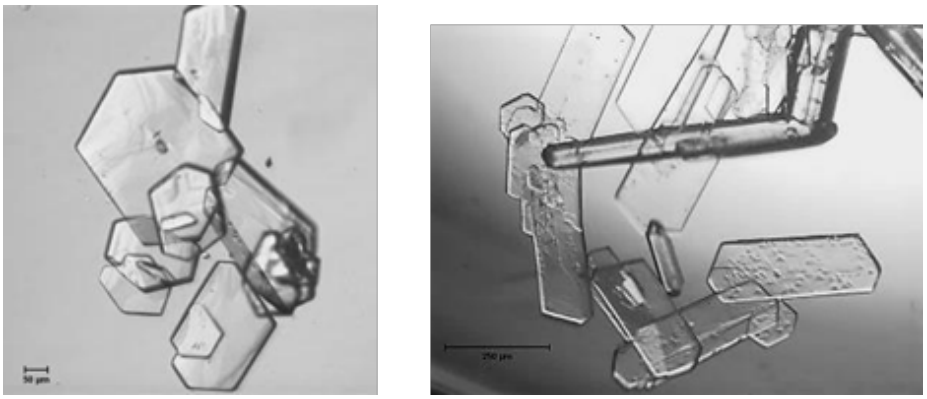

Figure 1.7. Morphology of mefenamic acid crystals grown in the presence of 2-((4-vinylphenyl)amino)benzoic acid. On left: no additive, on the right: 1 mol% additive.

selectively bind to the face of a crystal.[10, 14, 15, 21, 37-50] If the strong interactions between a tailor-made additive and a target compound could instead be applied at the surface of an insoluble polymer, it was hypothesized that the additive would act as crystallization promoter. As described in Chapter 4, additives were synthesized that mimic the pharmaceuticals acetaminophen or mefenamic acid and also possess polymerizable functionality. In solution, it was found that these additives face-selectively inhibit crystal growth and lead to overall slower crystal appearance (Figure 1.7).[35] However, when the additives were incorporated into an insoluble polymer, a decrease in the induction time for crystal appearance was observed for both pharmaceuticals relative to the induction time without polymer present. For acetaminophen crystallizations in the presence of the tailor-made copolymers, crystals appear on average within an hour, one hundredth of the time needed for crystallization to occur in the absence of polymer. This approach now allows for the synthesis of heteronucleants that can accelerate the rate of crystallization, for systems that are resistant to crystallization.[35, 36]

1.8 References

1. Bernstein, J., *Polymorphism in Molecular Crystals*. Oxford University Press: New York, 2002.
2. Davey, R.; Garside, J., *From Molecules to Crystallizers*. Oxford University Press: New York, 2000.
3. Givargizov, E. I., *Oriented Crystallization on Amorphous Substrates*. Plenum PRESS: New York, 1991.
4. Davey, R. J.; Blagden, N.; Potts, G. D.; Docherty, R., Polymorphism in molecular crystals: Stabilization of a metastable form by conformational mimicry. *J. Am. Chem. Soc.* **1997,** 119, (7), 1767-1772.
5. Bauer, J.; Spanton, S.; Henry, R.; Quick, J.; Dziki, W.; Porter, W.; Morris, J., Ritonavir: An Extraordinary Example of Conformational Polymorphism. *Pharm Res* **2001,** 18, (6), 859-866.
6. Chemburkar, S. R.; Bauer, J.; Deming, K.; Spiwek, H.; Patel, K.; Morris, J.; Henry, R.; Spanton, S.; Dziki, W.; Porter, W.; Quick, J.; Bauer, P.; Donaubauer, J.; Narayanan, B. A.; Soldani, M.; Riley, D.; McFarland, K., Dealing with the Impact of Ritonavir Polymorphs on the Late Stages of Bulk Drug Process Development. *Organic Process Research & Development* **2000,** 4, (5), 413-417.
7. Giron, D., Investigations of polymorphism and pseudo-polymorphism in pharmaceuticals by combined thermoanalytical techniques. *J. Therm. Anal.* **2001,** 64, (1), 37-60.
8. Burger, A.; Ramberger, R., Polymorphism of Pharmaceuticals and Other Molecular-Crystals. 1. Theory of Thermodynamic Rules *Mikrochim. Acta* **1979,** 2, (3-4), 259-271.
9. Kang, J. F.; Zaccaro, J.; Ulman, A.; Myerson, A., Nucleation and growth of glycine crystals on self-assembled monolayers on gold. *Langmuir* **2000,** 16, (8), 3791-3796.
10. Lee, A. Y.; Ulman, A.; Myerson, A. S., Crystallization of amino acids on self-assembled monolayers of rigid thiols on gold. *Langmuir* **2002,** 18, (15), 5886-5898.
11. Ulman, A.; Kang, J. F.; Shnidman, Y.; Liao, S.; Jordan, R.; Choi, G. Y.; Zaccaro, J.; Myerson, A. S.; Rafailovich, M.; Sokolov, J.; Fleischer, C., Self-assembled monolayers of rigid thiols. *Journal of biotechnology* **2000,** 74, (3), 175-88.
12. Capacci-Daniel, C.; Gaskell, K. J.; Swift, J. A., Nucleation and Growth of Metastable Polymorphs on Siloxane Monolayer Templates. *Cryst. Growth Des.* **2010,** 10, (2), 952-962.
13. Mitchell, C. A.; Yu, L.; Ward, M. D., Selective nucleation and discovery of organic polymorphs through epitaxy with single crystal substrates. *J. Am. Chem. Soc.* **2001,** 123, (44), 10830-10839.
14. Ward, M. D., Bulk crystals to surfaces: Combining X-ray diffraction and atomic force microscopy to probe the structure and formation of crystal interfaces. *Chem. Rev.* **2001,** 101, (6), 1697-1725.
15. Weissbuch, I.; Lahav, M.; Leiserowitz, L., Toward stereochentical control, monitoring, and understanding of crystal nucleation. *Cryst. Growth Des.* **2003,** 3, (2), 125-150.
16. Chen, J. H.; Shao, M.; Xiao, K.; He, Z. R.; Li, D. W.; Lokitz, B. S.; Hensley, D. K.; Kilbey, S. M.; Anthony, J. E.; Keum, J. K.; Rondinone, A. J.; Lee, W. Y.; Hong, S. Y.; Bao, Z. A., Conjugated Polymer-Mediated Polymorphism of a High Performance, Small-Molecule Organic Semiconductor with Tuned Intermolecular Interactions, Enhanced Long-Range Order, and Charge Transport. *Chem. Mat.* **2013,** 25, (21), 4378-4386.

17. Curcio, E.; López-Mejías, V.; Di Profio, G.; Fontananova, E.; Drioli, E.; Trout, B. L.; Myerson, A. S., Regulating Nucleation Kinetics through Molecular Interactions at the Polymer–Solute Interface. *Cryst. Growth Des.* **2013,** 14, (2), 678-686.
18. Diao, Y.; Helgeson, M. E.; Myerson, A. S.; Hatton, T. A.; Doyle, P. S.; Trout, B. L., Controlled Nucleation from Solution Using Polymer Microgels. *J. Am. Chem. Soc.* **2011,** 133, (11), 3756-3759.
19. Lee, M. K.; Lee, H.; Kim, I. W.; Lee, J., Novel polymorphic form of adefovir dipivoxil derived from polymer-directed crystallization. *Pharmazie* **2011,** 66, (10), 766-770.
20. McKellar, S. C.; Urquhart, A. J.; Lamprou, D. A.; Florence, A. J., Polymer Templating of Supercooled Indomethacin for Polymorph Selection. *ACS Combinatorial Science* **2012,** 14, (3), 155-159.
21. Staab, E.; Addadi, L.; Leiserowitz, L.; Lahav, M., Control of polymorphism by 'tailor-made' polymeric crystallization auxiliaries. Preferential precipitation of a metastable polar form for second harmonic generation. *Adv. Mater.* **1990,** 2, (1), 40-43.
22. Sudha, C.; Nandhini, R.; Srinivasan, K., Polymer-Induced Selective Nucleation of Mono or Ortho Polymorphs of Paracetamol through Swift Cooling of Boiled Aqueous Solution. *Cryst. Growth Des.* **2014,** 14, (2), 705-715.
23. Xu, A. W.; Dong, W. F.; Antonietti, M.; Colfen, H., Polymorph switching of calcium carbonate crystals by polymer-controlled crystallization. *Advanced Functional Materials* **2008,** 18, (8), 1307-1313.
24. Lopez-Mejias, V.; Kampf, J. W.; Matzger, A. J., Nonamorphism in Flufenamic Acid and a New Record for a Polymorphic Compound with Solved Structures. *J. Am. Chem. Soc.* **2012,** 134, (24), 9872-9875.
25. López-Mejías, V.; Kampf, J. W.; Matzger, A. J., Polymer-Induced Heteronucleation of Tolfenamic Acid: Structural Investigation of a Pentamorph. *J. Am. Chem. Soc.* **2009,** 131, (13), 4554-4555.
26. Price, C. P.; Grzesiak, A. L.; Matzger, A. J., Crystalline polymorph selection and discovery with polymer heteronuclei. *J. Am. Chem. Soc.* **2005,** 127, (15), 5512-5517.
27. Lopez-Mejias, V.; Knight, J. L.; Brooks, C. L.; Matzger, A. J., On the Mechanism of Crystalline Polymorph Selection by Polymer Heteronuclei. *Langmuir* **2011,** 27, (12), 7575-7579.
28. McClelland, A. A.; Lopez-Mejias, V.; Matzger, A. J.; Chen, Z., Peering at a Buried Polymer-Crystal Interface: Probing Heterogeneous Nucleation by Sum Frequency Generation Vibrational Spectroscopy. *Langmuir* **2011,** 27, (6), 2162-2165.
29. Atal, C. K.; Zutshi, U.; Rao, P. G., Scientific Evidence on the Role of Ayurvedic Herbals on Bioavailability of Drugs. *J. Ethnopharmacol.* **1981,** 4, (2), 229-232.
30. Mao, Q. Q.; Huang, Z.; Zhong, X. M.; Xian, Y. F.; Ip, S. P., Brain-derived neurotrophic factor signalling mediates the antidepressant-like effect of piperine in chronically stressed mice. *Behav. Brain Res.* **2014,** 261, 140-145.
31. Bano, G.; Raina, R. K.; Zutshi, U.; Bedi, K. L.; Johri, R. K.; Sharma, S. C., Effect of Piperine on Bioavailablity and Pharmacokinetics of Propanolol and Theophylline in Healthy-Volunteers. *Eur. J. Clin. Pharmacol.* **1991,** 41, (6), 615-617.
32. Mujumdar, A. M.; Dhuley, J. N.; Deshmukh, V. K.; Raman, P. H.; Thorat, S. L.; Naik, S. R., Effect of Piperine on Pentobarbital Induced Hypnosis in Rats. *Indian J. Exp. Biol.* **1990,** 28, (5), 486-487.
33. Grynpas, M.; Lindley, P. F., Crystal and Molecular-Structure of 1-Piperoylpiperidine *Acta Crystallogr. Sect. B-Struct. Commun.* **1975,** 31, (NOV15), 2663-2667.

34. Pfund, L. Y.; Matzger, A. J., Towards Exhaustive and Automated High-Throughput Screening for Crystalline Polymorphs. *ACS Combinatorial Science* **2014,** 16, (7), 309-313.
35. Pfund, L. Y.; Price, C. P.; Frick, J. J.; Matzger, A. J., Controlling Pharmaceutical Crystallization with Designed Polymeric Heteronuclei. *J. Am. Chem. Soc.* **2014**.
36. Dunitz, J. D.; Bernstein, J., Disappearing Polymorphs. *Accounts Chem. Res.* **1995,** 28, (4), 193-200.
37. Weissbuch, I.; Addadi, L.; Lahav, M.; Leiserowitz, L., Molecular Recognition at Crystal Interfaces *Science* **1991,** 253, (5020), 637-645.
38. Black, S. N.; Davey, R. J.; Halcrow, M., The Kinetics of Crystal- Growth in the Presence of Tailor-Made Additives. *J. Cryst. Growth* **1986,** 79, (1-3), 765-774.
39. Addadi, L.; Berkovitchyellin, Z.; Weissbuch, I.; Vanmil, J.; Shimon, L. J. W.; Lahav, M.; Leiserowitz, L., Growth and Dissolution of Organic-Crystals with Tailor-Made Inhibitors-Implications in Stereochemistry and Materials Science *Angew. Chem.-Int. Edit. Engl.* **1985,** 24, (6), 466-485.
40. Addadi, L.; Weinstein, S.; Gati, E.; Weissbuch, I.; Lahav, M., Resolution of Conglomerates with the Assistance of Tailor-Made Impurities- Generality and Mechanistic Aspects of the Rule of Reversal-A New Method for Assignment of Absolute-Configuration *J. Am. Chem. Soc.* **1982,** 104, (17), 4610-4617.
41. Berkovitchyellin, Z.; Vanmil, J.; Addadi, L.; Idelson, M.; Lahav, M.; Leiserowitz, L., Crystal Morphology Engineering by Tailor-Made Inhibitors- A New Probe to Fine Intermolecular Interactions. *J. Am. Chem. Soc.* **1985,** 107, (11), 3111-3122.
42. Farmanesh, S.; Ramamoorthy, S.; Chung, J. H.; Asplin, J. R.; Karande, P.; Rimer, J. D., Specificity of Growth Inhibitors and their Cooperative Effects in Calcium Oxalate Monohydrate Crystallization. *J. Am. Chem. Soc.* **2014,** 136, (1), 367-376.
43. He, X. R.; Stowell, J. G.; Morris, K. R.; Pfeiffer, R. R.; Li, H.; Stahly, G. P.; Byrn, S. R., Stabilization of a metastable polymorph of 4-methyl-2-nitroacetanilide by isomorphic additives. *Cryst. Growth Des.* **2001,** 1, (4), 305-312.
44. Li, T.; Morris, K.; Park, K., Influence of Tailor-Made Additives on Etching Patterns of Acetaminophen Single Crystals. *Pharm Res* **2001,** 18, (3), 398-402.
45. Li, T. L.; Wen, H.; Park, K.; Morris, K. R., How specific interactions between acetaminophen and its additive 4-methylacetanilide affect growth morphology: Elucidation using etching patterns. *Cryst. Growth Des.* **2002,** 2, (3), 185-189.
46. Lovette, M. A.; Browning, A. R.; Griffin, D. W.; Sizemore, J. P.; Snyder, R. C.; Doherty, M. F., Crystal Shape Engineering. *Ind. Eng. Chem. Res.* **2008,** 47, (24), 9812-9833.
47. Shtukenberg, A. G.; Lee, S. S.; Kahr, B.; Ward, M. D., Manipulating Crystallization with Molecular Additives. *Annu. Rev. Chem. Biomol. Eng.* **2014,** 5, 77-96.
48. Torbeev, V. Y.; Shavit, E.; Weissbuch, I.; Leiserowitz, L.; Lahav, M., Control of crystal polymorphism by tuning the structure of auxiliary molecules as nucleation inhibitors. The beta-polymorph of glycine grown in aqueous solutions. *Cryst. Growth Des.* **2005,** 5, (6), 2190-2196.
49. van Enckevort, W. J. P.; Los, J. H., "Tailor-Made" inhibitors in crystal growth: a Monte Carlo simulation study. *J. Phys. Chem. C* **2008,** 112, (16), 6380-6389.
50. Weissbuch, I.; Leisorowitz, L.; Lahav, M., Tailor-Made and Charge-Transfer Auxiliaries for the Control of the Crystal Polymorphism of Glycine. *Adv. Mater.* **1994,** 6, (12), 952-956.

Chapter 2 Discovery of Two Novel Polymorphs of the Bioenhancer Piperine

Unpublished Work

2.1 Introduction

Piperine (1-[5-(1,3-benzodioxol-5-yl)-1-oxo-2,4-pentadienyl]piperidine) is a natural alkaloid that is produced via extraction from both long and black pepper (Figure 2.1).[1, 2] Piperine has been used in herbal medicine as an anti-inflammatory, anti-arthritic, and anti-depressant.[1, 2] Moreover, it has been reported to act as a bioenhancer[2], a compound used in combination with a pharmaceutical in order to increase drug bioavailability, in combination with propranolol, theophylline, ciprofloxacin, and tetracycline.[2-5] Recently, piperine was used as a bioenhancer with the antitubercular drug, rifampicin.[2] Rifampicin inhibits transcription within *mycobacterium smegmatis* by binding to the σ-subunit of RNA polymerase.[2] Piperine has been shown to have no effect on *mycobacterium smegmatis* growth, but when piperine was administered with rifampicin it was found to increase the binding ability of rifampicin to RNA polymerase.[2] The combined therapy of the drug with piperine has enabled the therapeutic dose of rifampicin to be reduced by 50%. This formulation has been successfully patented and undergone phase I, II, and III clinical trials.[2]

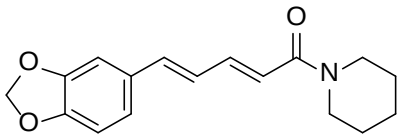

Figure 2.1. Structure of piperine.

Despite its success as a bioenhancer, the aqueous solubility of piperine is only 40 mg/L, which limits its efficacy.[1] However, solubility often depends on crystalline form and crystalline

polymorphs can exhibit significant differences in solubility and hence, activity within the human body.[6] Now, the polymorphism of piperine is studied with polymer-induced heteronucleation (PIHn),[7-9] a powerful crystalline polymorph discovery method, with the goal of discovering novel crystalline forms which have an enhanced solubility as compared to the known piperine form. Previously, only one crystal form of piperine was known. Herein, it is shown that piperine is at least trimorphic and both new piperine forms have enhanced aqueous solubility as compared to the known polymorph.

2.2 Results and Discussion

In order to explore the potential polymorphism of piperine, the compound was crystallized by solvent evaporation in the presence of polymer heteronucleants.[7-9] Initial characterization of the piperine polymorphs was carried out by Raman spectroscopy. All of the forms were observed to have characteristic peaks in the 1100-1700 cm^{-1} region (Figure 2.2). Strong bands were observed for the aromatic ring vibrations (1583.1, 1591.6, and 1600.4 cm^{-1} for form I, II, and III respectively) and CH_2 bending (1445.8, 1450.7, and 1442.8 cm^{-1} for form I, II, and III respectively). Additionally, there was significant peak shifting in the 1620-1640 cm^{-1} region, which can be attributed to the stretching of the amide carbonyl. This region is characterized by at least two peaks for all of the forms with the peak positions of forms II and III shifting towards higher frequencies relative to form I. The shifting of the amide carbonyl vibrational modes gives insight into the expected conformation of the two new forms of piperine as peak shifting can be attributed to local conformational effects and resonance via conjugation of the pentadiene chain. The local conformational effect is present due to the nitrogen of the piperidine ring acting as an electron donor. When the carbonyl group is in a planar conformation, electrons are readily donated, thereby shifting the peak observed for the stretching of the amide carbonyl to lower

frequencies as observed in form I. It is also possible for this region of the molecule to experience distortions such as local bond rotation, which would hinder the electron donating ability of the nitrogen. In this case, the peaks corresponding to amide carbonyl stretching would shift towards higher energy. Therefore the Raman data suggests that both forms II and III have increased rotation around either the O=C–N or O=C–C bond.

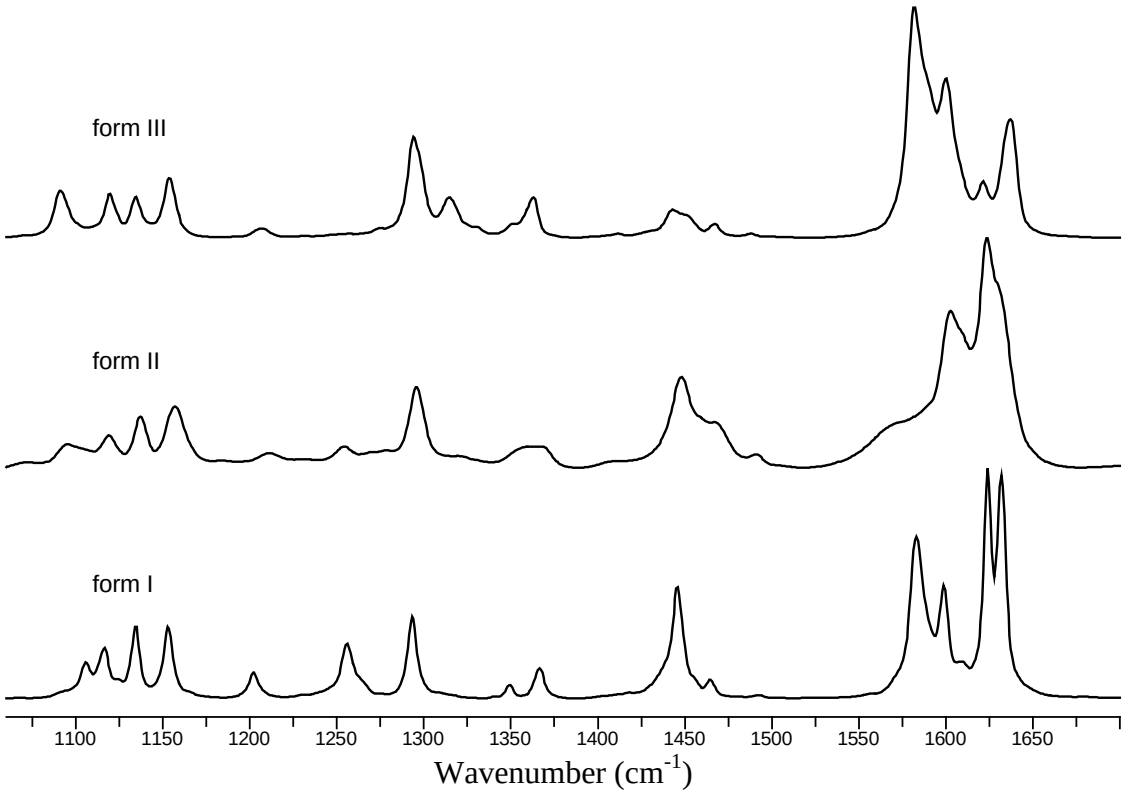

Figure 2.2. Raman spectra of piperine polymorphs: forms I, II, and III.

Crystalline samples of all the forms were also characterized by powder X-ray diffraction (PXRD) (Figure 2.3). Form I exhibits peaks at 2θ = 13.0°, 14.3°, 14.8°, 16.0°, 19.7°, and 20.7°, which agrees well with the literature powder pattern.[10] Form II was found to possess peaks at 2θ

=13.3°, 13.9°, 16.8°, 19.4°, and 21.7°. Form III was found to be distinct from both forms I and II by the presence of peaks at 2θ = 13.5°, 17.8°, 21.4°, and 22.7°. Thus it was confirmed that forms II and III were in fact different from form I by their distinct powder patterns.

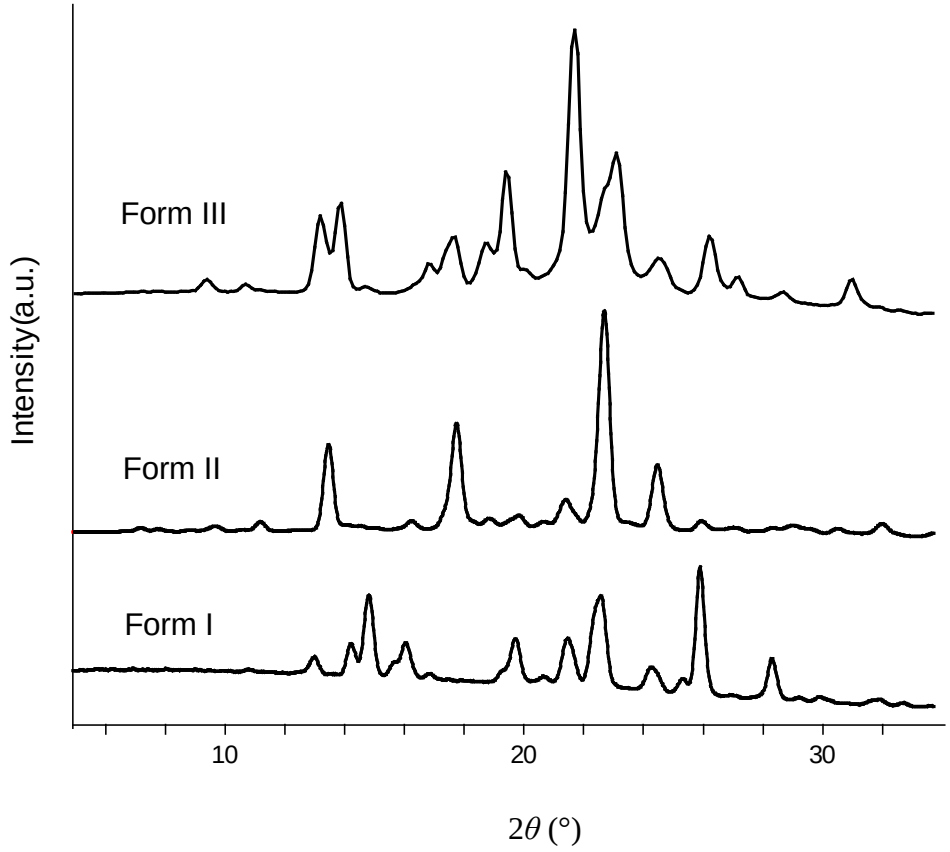

Figure 2.3. Powder X-ray diffraction patterns for piperine forms I, II, and III.

When initially examining the known crystal structure of piperine it was found that it was completely devoid of any π-π interactions despite the extended conjugation present in the molecule.[10] It was hypothesized that if alternative arrangements of piperine could be found, they would possess π-π interactions. Single crystal X-ray analysis of form II at 95 K revealed a monoclinic unit cell in the space group $P2_1/n$ with the following unit cell parameters: a = 16.6510(2) Å, b = 9.5153(7) Å, c = 18.0362(1) Å, β = 99.587(7)° (see Figure 2.4, Table 2.1).

The asymmetric unit consists of two symmetry independent molecules with a total of eight molecules within the unit cell. Unlike form I, form II does exhibit strong π-π interactions with the close contacts for π stacking at a distance of 3.110 Å and 3.303 Å for each of the molecules in the asymmetric unit (Figure 2.5). These distances are very close; commonly the distance for π-π interactions in a crystal structure is between 3.3-3.6 Å.[11-13] Single crystal X-ray analysis of form III at 85 K revealed a monoclinic unit cell in the space group *C*2/*c* with the following unit cell parameters: a = 23.3983(4) Å, b = 10.0341(2) Å, c = 25.8291(18) Å, β = 108.545(8)° (see Table 2.1, Figure 2.4). The asymmetric unit consists of two symmetry independent molecules with a total of sixteen molecules within the unit cell. In form III the piperidine rings adopt a chair conformation, similar to what is observed in forms I and II. π-π Interactions are also present in form III, with the close contacts for π stacking at a distance of 3.327 Å for both molecules in the asymmetric unit (Figure 2.6). Thus, both novel forms exhibited π-π interactions as would be expected in a molecule with extended conjugation.

Table 2.1. Crystallographic parameters of piperine forms I, II, and III.

	Form I[10]	Form II	Form III
Crystal System	Monoclinic	Monoclinic	Monoclinic
Space Group	$P2_1/n$	$P2_1/n$	$C2/c$
a (Å)=	8.743(2)	16.6510(16)	23.3983(4)
b (Å)=	13.364(3)	9.5153(7)	10.0341(2)
c (Å)=	13.147(3)	18.0362(13)	25.8291(18)
α (°)=	90.00	90.00	90.00
β (°)=	108.66(1)	99.587(7)	108.545
γ (°) =	90.00	90.00	90.00
Volume ($Å^3$)	1455.36	2817.7(4)	5749.3(4)
Z	4	8	16
Final R indices (obs data)	0.056	0.0398	0.054
Temperature	283-303 K	95(2) K	85(1) K

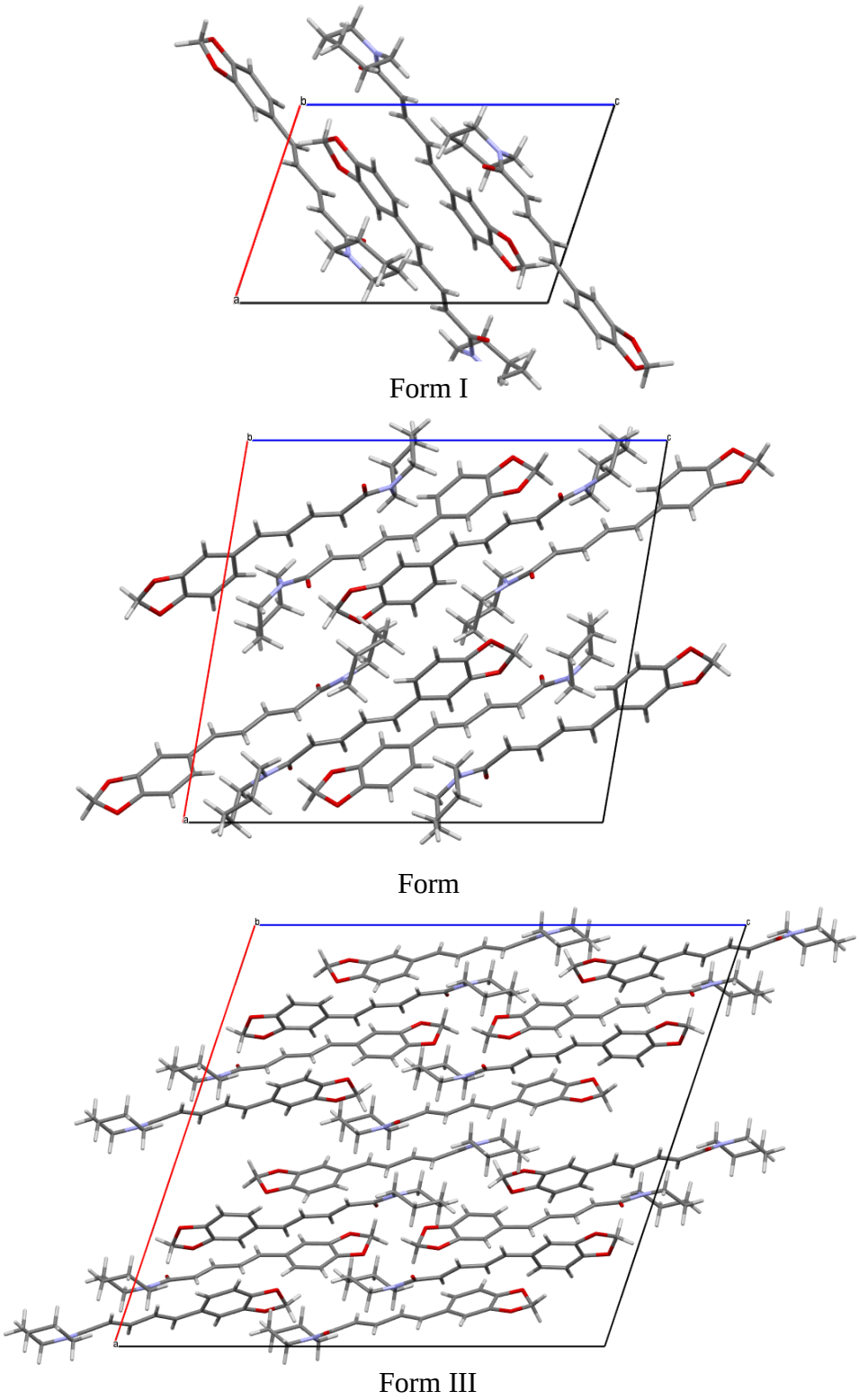

Figure 2.4. Crystal packing diagrams of piperine polymorphs form I, II, and III as viewed down the *b*-axis

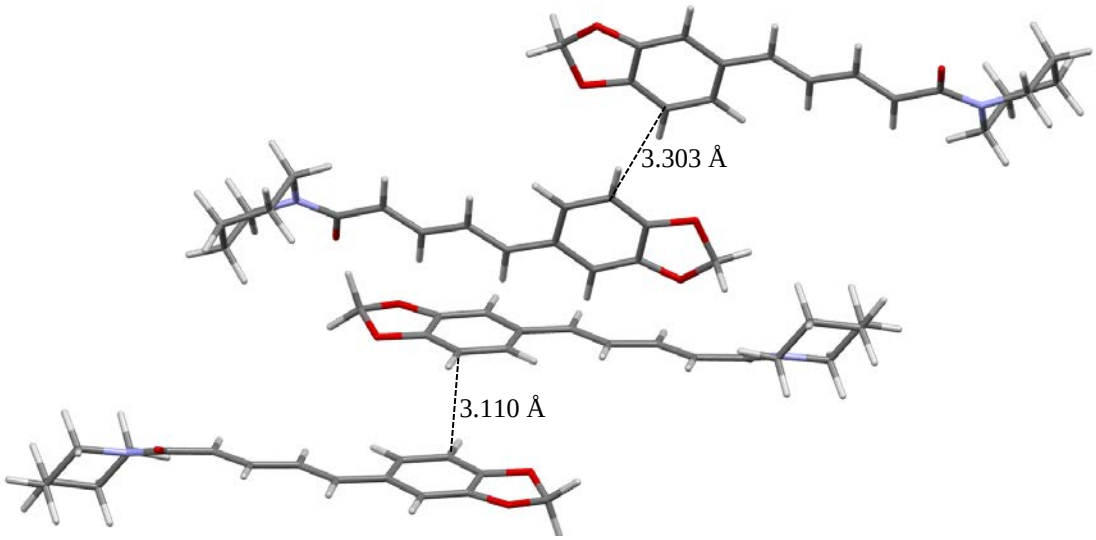

Figure 2.5. π-π Interactions present in form II. As shown in the figure π stacking close contacts are at a distance of 3.110 Å and 3.303 Å for each of the molecules in the asymmetric unit.

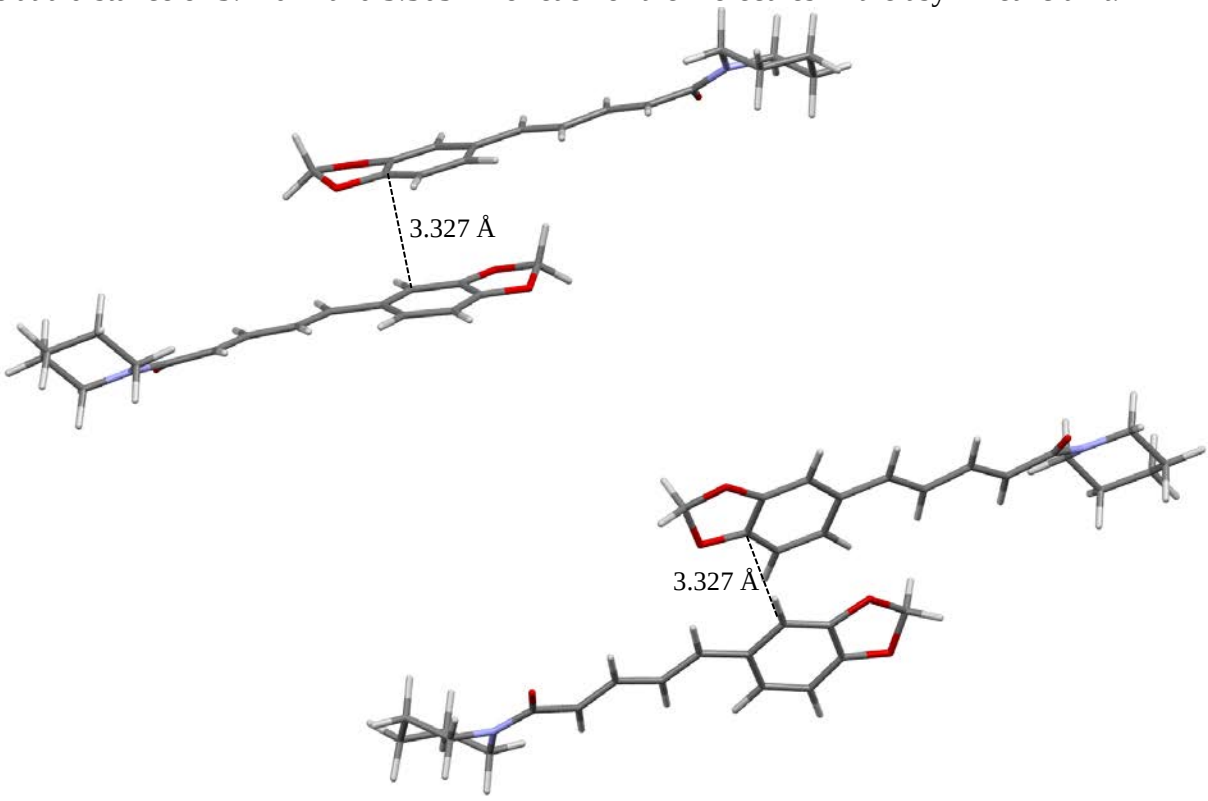

Figure 2.6. π-π Interactions present in form III. As shown in the figure the π stacking close contacts are at a distance of 3.327 Å for both of the molecules in the asymmetric unit.

Hirshfeld surface (HSs)[14] analysis was performed to determine the relative contribution of the important intermolecular contacts present in each of the molecules in the asymmetric unit of the piperine polymorphs (see section 2.4.7). For form I, the C···C contacts compose only 2.2% of the HSs, while for form III this is increased to 3.0% most likely due to the close π-π interactions present in this structure. Although the crystal phases differ in their packing arrangements and conformations, the strong hydrogen bonding contacts (O···H and N···H) and the H···H contacts remain fairly constant among all three forms of piperine (Figure 2.7).

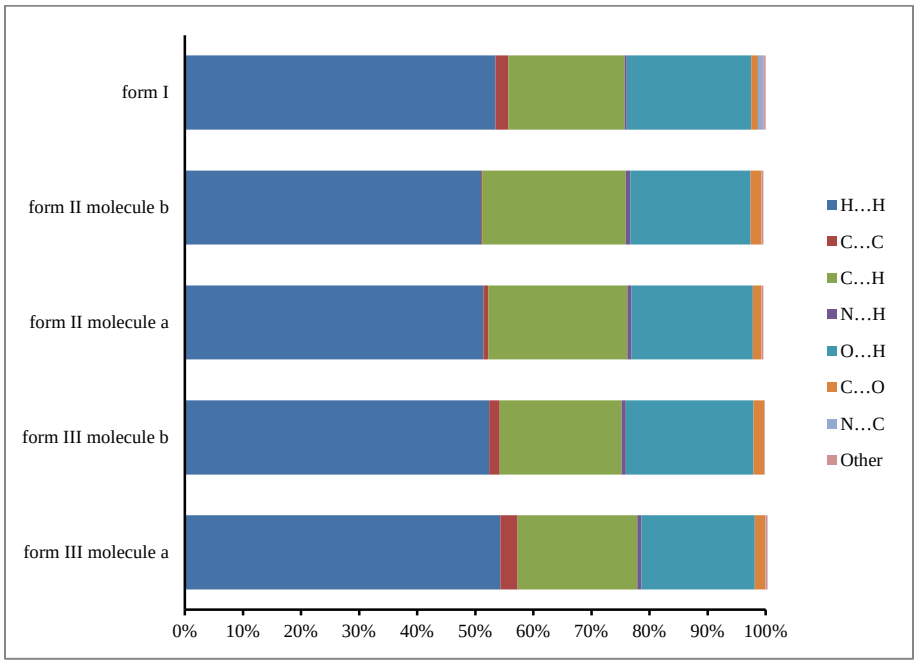

Figure 2.7. Graph of quantitative data collected from Hirshfeld surface analysis of piperine polymorphs form I and form II.

To assess the effect of the structural differences on the energies of the polymorphs, the relative free energies were established experimentally for each of the novel forms. The optical absorbance of the piperine polymorphs in water was monitored in situ over time to determine the absorbance at equilibrium. It was found that both forms II and III converted to form I over time as confirmed by PXRD (see section 2.4.8.). Form I was found to be the most thermodynamically

stable form by at least 0.39 kcal/mol (see section 2.4.8.). In addition to determining the relative free energies of the polymorphs, by measuring the optical absorbance of different polymorphs in situ one can also determine the relative solubilities of each form. It is well established that metastable forms exhibit higher solubilities than the thermodynamically stable form.[6, 15] Accordingly, form II was found to be one and a half times more soluble than form I, whereas form III exhibited solubility twice that of the thermodynamically stable form (see section 2.4.8.).

The thermodynamic relationship between polymorphs can be described as enantiotropic or monotropic. If polymorphs are enantiotropically related then the phase transition from one form to another is reversible and the enthalpy change corresponding to this transition is endothermic on heating.[15] For monotropically related polymorphs, the phase transition from one polymorph to another is irreversible meaning that only one form is stable at all temperatures and the transformation from a metastable form to the stable form is generally exothermic on heating.[15] Differential scanning calorimetry (DSC), an analytical technique which can measure the enthalpy associated with events including melting, can be used to determine if polymorphs are enantiotropes or monotropes. If the higher melting form has the lower melting enthalpy then the forms are enantiotropically related; if the higher melting form has the higher melting enthalpy then the forms are monotropically related. [15, 16] Form I was found to melt at 132.49 °C, while form II melts at 127.97 °C, and form III melts at 116.48 °C; making form I the highest melting form. The melting enthalpy of form I (7.5 kcal/mol) is higher than that of form II (6.0 kcal/mol) and form III (5.9 kcal/mol), thus both of the metastable forms are monotropically related to form I (Figure 2.8). Also by examining the DSC scan for form III, it was found that the form first melts and then recrystallizes into form I as confirmed by the subsequent melt at 132.50 °C.

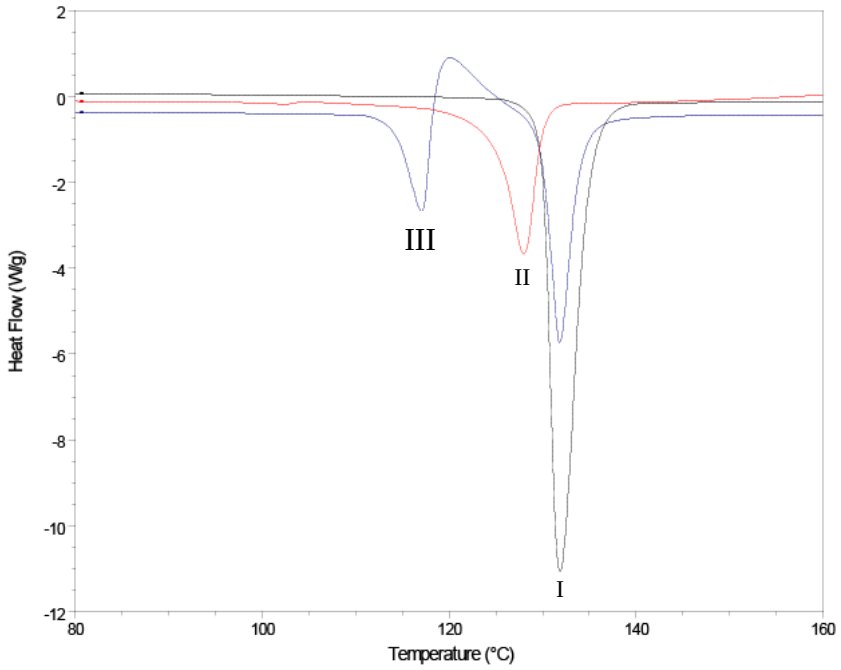

Figure 2.8. DSC scans of forms I, II, and III.

2.3 Conclusion

Piperine is at minimum trimorphic, with two of these forms structurally characterized for the first time. The novel crystal forms were found to possess π-π interactions which are lacking in the known form despite the extended conjugation in the molecule. The polymorphs were also found to have an enhanced solubility relative to the known form, allowing them to potentially enhance piperine's efficacy as a bioenhancer.

2.4 Experimental

2.4.1 Creation of Acidic Polymer Library

The components used to build the acidic polymer library are methyl methacrylate (MMA), acrylic acid (AA), methacrylic acid (MAA), 2-hydroxyethyl methacrylate (HEMA), 2-ethoxyethyl methacrylate (EEMA), styrene (STY), and divinylbenzene (DVB). For each library six 1:1 (v/v) monomer solutions in ethanol were dispensed as 90 pair wise combinations of varied ratios (86:14, 71:29, 57:43, 43:57, 29:71, and 14:86) and six pure monomer solutions by a Gilson 215 liquid handler to a volume of 120 μL. To this was added 40 μL of a 1:1 solution of DVB in ethanol containing 2 mol% 2,2'-azobis(2-methylpropionitrile) (AIBN) with respect to DVB.). The monomer solutions were then photopolymerized with four 15W UVA bulbs in an atmosphere of N_2 for two hours. Following polymerization the polymers were annealed at 85 °C under vacuum for 2 hours to produce the cross-linked polymer libraries.

2.4.2 Crystallization of Piperine Polymorphs

Piperine form I was obtained commercially from Acros Organics (NJ). Forms II and III were discovered through polymer-induced heteronucleation (PIHn).[7] A dry ethanol solution of piperine (70.5 mg/mL) was prepared by heating at 80 °C and immediate filtering through a 0.45 μm PTFE filter. Approximately 0.15 mL of the solution was then added to each well of a 96-well polypropylene plate containing various ratios of acidic polymers in each well. Form II was present most reliably on cross-linked polymers derived from hydroxyethylmethacrylate (HEMA) and acrylic acid (AA) or methylmethacrylate (MMA) and methacrylic acid (MAA). Form II was consistently observed on a polymer derived from DVB:HEMA:AA (33:71:29). Form III was present most reliably on cross-linked polymers derived from acrylic acid (AA), styrene (STY), and 2-ethoxyethyl methacrylate (EEMA). Form III was consistently observed on cross linked

polymers derived from DVB:STY (33:100) and DVB:EEMA (33:100). Form III was also obtained by heating form I past the melting point followed by immediate supercooling to -40 °C and then reheating the sample to 105 °C the resulting solid was confirmed to be form III by both Raman spectroscopy and powder X-ray diffraction (PXRD).

2.4.3 Optical Microscopy

Images of forms I, II, and III were collected using a Spot Advanced camera through a Leica microscope. All images were processed using Spot Advanced software (Version 4.6).

Form I

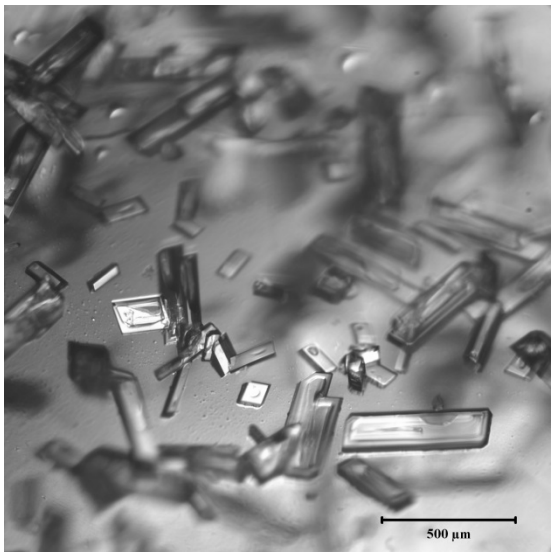

Form II

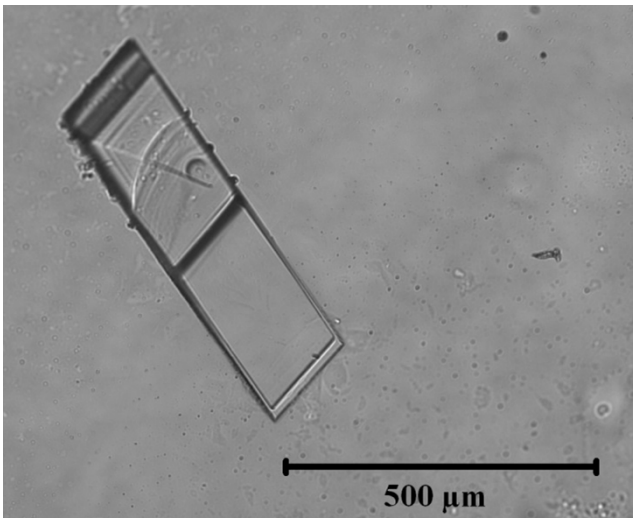

Figure 2.9. Optical microscopy of piperine forms I, and II.

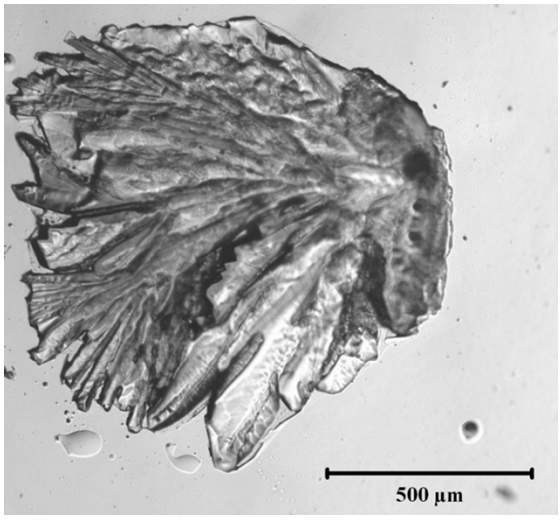

Figure 2.10. Optical microscopy of piperine form III.

2.4.4 Raman Spectroscopy

Raman spectra were collected using a Renishaw inVia Raman microscope equipped with a Leica microscope, RenCam CCD detector, 633 nm Kr^{+} laser, 1800 lines/nm grating, and 50 µm slit. Spectra were collected in extended scan mode in the range of 100-3600 cm^{-1} and then analyzed using the Wire 3.4 software package. Calibration was performed using a silicon standard.

2.4.5 Powder X-ray Diffraction of Piperine Polymorphs I, II and III

Powder X-ray diffraction (PXRD) patterns were collected at ambient temperature using a Rigaku R-Axis Spider diffractometer with an image plate detector and graphite monochromated Cu-Kα radiation (1.5406 Å). Samples were mounted on a CryoLoop™ and images were collected for five minutes while rotating the sample about the φ-axis at 10°/sec, oscillating ω between 120° and 180° at 1°/sec and with χ fixed at 45°. Images were integrated from 2° to 70° with a 0.02° step size using the AreaMax software. Powder patterns were processed in Jade Plus to calculate peak positions and intensities.

2.4.6 Single X-ray Diffraction of Piperine Polymorphs II and III

Single crystal X-ray diffraction data of form II was recorded on a Rigaku R-axis Spider diffractometer with an image plate detector using graphite monochromated Cu-Kα radiation (1.5406 Å). The data collection was made at 95 K and the structure was solved using direct methods.[18] All calculations were performed using CrystalStructure[19] crystallographic software package except for refinement, which was performed using SHELXL-97.[20] A crystal of piperine form III with dimensions 0.12 x 0.10 x 0.02 mm was mounted on a Rigaku AFC10K Saturn 944+ CCD-based X-ray diffractometer equipped with a low temperature device and Micromax-007HF Cu-target micro-focus rotating anode (λ = 1.54187 A) operated at 1.2 kW power (40 kV, 30 mA). The X-ray intensities were measured at 85(1) K with the detector placed at a distance 42.00 mm from the crystal. A total of 3935 images were collected with an oscillation width of 1.0° in ω. The exposure time was 1 second for the low angle images, 8 seconds for high angle. The integration of the data yielded a total of 77393 reflections to a maximum 2θ value of 136.46° of which 5221 were independent and 4436 were greater than 2σ(I). The final cell constants (Table 2.1) were based on the xyz centroids 46619 reflections above 10σ(I). Analysis of the data showed negligible decay during data collection; the data were processed with CrystalClear 2.0 and corrected for absorption.[21] The structure was solved and refined with the Bruker SHELXTL (version 2008/4) software package, using the space group C2/c with Z = 16 for the formula $C_{17}H_{19}NO_3$. There are two crystallographically independent molecules in the asymmetric unit.[22] All non-hydrogen atoms were refined anisotropically with the hydrogen atoms placed in idealized positions. Full matrix least-squares refinement based on F^2 converged at R1 = 0.0540 and wR2 = 0.1496 [based on I > 2sigma(I)], R1 = 0.0599 and wR2 = 0.1545 for

all data. Additional details are presented in Table 2.1. Acknowledgement is made for funding from NSF grant CHE-0840456 for X-ray instrumentation.

2.4.7 Hirshfeld Surface Analysis of Piperine forms I, II, and III

Hirshfeld surfaces of each of the molecules in the asymmetric unit of the ordered polymorphs of piperine were constructed using the program CrystalExplorer (Version 3.1).[14] Crystallographic information files were uploaded to the program after the normalization of N-H, O-H and C-H bond lengths (1.008, 0.983, and 1.083 Å, respectively) to average neutron values was performed.[23, 24]

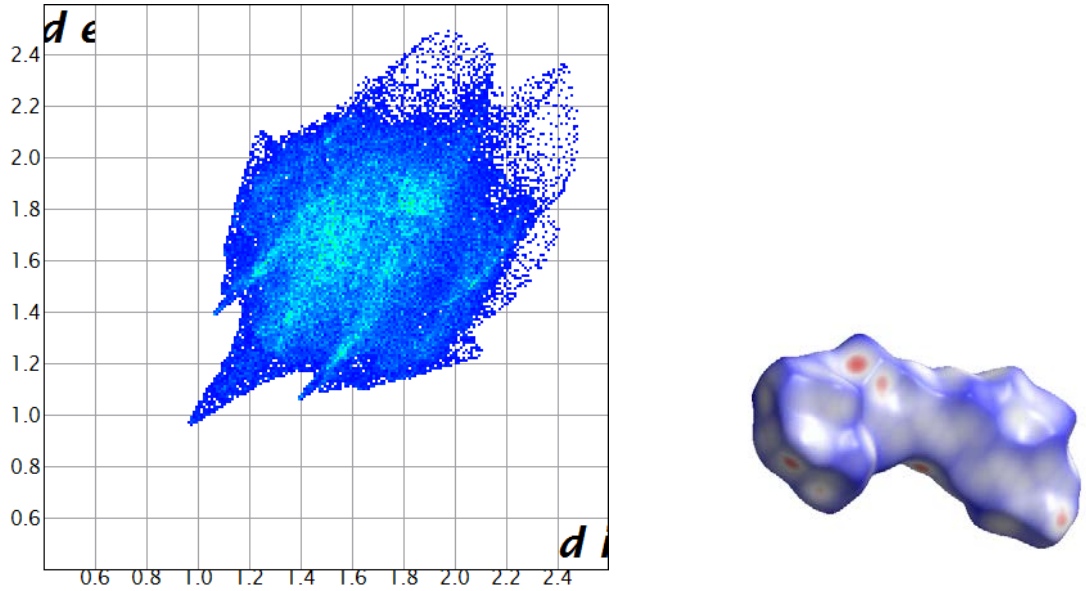

Figure 2.11. 2D finger plot and the Hirshfeld surface for piperine form I.

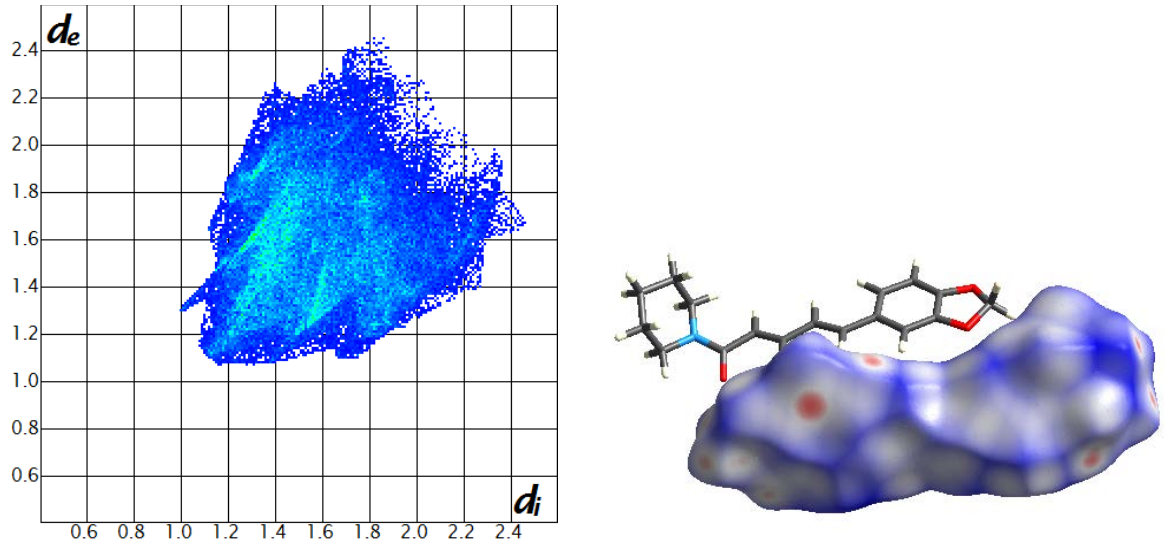

Figure 2.12. 2D finger plot for the Hirshfeld surface for one molecule in the asymmetric unit of piperine form II.

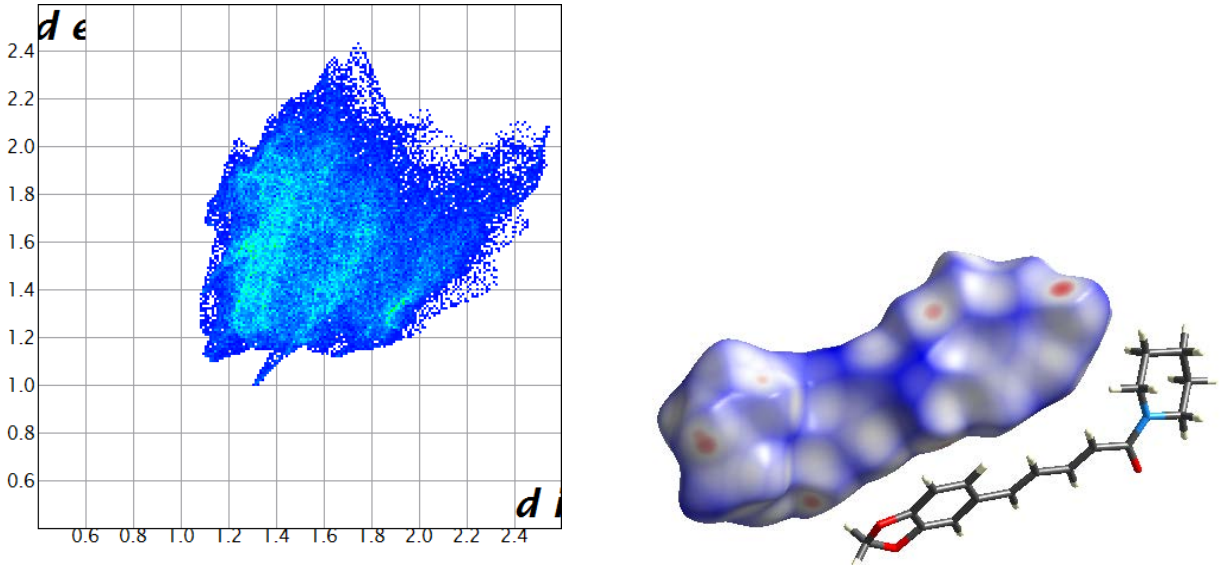

Figure 2.13. 2D finger plot and the Hirshfeld surface for the second molecule in the asymmetric unit of piperine form II.

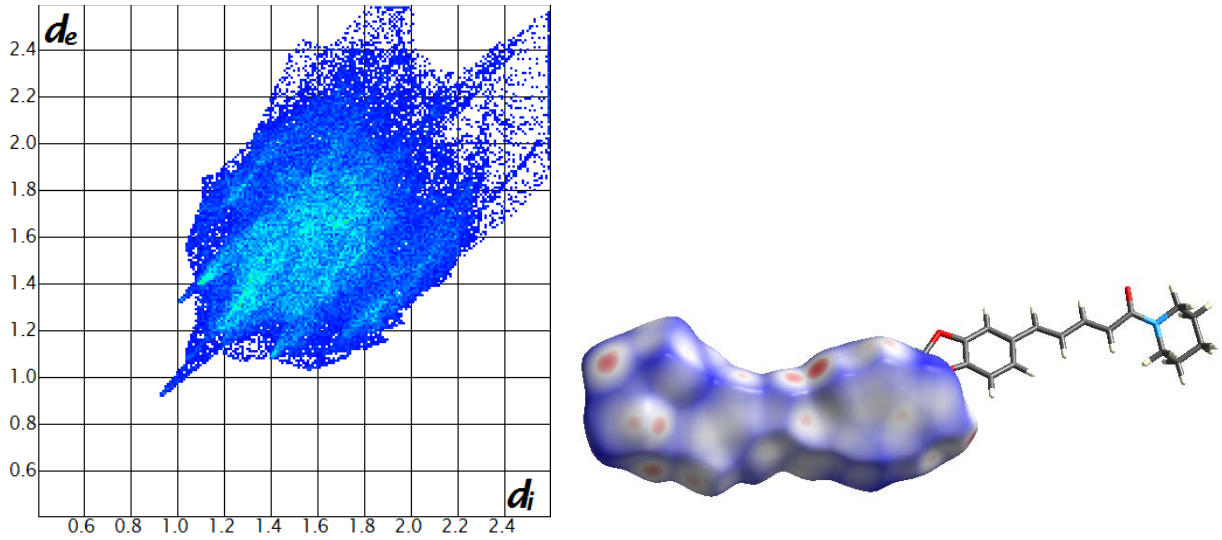

Figure 2.14. 2D finger plot and the Hirshfeld surface for one molecule in the asymmetric unit of piperine form III.

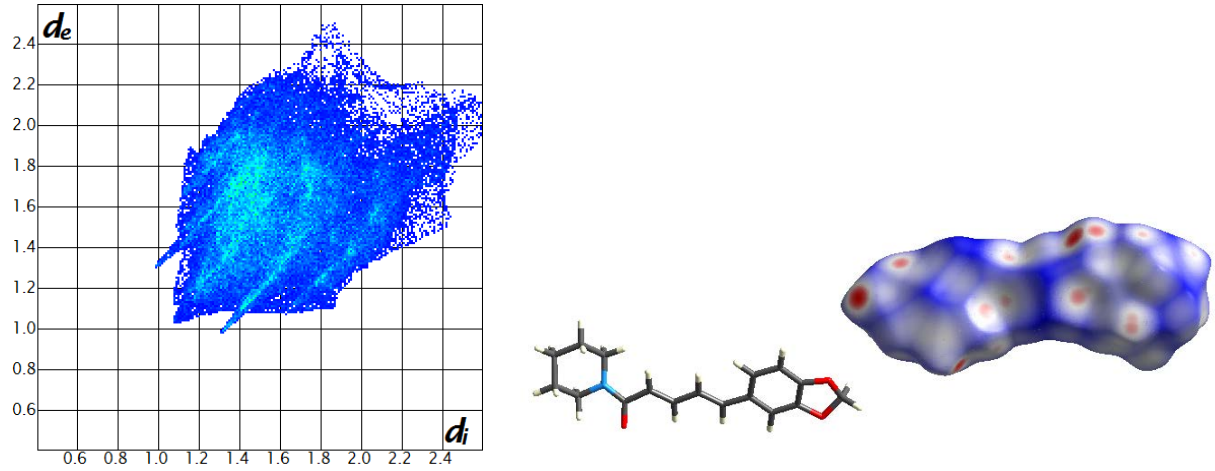

Figure 2.15. 2D finger plot and the Hirshfeld surface for the second molecule in the asymmetric unit of piperine form III.

2.4.8 Differential Scanning Calorimetry of Piperine Polymorphs I, II, and III

Thermograms of the samples were recorded on a TA Instruments Q20 DSC. The thermal behavior of the samples, placed in sealed aluminum pans, was studied under nitrogen purge with a heating/cooling rate of 10 °C min^{-1}covering the temperature range 25 °C to 300 °C. The

instrument was calibrated with an indium standard. Differential scanning calorimetry was performed on piperine forms I, II, and III. Form I showed no transitions prior to a melt centered at 132.49 °C. Form II was found to melt at 127.97 °C. Form III exhibited an initial melt centered at 116.48 °C followed by an exothermic transition between 118 °C and 128 °C. This exothermic transition represents the recrystallization of form III into form I, shown by the subsequent melt centered at 132.5 °C.

2.4.9 Free Energy Relationships Among the Piperine Polymorphs

The optical absorbance of the piperine polymorphs in water was monitored in situ over time using a Pion *μDISS Profiler* in the range of 500-200 nm at 300 ± 1 K., 22 mL glass cells were used for the experiment. The lambda maximum (λmax.) of absorbance of piperine in water was located at 340 nm. A time-dependent absorbance curve was used to determine the absorbance at equilibrium and these values were employed in determining the relative free energy (ΔG) for each of the polymorphs as well as to monitor conversions in solution over a longer period of time (see equation 1). The solute remaining was identified using PXRD. In the case of form I, no transformation was observed within the time frame of the experiment. However it was found that both forms II and III converted to form I during the course of the experiment, as confirmed by PXRD. Furthermore, the relative solubilities of each of the forms were found by determining the absorbance at equilibrium for each of the polymorphs in water and then taking the ratio of the relative absorbance of the metastable forms relative to the stable form.

$$\Delta G = RT \ln(S_2/S_1) \qquad (1)$$

Form	ΔG (kcal/mol)
I	0
II	0.24*
III	0.39*

*Polymorphs II and III transformed during the experimental time frame to form I, therefore the free energies presented in this table are a slight underestimation of the free energies due to polymorphic transformation preventing full supersaturation from being achieved.

Table 2.2. Relative free energies of the piperine polymorphs.

2.5 References

1. Meghwal, M.; Goswami, T. K., Piper nigrum and Piperine: An Update. *Phytother. Res.* **2013,** 27, (8), 1121-1130.
2. Atal, C. K.; Zutshi, U.; Rao, P. G., Scientific Evidence on the Role of Ayurvedic Herbals on Bioavailability of Drugs. *J. Ethnopharmacol.* **1981,** 4, (2), 229-232.
3. Mao, Q. Q.; Huang, Z.; Zhong, X. M.; Xian, Y. F.; Ip, S. P., Brain-derived neurotrophic factor signalling mediates the antidepressant-like effect of piperine in chronically stressed mice. *Behav. Brain Res.* **2014,** 261, 140-145.
4. Bano, G.; Raina, R. K.; Zutshi, U.; Bedi, K. L.; Johri, R. K.; Sharma, S. C., Effect of Piperine on Bioavailablity and Pharmacokinetics of Propanolol and Theophylline in Healthy-Volunteers. *Eur. J. Clin. Pharmacol.* **1991,** 41, (6), 615-617.
5. Mujumdar, A. M.; Dhuley, J. N.; Deshmukh, V. K.; Raman, P. H.; Thorat, S. L.; Naik, S. R., Effect of Piperine on Pentobarbital Induced Hypnosis in Rats. *Indian J. Exp. Biol.* **1990,** 28, (5), 486-487.
6. Bernstein, J., *Polymorphism in Molecular Crystals*. Oxford University Press: New York, 2002.
7. Price, C. P.; Grzesiak, A. L.; Matzger, A. J., Crystalline polymorph selection and discovery with polymer heteronuclei. *J. Am. Chem. Soc.* **2005,** 127, (15), 5512-5517.
8. Lopez-Mejias, V.; Kampf, J. W.; Matzger, A. J., Polymer-Induced Heteronucleation of Tolfenamic Acid: Structural Investigation of a Pentamorph. *J. Am. Chem. Soc.* **2009,** 131, (13), 4554-4555.
9. Lopez-Mejias, V.; Kampf, J. W.; Matzger, A. J., Nonamorphism in Flufenamic Acid and a New Record for a Polymorphic Compound with Solved Structures. *J. Am. Chem. Soc.* **2012,** 134, (24), 9872-9875.
10. Grynpas, M.; Lindley, P. F., Crystal and Molecular-Structure of 1-Piperoylpiperidine *Acta Crystallogr. Sect. B-Struct. Commun.* **1975,** 31, (NOV15), 2663-2667.
11. Rajesh, C.; Majumder, C.; Mizuseki, H.; Kawazoe, Y., A theoretical study on the interaction of aromatic amino acids with graphene and single walled carbon nanotube. *J. Chem. Phys.* **2009,** 130, (12).
12. Sinnokrot, M. O.; Valeev, E. F.; Sherrill, C. D., Estimates of the Ab Initio Limit for π−π Interactions: The Benzene Dimer. *J. Am. Chem. Soc.* **2002,** 124, (36), 10887-10893.
13. Dahl, T., The nature of stacking interactions between organic molecules elucidated by analysis of crystal structures. **1994**.
14. Wolff, S. K.; Grimwood, D. J.; McKinnon, J. J.; Turner, M. J.; Jayatilaka, D.; M.A. Spackman *CrystalExplorer* 3.1; University of Western Australia: 2012.
15. Burger, A.; Ramberger, R., Polymorphism of Pharmaceuticals and Other Molecular-Crystals. 1. Theory of Thermodynamic Rules *Mikrochim. Acta* **1979,** 2, (3-4), 259-271.
16. Giron, D., Investigations of polymorphism and pseudo-polymorphism in pharmaceuticals by combined thermoanalytical techniques. *J. Therm. Anal.* **2001,** 64, (1), 37-60.
17. Threlfall, T., Structural and Thermodynamic Explanations of Ostwald's Rule. *Organic Process Research & Development* **2003,** 7, (6), 1017-1027.
18. Burla, M. C.; Caliandro, R.; Camalli, M.; Carrozzini, B.; Cascarano, G. L.; De Caro, L.; Giacovazzo, C.; Polidori, G.; Spagna, R., SIR2004: an improved tool for crystal structure determination and refinement. *Journal of Applied Crystallography* **2005,** 38, (2), 381-388.

19. Rigaku/MSC, R. a. *CrystalStructure 3.7.0 ed.; Crystal Structure Analysis Package;* , Rigaku and Rigaku/MSC: The Woodlands, TX 77381, 2000−2005.
20. Sheldrick, G. M. *SHELXS97 and SHELXL97*, University of Göttingen: Germany, 1997: Germany, 1995-2000.
21. (2011), R. A. a. R. C. *CrystalClear Expert 2.0 r12*, Rigaku Americas and Rigaku Corporation: 9009, TX, USA 77381-5209, Rigaku Tokyo, 196-8666, Japan, 2011.
22. Sheldrick, G. M. *SHELXTL, v. 2008/4*, Bruker Analytical X-ray: Madison, WI, 2008.
23. McKinnon, J. J.; Spackman, M. A.; Mitchell, A. S., Novel tools for visualizing and exploring intermolecular interactions in molecular crystals. *Acta Crystallographica Section B* **2004,** 60, (6), 627-668.
24. Spackman, M. A.; McKinnon, J. J., Fingerprinting intermolecular interactions in molecular crystals. *Crystengcomm* **2002,** 4, (66), 378-392.

Chapter 3 Towards Exhaustive and Automated High Throughput Screening for Crystalline Polymorphs

Published: Pfund, L. Y.; Matzger, A. J., *ACS Combinatorial Science* **2014,** 16, (7), 309-313.

3.1 Introduction

The recognition that pharmaceuticals often exist in multiple crystalline forms solely differing in the arrangement of molecules, crystalline polymorphs,[1] has led to an increase in activity directed towards efficiently screening for solid form diversity. The ideal technique should facilitate formation and identification of all possible polymorphs of a molecule while utilizing minimal amounts of the target compound and automated form identification. This goal remains elusive in part due to the fact that the nucleation of a specified polymorph is influenced by a wide array of factors, making polymorph discovery an often time-consuming, Edisonian process. A traditional screen typically involves changes in variables such as solvent, temperature, and degree of supersaturation. These variables have empirically been shown to influence the polymorphic form obtained from a crystallization trial, albeit through a mechanism that is obscure. More sophisticated approaches involving heterogeneous nucleation, where a foreign surface is present that can interact with the crystallizing material in solution[2] are emerging. For example, self-assembled monolayers (SAMs)[3-6], crystalline heteronucleants[7, 8], and amorphous polymers[9-13] have all been employed with varying degrees of success. In particular, polymer-induced heteronucleation (PIHn) has proven to be a powerful discovery method utilizing

hundreds of unique amorphous polymers as crystallization directors for obtaining novel solid forms.[14-16] The polymer selectively promotes the growth of one form above others through a kinetic mechanism involving selective stabilization at the stage of nucleation.[17, 18] It has been established that functional group interactions at the polymer-crystal interface are responsible for directing and controlling the nucleation of different crystal phases on specific polymer heteronucleants.[17, 18] Recently nonamorphism in the anti-inflammatory compound flufenamic acid was demonstrated using PIHn, setting a new record for the organic compound with the most structurally characterized polymorphs.[19]

Although PIHn has been extremely successful in both form selection and in obtaining novel polymorphs, there are still several challenges that must be overcome to improve screening efficiency and accuracy. Raman spectroscopy, an analytical technique used to study the vibrational modes in a material, is often employed to distinguish among polymorphs due to its short analysis times, minimal sample preparation requirements, and high sensitivity. However, the relatively large amount of polymer heteronucleant present often leads to problematic levels of background Raman scattering; this can obscure the Raman spectrum of the compound of interest and hamper automated analysis. Furthermore, PIHn relies on relatively large amounts of sample, limiting polymorph screening to compounds that are readily available.

Previous work on high throughput platforms focused on the creation of polymer microarrays by a piezo jet-printer.[20] This system employed hundreds of soluble commercial polymers and a few synthesized cross-linked and linear copolymers as polymer heteronucleants and demonstrated some success in form selection.[20] Here PIHn is adapted into a high density format in which hundreds of distinct amorphous, insoluble cross-linked terpolymers are arrayed on a single substrate by using simple pin tools, making automated, high throughput screening

possible. The cross-linked terpolymers used in this study are readily generated from simple feedstocks of monomer solutions which are combined in various, allowing for diversity and flexibility in the composition of the cross-linked terpolymers that are utilized as the heteronucleants in this high density platform. This new format is distinct from traditional PIHn in that the amount of polymer, the platform on which the crystallizations occur, the volume of solvent used for crystallization, and the total amount of material used for the crystallization have been dramatically decreased. The reduction in scale is advantageous for a number of reasons. The reduction in polymer thickness yields Raman spectra of compounds with minimal spectral interference from the polymer heteronucleant, enabling completely automated analysis. The amount of material needed has been considerably reduced (to ~1 mg) as compared to the amounts previously needed for polymorph discovery with PIHn (~300 mg). Hence, screening newly synthesized compounds for which typically only small quantities are available becomes feasible. Here the efficacy of this new, high density format using the compounds acetaminophen[14], tolfenamic acid[16], ROY,[21] and curcumin[22] is demonstrated. Furthermore, the consequence of this reduction in scale on polymorph selection efficacy, as compared with PIHn deployed in a traditional format, is explored.

3.2 Results and Discussion

Most high throughput crystallizations are currently conducted using 96, 384, or 1536 well microtiter plates due to their high densities and compatibility with liquid handling robotics. However, using these plates for polymorph screening can be problematic for several reasons. *In situ* Raman analysis is challenging due to the high aspect ratio and narrow width of the wells in these microtiter plates. When laser light from the Raman spectrometer is focused on a crystal at the bottom of a well, it is hindered from reaching the sample due to the refraction of light at the

top of the well arising from its narrow diameter. This also results in an increase in the focal volume of the laser.[23] Even for the portion of the laser light reaching the sample, the light does not scatter directly upwards but rather will scatter off of the opaque walls of the plate, limiting the amount of light that reaches the detector. These issues effectively reduce sample throughput by increasing the time needed to collect individual spectra. In order to quantitatively understand these effects, an experiment was performed with a Delrin aperture (hole diameter of 3.30 mm with a 6.0 mm height) placed above a crystal of the nutraceutical piperine, monitoring the signal intensity as the number of Delrin pieces was increased. When one Delrin aperture was used the signal was diminished by 41%; when two were used (effectively mimicking the depth in a standard 384 microtiter plate) the signal was diminished by 72% as compared to having the same crystal on a planar substrate. This experiment demonstrates how the signal in Raman spectroscopy is affected by the depth and narrowness of a well (see Section 3.4.8). Direct interrogation of crystals within a microtiter plate by X-rays is not possible due to the geometric requirements for diffraction. The geometry of the microtiter plates also makes it very difficult to manually manipulate crystals for *ex situ* analysis. After examining all of these disadvantages, it is apparent that microtiter plates are not optimal for conducting efficient polymorph screening.

To overcome the limitations of current approaches to high throughput polymorph screening, a platform which takes advantage of the benefits of a high density microtiter plate, but limits the drawbacks currently associated with them was devised. A CO_2 laser

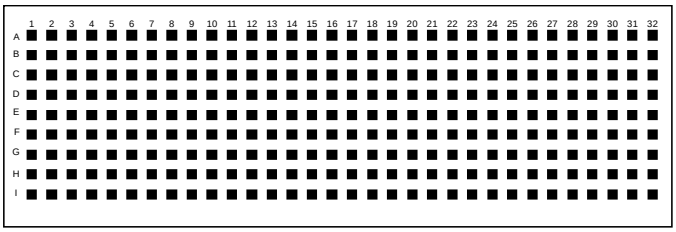

Figure 3.1. Schematic of quartz slide with an array of depressions (1 mm wide) with a 2.25 mm spacing from center of one depression to another, implemented in this study as the crystallization platform.

was utilized to create an array of 288 depressions approximately 300 μm deep on a standard quartz microscope slide (75 mm × 25 mm × 1 mm). This geometry eliminates any constraints to *in situ* analysis and crystal harvesting (Figure 3.1, see Section 3.4.4). This precisely-defined array possesses the spacing of a 1536 well plate (2.25 mm from the center of one depression to another) maintaining compatibility with liquid handling robots. For demonstration purposes the three distinct polymer libraries commonly employed in PIHn studies were chosen; these are characterized by the functionalities of their constituent monomers: acidic, nonpolar aromatic, and polar nitrogen.[14] For each of these libraries there are 96 cross-linked polymers, for a total of 288 unique cross-linked polymers. Therefore, the three libraries can be deposited on a single quartz slide with a unique polymer in each depression. This manipulation was accomplished by taking advantage of the geometry of a 1536 well plate relative to a 384 well plate. On a 384 microtiter plate the spacing from the center of one well to another is 4.5 mm (exactly double the spacing in a 1536 well plate). With this in mind, a custom pin tool[24] was fabricated comprised of five Delrin combs held together in a poly(methyl methacrylate) lattice (Figure 3.2). This pin tool enables rapid contact-printing of up to 80 distinct monomer solutions simultaneously from a 384 well plate containing the monomer solutions onto the individual depressions on the laser-etched quartz slide. The number of monomer solutions printed onto the quartz slide can be easily changed by removing a comb from the lattice; depending on the number of combs present, 16-80 distinct monomer solutions can be dispensed at one time. Immediately after each print from the 384 well plate onto the quartz slide,

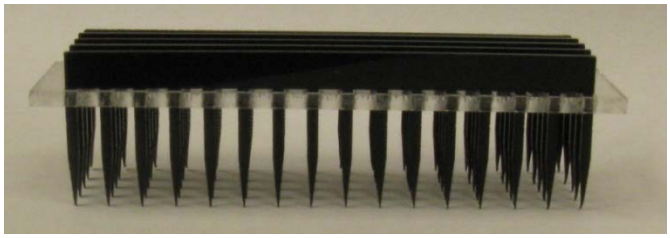

Figure 3.2. Pin tool used for deposition of material onto a μPIHn plate.

the monomer solutions were photopolymerized, yielding thin polymer films in each depression. Four applications of the printing tool were required to print all 288 distinct monomer solutions (see Section 3.4.5) and after polymerization was completed, the μPIHn plate was applied to crystallization studies. An additional comb was then used to dispense the crystallization solution of the molecule to be investigated onto the μPIHn plate. This contact printing leads to very low volume transfer (~0.3 μL per well) and therefore small sample requirements. The extremely thin polymer films allow for analysis of polymorphs directly on the plate without significant signal interference from the polymer heteronucleant, thus enabling automated Raman microscopy mapping. The efficacy of this platform was demonstrated with four model polymorphic compounds: acetaminophen (ACM), tolfenamic acid (TA), ROY, and curcumin.

Acetaminophen. Acetaminophen is typically found in one of two stable polymorphic forms: form I (monoclinic) and form II (orthorhombic).[14] Previously, when PIHn was used to study the polymorphism of ACM, both the monoclinic and orthorhombic forms were found utilizing roughly half of a gram of material for one screen.[14] With μPIHn both forms I and II of ACM were obtained using less than one milligram of material (Figure 3.3). Form I of ACM was crystallized by room temperature evaporation of aqueous solutions in the presence of acidic polymers whereas form II nucleated on polymers within the nonpolar aromatic library (see Section 3.4.6).

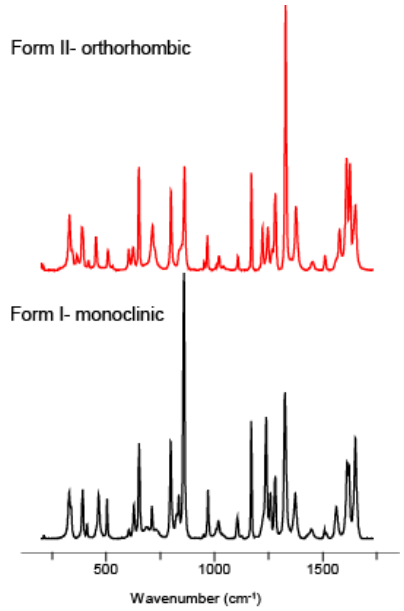

Figure 3.3. Raman spectra of acetaminophen forms I and II obtained directly from crystals on the µPIHn plate.

ROY. ROY, an intermediate in the production of the pharmaceutical olanzapine, is known for the color of its red, orange, and yellow polymorphs.[21] Using µPIHn, four of the seven structurally characterized forms were obtained: red prism (R), yellow needle (YN), orange needle (ON), and yellow prism (Y) (Figure 3.4). Red and yellow prisms nucleated on polymers within the polar nitrogen library. However, polymers in the nonpolar aromatic library facilitated the formation of yellow needles. Orange needles were found on polymers in the acidic library (see Section 3.4.6).

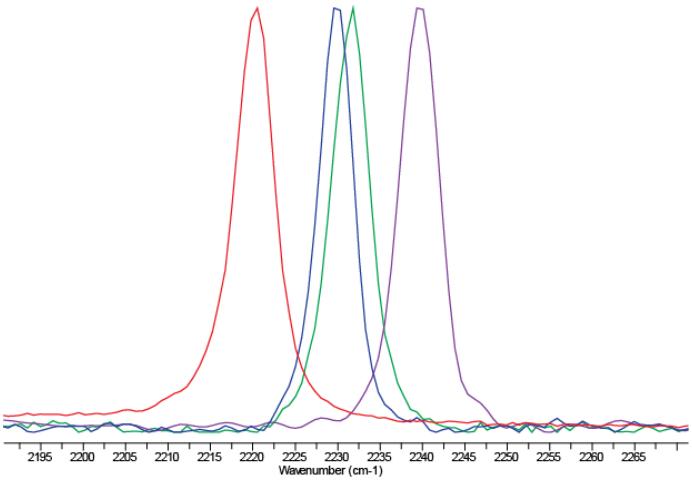

Figure 3.4. Raman Spectra of the diagnostic nitrile region for ROY, in order from left to right: red prism, yellow needles, orange needles, yellow prims, obtained directly from crystals on a µPIHn plate.

Tolfenamic acid. Tolfenamic acid (TA) is a pentamorphic, non-steroidal anti-inflammatory drug.[16] Previously when TA was subjected to traditional PIHn screening, five polymorphs were found, with three forms discovered for the first time.[16] Now with µPIHn all five known forms of TA were obtained using only 0.2 mg of TA (Figure 3.5). Forms I, II, and V of TA were found to nucleate on polymers within the polar nitrogen library, whereas forms III and IV nucleated on polymers in the nonpolar aromatic library (see Section 3.4.6).

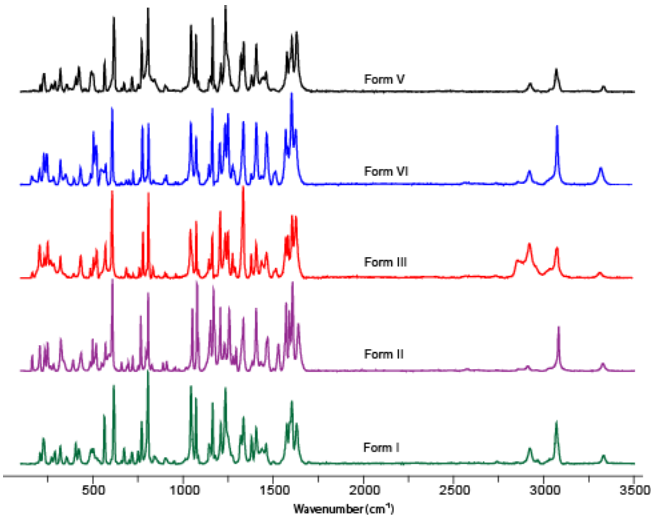

Figure 3.5. Raman Spectra of tolfenamic acid forms I, II, III, VI, and V, obtained directly from crystals on a µPIHn plate.

Curcumin. Curcumin is the primary curcuminoid in the spice turmeric. Curcumin has been found to act as an anti-inflammatory, anti-cancer, and anti-HIV agent.[25] Nangia and coworkers discovered two new polymorphs of curcumin while attempting to form cocrystals.[22] All three polymorphs of curcumin were found in the present study (Figure 3.6). Form I and II formed on polymers within the polar nitrogen library, whereas form III nucleated on polymers within the acidic library (see Section 3.4.6).

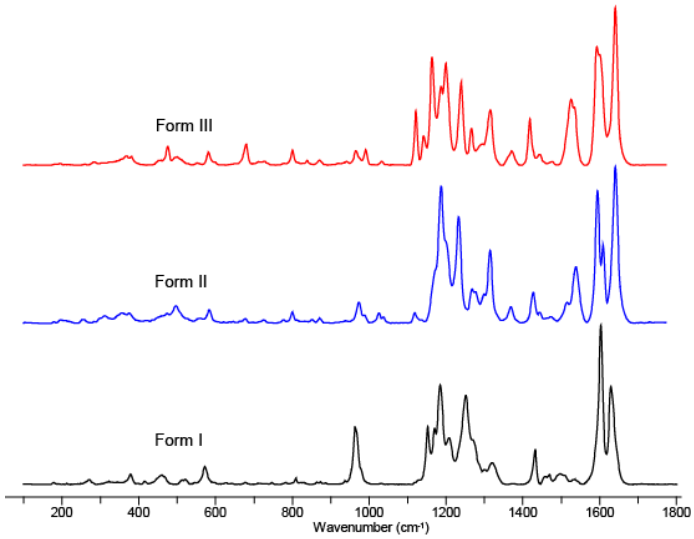

Figure 3.6. Raman Spectra of curcumin forms I, II, and III, obtained directly from crystals on a µPIHn plate.

In the present study, automated Raman mapping was used to identify all of the pharmaceutical polymorphs. The above results illustrate that using ~1 mg is viable for efficient polymorph screening for all of the compounds studied with µPIHn. However, the polymers responsible for promoting the formation of a particular polymorph in some cases were different from those of traditional PIHn. For example, with µPIHn, forms II and V of tolfenamic acid were found to nucleate on polymers within the polar nitrogen library whereas with traditional PIHn, these forms were obtained exclusively on polymers within the aromatic library. This difference may arise from the dramatic increase in the rate of evaporation of the crystallizing solution with

μPIHn as compared with traditional PIHn. This enhanced evaporation rate is a direct result of the extremely small amount of solvent that is printed into each depression (~0.3 μL) and the relatively open nature of conducting crystallization on an open plate. Despite this drastic difference in the kinetics of the crystallization, the efficacy of PIHn was still maintained.

3.3 Conclusions

The above results have important implications for the stage at which comprehensive polymorph discovery can take place. Solid form screening, as currently practiced, requires substantial sample quantities and it has thus far not been feasible to perform solid form screening as an early-stage selection criterion for choosing which bioactive compounds to advance in the pipeline. Hence, the process by which a drug candidate is chosen neglects solid form considerations until a rather late stage where the cost of failure is greater.[26, 27] With μPIHn only a small amount of material is needed in order to study the potential polymorphism of a newly synthesized compound. Therefore, this new polymorph discovery platform can shift solid form considerations to an earlier stage in the pharmaceutical development process.

PIHn has been transformed into a high density format in which hundreds of distinct polymers are arrayed on one substrate, making automated, high throughput analysis possible. This new format is dissimilar from traditional PIHn in that the amount of polymer, the substrate on which the crystallizations occur, the volume of solvent utilized for crystallization, and the total amount of material used for the crystallization (~1 mg) have been decreased dramatically. The reduction in polymer thickness yields Raman spectra with minimal spectral interference from the polymer heteronucleant, enabling completely automated analysis.

From the present study, it is apparent that although aspects of the crystallizations with μPIHn have changed from traditional PIHn, the method's efficacy has been maintained. This is a direct

result of the mechanism of PIHn: it is a surface-mediated process dominated by functional group interactions at the polymer-crystal interface, and is therefore independent of the amount of polymer present.[17, 18] μPIHn can now be implemented to study the potential of polymorphism in newly synthesized compounds. As a result of the unique configuration of this platform, countless crystallization conditions can be explored in the presence of hundreds of distinct polymers including, but not limited to, varying parameters such as the temperature,[9] the degree of supersaturation, and solvent, enabling the structural landscape of a compound to be thoroughly explored. Although it is not possible to determine if all of the polymorphs of a compound have been found, by conducting a comprehensive experimental screening in combination with modern methods for computationally predicting which polymorphs are viable on the crystal energy landscape, one can have high confidence that all relevant polymorphs have been discovered. By considering all possible solid forms early in the drug development process, knowledge of solid form diversity can be leveraged to select which drug candidates to advance in the pipeline.

3.4 Experimental Procedures

3.4.1 Preparation of the polymer libraries

The components used to build the non-polar aromatic polymer library were 4-acetoxystyrene (AOS), n-butyl methacrylate (n-BuMA), tert-butyl methacrylate (t-BuMA), benzyl methacrylate (BzMA), methyl methacrylate (MMA), styrene (STY), and divinylbenzene (DVB). The components used to build the polar nitrogen polymer library were 2-methyl-2-nitropropyl methacrylate (MNPMA), methacrylonitrile (MAN), 2-(dimethylamino)ethyl methacrylate (DMAEMA), N,N-dimethylmethacrylamide (DMMAA), 2-vinylpyridine (2VP), 4-vinylpyridine (4VP), and divinylbenzene (DVB). The components used to build the acidic polymer library are methyl methacrylate (MMA), acrylic acid (AA), methacrylic acid (MAA), 2-

hydroxyethyl methacrylate (HEMA), 2-ethoxyethyl methacrylate (EEMA), styrene (STY), and divinylbenzene (DVB). For each library six 1:1 (v/v) monomer solutions in ethanol were dispensed as 90 pair wise combinations of varied ratios (86:14, 71:29, 57:43, 43:57, 29:71, and 14:86) and six pure monomer solutions by a Gilson 215 liquid handler to a volume of 120 μL. To this was added 40 μL of a 1:1 solution of DVB in ethanol containing 2 mol% 2,2'-Azobis(2-methylpropionitrile) (AIBN) with respect to DVB. The three 96 well plates containing the monomer solutions were transferred into a flat bottom 384 well plate by using an Eppendorf epmotion® 5070 liquid handling robot. Using a pin tool comprised of Delrin combs in a PMMA lattice four prints were performed from a 384 well plate containing monomer solutions onto the depressions on the laser etched quartz slide. In order to print all 288 monomer solutions four prints were performed from the 384 well plate onto the quartz slide (See Supporting Information). After each print the monomer solutions were photopolymerized with four 15W UVA bulbs in an atmosphere of N_2 for 1 minute. Following polymerization the μPIHn plates were annealed at 85 °C under vacuum for 2 hours to produce the cross-linked polymer libraries.

3.4.2 Materials

Acetaminophen (ACM) and tolfenamic acid (TA) were obtained from Sigma-Aldrich (MO). Curcumin was purchased from Acros Organics (NJ). ROY was synthesized by following the literature procedure.[28] Ethanol was purchased from Decon Laboratories, Inc. (PA).

Delrin® in sheets 1.19 mm thick and poly(methyl methacrylate) (PMMA) in sheets 3.175 mm thick were obtained from McMaster-Carr (OH). Quartz slides (75 mm × 25 mm × 1 mm) were purchased from Chemglass (NJ).

3.4.3 Pin tool preparation

All pin tools used in this study were created using a Universal Laser System desktop VLS2.30 equipped with a 30W CO_2 laser and High Power Density Focusing Optics (HPDFO). The system described above is capable of cutting in two different manners: vector (used to cut through a material) and raster (used to create depressions in a material). Additionally, the power and the speed of the cutting can be controlled. Both the Delrin combs and the PMMA lattice were created by using the vector configuration of the system. The combs were created by cutting Delrin sheets at 100% power and 17% speed. In order to create the PMMA lattice, PMMA sheets were cut at 100% power and 7% speed (Adobe Illustrator files used to define the cutting geometries are available in Supporting Information).

3.4.4 Creation of a quartz slide with an array of depressions

Quartz slides with a precisely defined array of depressions were cut in raster mode at 100% power and 10% speed. The width of each depression was 1 mm and the spacing from the center of one depression to another was 2.25 mm (the Adobe Illustrator file is available in Supporting Information).

3.4.5 Printing procedure to produce a μPIHn plate.

Using a pin tool comprised of a set of Delrin combs in a PMMA lattice four prints were performed from a 384 well plate containing monomer solutions onto the depressions on the laser etched quartz slide. For the first two prints five combs were used in the PMMA lattice. For the final two prints four combs were used in the PMMA lattice. Immediately after each print from the 384 well plate onto the quartz slide, the monomer solutions were photopolymerized with four 15 W UVA blubs in an N_2 atmosphere, yielding thin polymer films in each depression.

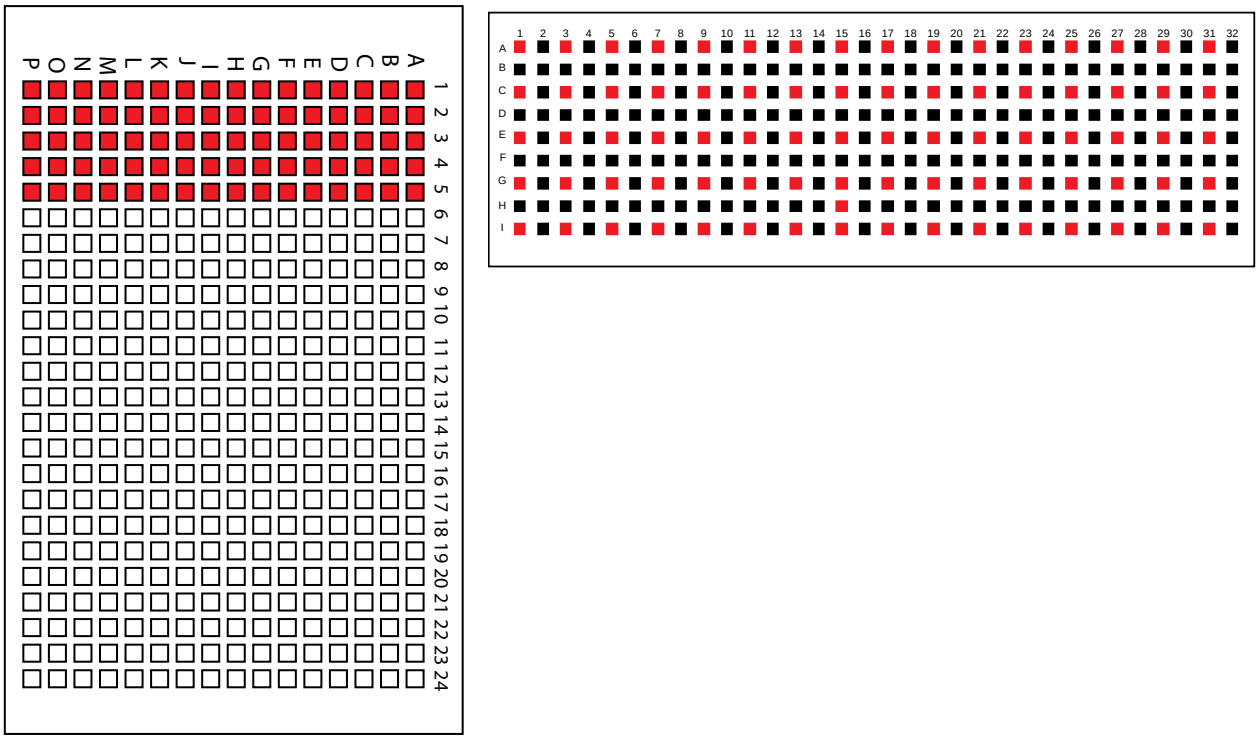

Figure 3.7. First print from a 384 well plate onto quartz slide with an array of depressions.

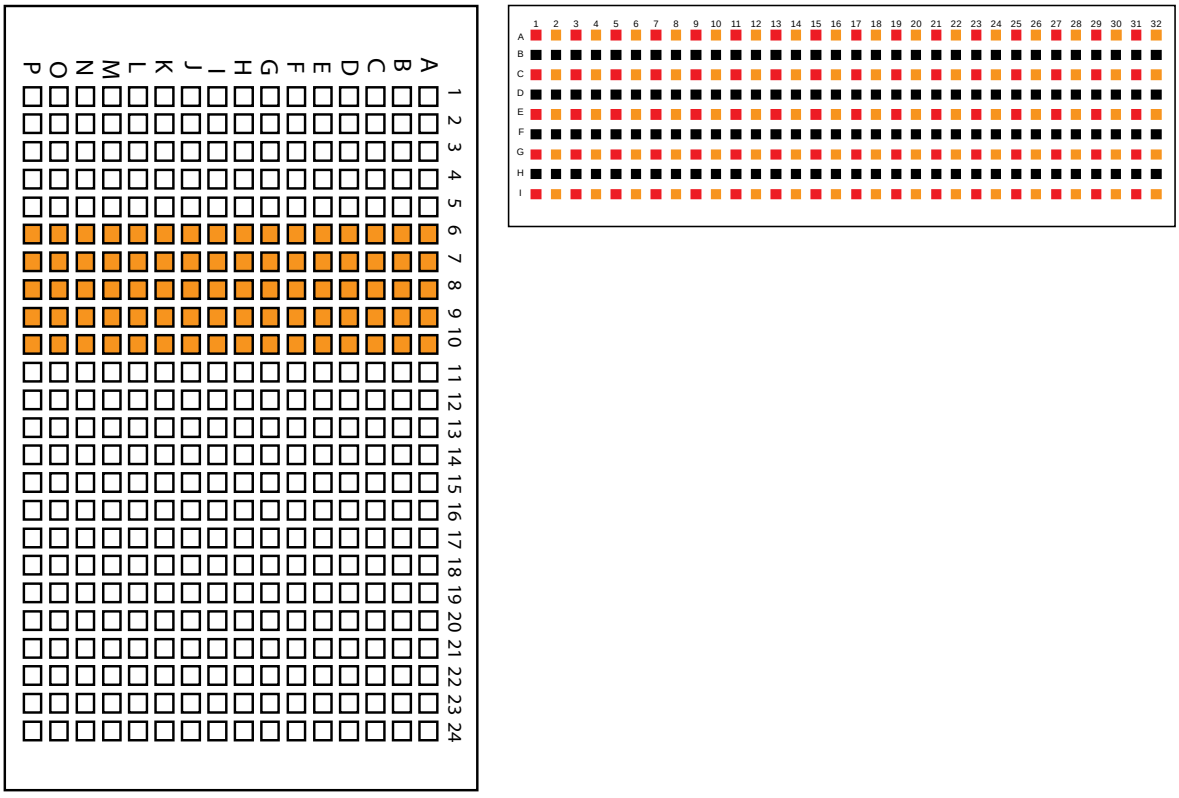

Figure 3.8. Second print from a 384 well plate onto quartz slide with an array of depressions.

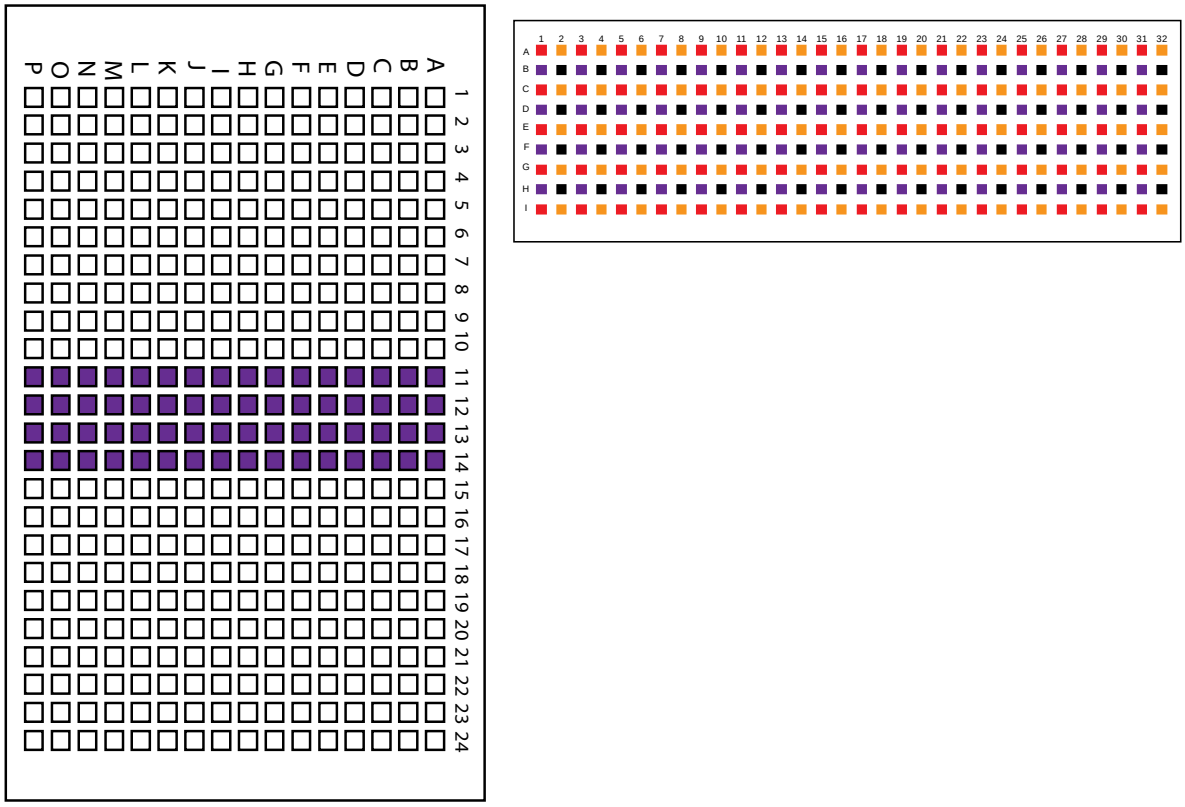

Figure 3.9. Third print from a 384 well plate onto quartz slide with an array of depressions.

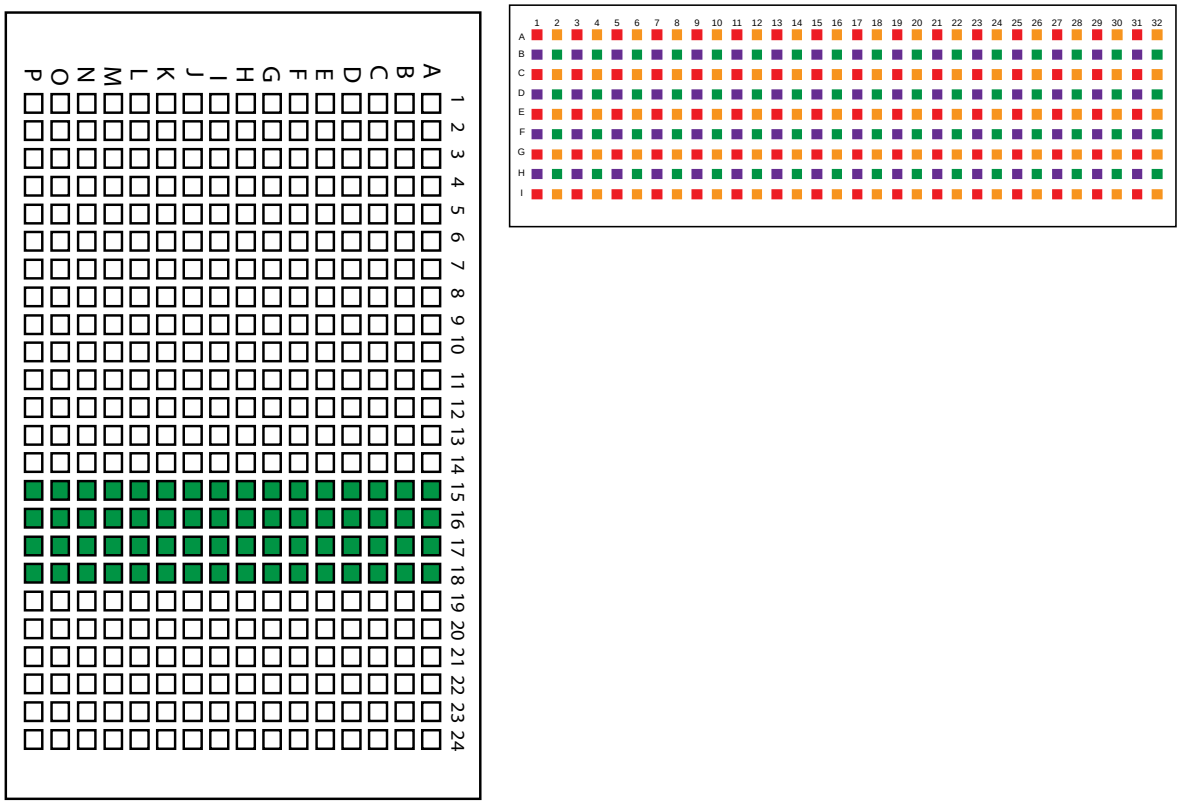

Figure 3.10. Fourth print from a 384 well plate onto quartz slide with an array of depressions.

3.4.6 Crystallizations

ACM. A solution of ACM was prepared by dissolving 10 mg of ACM in 1 mL of water. The solution was then filtered using a 0.45 μm pore size PTFE filter. Following filtration the solution was dispensed onto a μPIHn plate by using Delrin combs. Form I (monoclinic) was present most reliably on cross-linked polymers derived from methyl methacrylate (MMA) and methacrylic acid (MAA). Form I was consistently observed on a polymer derived from DVB:MMA:MAA (33:57:43). Form II nucleated consistently on cross-linked polymers derived from styrene (STY) and 2-ethoxyethyl methacrylate (EEMA). In particular, cross-linked polymers derived from DVB:STY (33:100) assisted in the formation of form II.

ROY. A solution of ROY was made by dissolving 10 mg of the material in 1 mL of ethanol. The solution was then filtered using a 0.45 μm pore size PTFE filter and printed onto a μPIHn plate with Delrin combs. Red prisms were found to nucleate on cross-linked polymers which were derived from 2-vinylpyridine (2VP) and 4-vinylpyridine (4VP). Specifically, red prisms were found consistently on a DVB:2VP:4VP (33:29:71) derived polymer. Yellow prisms formed on cross-linked polymers which were derived from 2-methyl-2-nitropropyl methacrylate (MNPMA). This form was most reliably obtained on cross-linked polymers derived from DVB:MNPMA (33:100). Yellow needles were observed on cross-linked polymers derived from styrene (STY) and 4-acetoxystyrene (AOS), especially on polymers derived from DVB:STY (33:100). Orange needles were present on several cross-linked polymers, particularly on those derived from 2-hydroxyethyl methacrylate (HEMA) and acrylic acid (AA). Cross-linked polymers derived from DVB:HEMA:AA (33:57:43) consistently facilitated the formation of orange needles.

Curcumin. A solution of curcumin was made by dissolving 25 mg of curcumin in 1 mL of dimethyl sulfoxide (DMSO). The solution was then filtered using a 0.45 μm pore size PTFE filter. This solution was then contact printed onto a μPIHn plate with Delrin combs. The plate was then placed in a closed vessel in which a dish of water had been placed. Form I formed on many cross-linked polymers especially those derived from methacrylonitrile (MAN). In particular, cross-linked polymers derived from DVB:MAN:2VP (33:71:29) aided in the nucleation of form I. Form II was found on several cross-linked polymers particularly on those derived from methyl methacrylate (MMA), the form was specifically found on polymers derived from DVB:MMA:MNPMA (33:86:14). Form III nucleated on cross-linked polymers derived from methyl methacrylate (MMA), particularly on polymers derived from DVB:HEMA:MMA (33:43:57).

TA. A solution of TA was prepared by dissolving 7.2 mg of TA in 1 mL of ethanol. The solution was then filtered using a 0.45 μm pore size PTFE filter. The filtered solution was then transferred onto a μPIHn plate by pipetting 0.1μL into each well with an Eppendorf Research Pipette. Form I was found on cross linked polymers derived from methacrylonitrile (MAN), specifically on polymers derived from DVB:MAN:2VP (33:71:29). Form II nucleated on numerous cross-linked polymers especially those derived from 2-methyl-2-nitropropyl methacrylate (MNPMA), in particular on polymers derived from DVB:MNPMA (33:100). Form III formed on cross-linked polymers derived from 4-acetoxystyrene (AOS), especially on polymers derived from DVB:AOS:*t*-BuMa (33:57:43). Form IV nucleated on cross-linked polymers derived from 2-ethoxyethyl methacrylate (EEMA). Particularly, cross-linked polymers derived from DVB:EEMA:MMA (33:86:14) facilitated the formation of form IV. Cross-linked

polymers derived from 2-vinylpyridine (2VP) assisted in the formation of form V, derived from DVB:MNPMA:2VP (33:14:86).

3.4.7 Raman vibrational spectroscopy

Automated Raman mapping was performed using a Renishaw inVia Raman Microscope equipped with a RenCam CCD detector, 785 nm laser, 1200 lines/nm grating, and 65 μm slit. An image of the μPIHn plate was captured by using an automatic Renishaw MS20 encoded stage in combination with the ability to montage an image using the camera. This image was used as a template for the mapping experiment. Using point by point mapping nine points were selected in each depression on the image of the μPIHn plate: three across the top, three across the center, and three at the bottom. These defined positions are the locations in which the spectra were collected during the mapping experiment. Twenty second static scans were used to determine the polymorphic composition of each well. The center for the static scans varied depending on which compound was studied: 2200 cm^{-1} for ROY, 1050 cm^{-1} for ACM, and 1450 cm^{-1} for TA. The spectra obtained by mapping were then analyzed using the Wire 3.4 software package principal component analysis routines. For full characterization of a polymorph on the above system or on the Renishaw inVia Raman Microscope equipped RenCam CCD detector, 633 nm laser, 1800 lines/nm grating, and 50 μm slit, long scans were conducted. Spectra were collected in extended scan mode in the range of 4000-100 cm^{-1} and then analyzed using Wire 3.4 software package. Calibration was performed for all experiments using a silicon standard.

3.4.8 Quantifying the effect of well depth on Raman laser intensity

An experiment was performed with a Delrin aperture (hole diameter of 3.30 mm with a 6.0 mm height) placed above a crystal of the nutraceutical piperine, monitoring the signal intensity as the number of Delrin pieces was increased. In order to compare the signal in each spectrum, the

intensity of the peak at 1624 cm^{-1} was monitored. When one Delrin aperture was used the signal was diminished by 41%; when two were used (effectively mimicking the depth in a 384 microtiter plate) the signal was diminished by 72% as compared to having the same crystal on a planar substrate.

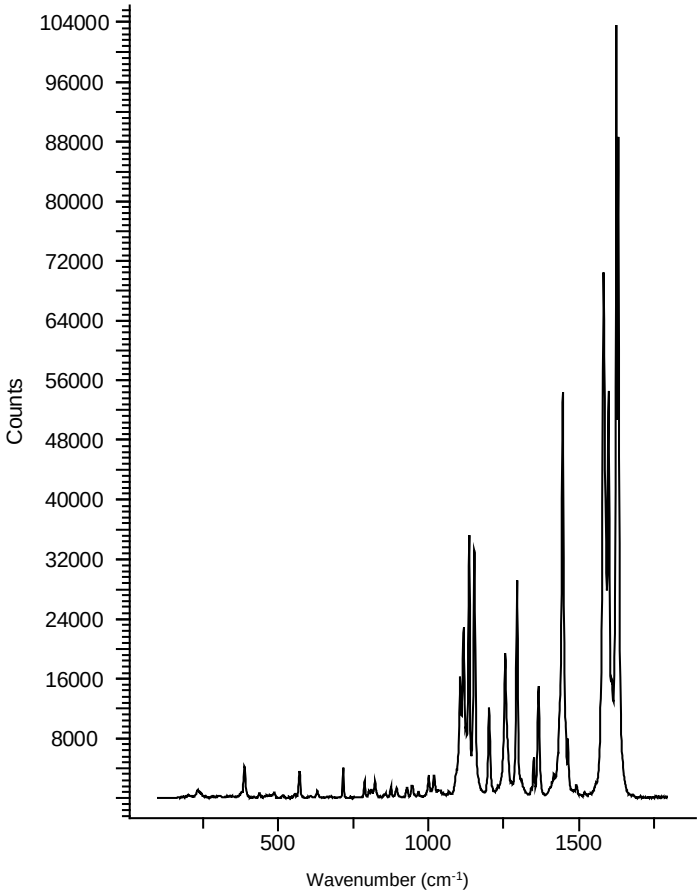

Figure 3.11. Raman spectrum of piperine on a planar substrate.

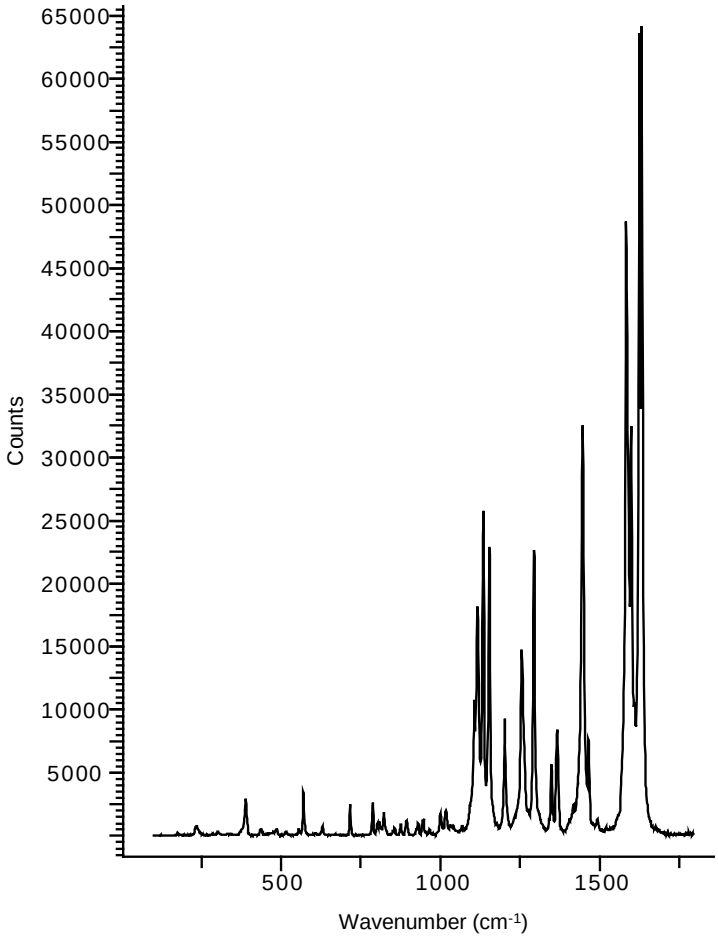

Figure 3.12. Raman spectrum of piperine with one Delrin aperture.

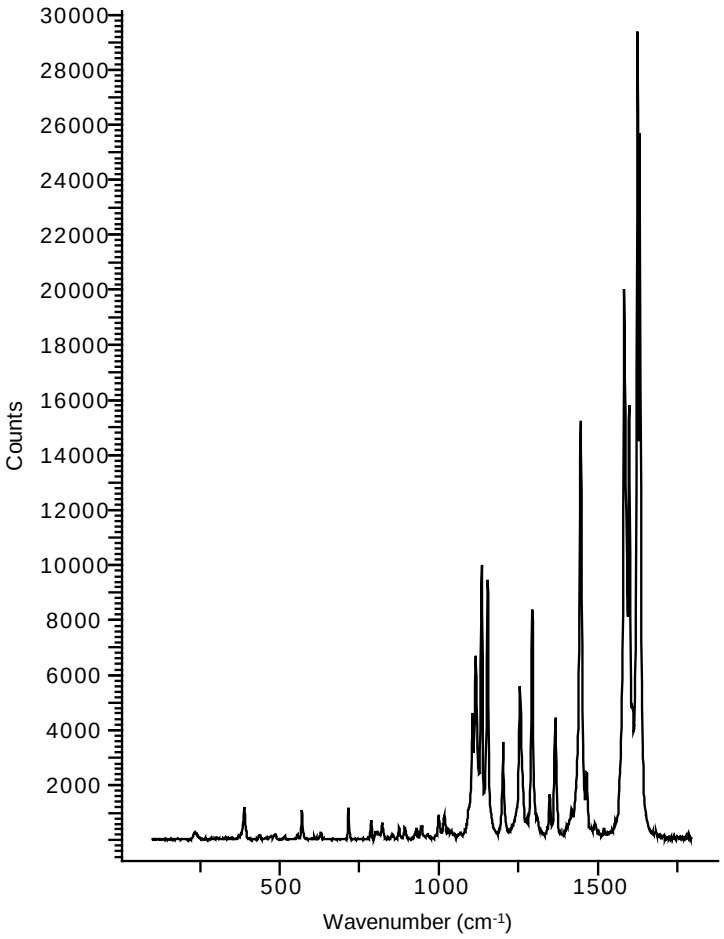

Figure 3.13. Raman spectrum of piperine with two Delrin apertures.

3.5 References

1. Bernstein, J., *Polymorphism in Molecular Crystals*. Oxford University Press: New York, 2002.
2. Davey, R.; Garside, J., *From Molecules to Crystallizers*. Oxford University Press: New York, 2000.
3. Lee, A. Y.; Ulman, A.; Myerson, A. S., Crystallization of amino acids on self-assembled monolayers of rigid thiols on gold. *Langmuir* **2002,** 18, (15), 5886-5898.
4. Kang, J. F.; Zaccaro, J.; Ulman, A.; Myerson, A., Nucleation and growth of glycine crystals on self-assembled monolayers on gold. *Langmuir* **2000,** 16, (8), 3791-3796.
5. Capacci-Daniel, C.; Gaskell, K. J.; Swift, J. A., Nucleation and Growth of Metastable Polymorphs on Siloxane Monolayer Templates. *Cryst. Growth Des.* **2010,** 10, (2), 952-962.
6. Ulman, A.; Kang, J. F.; Shnidman, Y.; Liao, S.; Jordan, R.; Choi, G. Y.; Zaccaro, J.; Myerson, A. S.; Rafailovich, M.; Sokolov, J.; Fleischer, C., Self-assembled monolayers of rigid thiols. *J. biotechnol.* **2000,** 74, (3), 175-88.
7. Mitchell, C. A.; Yu, L.; Ward, M. D., Selective nucleation and discovery of organic polymorphs through epitaxy with single crystal substrates. *J. Am. Chem. Soc.* **2001,** 123, (44), 10830-10839.
8. Munroe, A.; Croker, D.; Hodnett, B. K.; Seaton, C. C., Epitaxial growth of polymorphic systems: The case of sulfathiazole. *Crystengcomm* **2011,** 13, (19), 5903-5907.
9. McKellar, S. C.; Urquhart, A. J.; Lamprou, D. A.; Florence, A. J., Polymer Templating of Supercooled Indomethacin for Polymorph Selection. *ACS Combinatorial Science* **2012,** 14, (3), 155-159.
10. Lee, M. K.; Lee, H.; Kim, I. W.; Lee, J., Novel polymorphic form of adefovir dipivoxil derived from polymer-directed crystallization. *Pharmazie* **2011,** 66, (10), 766-770.
11. Sudha, C.; Nandhini, R.; Srinivasan, K., Polymer-Induced Selective Nucleation of Mono or Ortho Polymorphs of Paracetamol through Swift Cooling of Boiled Aqueous Solution. *Cryst. Growth Des.* **2014,** 14, (2), 705-715.
12. Xu, A. W.; Dong, W. F.; Antonietti, M.; Colfen, H., Polymorph switching of calcium carbonate crystals by polymer-controlled crystallization. *Advanced Functional Materials* **2008,** 18, (8), 1307-1313.
13. Chen, J. H.; Shao, M.; Xiao, K.; He, Z. R.; Li, D. W.; Lokitz, B. S.; Hensley, D. K.; Kilbey, S. M.; Anthony, J. E.; Keum, J. K.; Rondinone, A. J.; Lee, W. Y.; Hong, S. Y.; Bao, Z. A., Conjugated Polymer-Mediated Polymorphism of a High Performance, Small-Molecule Organic Semiconductor with Tuned Intermolecular Interactions, Enhanced Long-Range Order, and Charge Transport. *Chem. Mat.* **2013,** 25, (21), 4378-4386.
14. Price, C. P.; Grzesiak, A. L.; Matzger, A. J., Crystalline polymorph selection and discovery with polymer heteronuclei. *J. Am. Chem. Soc.* **2005,** 127, (15), 5512-5517.
15. Grzesiak, A. L.; Matzger, A. J., Selection and discovery of polymorphs of platinum complexes facilitated by polymer-induced heteronucleation. *Inorg. Chem.* **2007,** 46, (2), 453-457.
16. Lopez-Mejias, V.; Kampf, J. W.; Matzger, A. J., Polymer-Induced Heteronucleation of Tolfenamic Acid: Structural Investigation of a Pentamorph. *J. Am. Chem. Soc.* **2009,** 131, (13), 4554-4555.
17. Lopez-Mejias, V.; Knight, J. L.; Brooks, C. L.; Matzger, A. J., On the Mechanism of Crystalline Polymorph Selection by Polymer Heteronuclei. *Langmuir* **2011,** 27, (12), 7575-7579.

18. McClelland, A. A.; Lopez-Mejias, V.; Matzger, A. J.; Chen, Z., Peering at a Buried Polymer-Crystal Interface: Probing Heterogeneous Nucleation by Sum Frequency Generation Vibrational Spectroscopy. *Langmuir* **2011,** 27, (6), 2162-2165.
19. Lopez-Mejias, V.; Kampf, J. W.; Matzger, A. J., Nonamorphism in Flufenamic Acid and a New Record for a Polymorphic Compound with Solved Structures. *J. Am. Chem. Soc.* **2012,** 134, (24), 9872-9875.
20. Liberski, A. R.; Tizzard, G. J.; Diaz-Mochon, J. J.; Hursthouse, M. B.; Milnes, P.; Bradley, M., Screening for polymorphs on polymer microarrays. *J. Comb. Chem.* **2008,** 10, (1), 24-27.
21. Yu, L. A., Polymorphism in Molecular Solids: An Extraordinary System of Red, Orange, and Yellow Crystals. *Accounts Chem. Res.* **2010,** 43, (9), 1257-1266.
22. Sanphui, P.; Goud, N. R.; Khandavilli, U. B. R.; Bhanoth, S.; Nangia, A., New polymorphs of curcumin. *Chem. Commun.* **2011,** 47, (17), 5013-5015.
23. Leiws, I.; Edwards, H., *Handbook of Raman Spectroscopy* Marcel Dekker, Inc: New York 2001; Vol. 28.
24. Barbulovic-Nad, I.; Lucente, M.; Sun, Y.; Zhang, M. J.; Wheeler, A. R.; Bussmann, M., Bio-microarray fabrication techniques - A review. *Crit. Rev. Biotechnol.* **2006,** 26, (4), 237-259.
25. Hatcher, H.; Planalp, R.; Cho, J.; Tortia, F. M.; Torti, S. V., Curcumin: From ancient medicine to current clinical trials. *Cell. Mol. Life Sci.* **2008,** 65, (11), 1631-1652.
26. Almarsson, O.; Zaworotko, M. J., Crystal Engineering of the Composition of Pharmaceutical Phases. Do Pharmaceutical Co-crystals Represent a New Path to Improved Medicines? *Chem. Commun.* **2004**, (17), 1889-1896.
27. Sun, Y.; Xi, H. M.; Ediger, M. D.; Richert, R.; Yu, L., Diffusion-controlled and "diffusionless" crystal growth near the glass transition temperature: Relation between liquid dynamics and growth kinetics of seven ROY polymorphs. *J. Chem. Phys.* **2009,** 131, (7).
28. Leyva-Perez, A.; Cabrero-Antonino, J. R.; Corma, A., Bifunctional solid catalysts for chemoselective hydrogenation-cyclisation-amination cascade reactions of relevance for the synthesis of pharmaceuticals. *Tetrahedron* **2010,** 66, (41), 8203-8209.

Chapter 4 Controlling Pharmaceutical Crystallization with Designed Polymeric Heteronuclei

Published: Pfund, L. Y.; Price, C. P.; Frick, J. J.; Matzger, A. J., *J. Am. Chem. Soc,* Just Accepted Manuscript **2015**.

4.1 Introduction

There is often a large barrier to the formation of an ordered three-dimensional lattice from an isotropic state. The initial stage of crystallization, nucleation, can be accelerated if a surface is present to facilitate the organization of molecules by heteronucleation.[1] Among the various methods utilized for heteronucleation[2-6], polymer-induced heteronucleation (PIHn) has proven to be a powerful polymorph discovery method utilizing hundreds of unique insoluble polymers as crystallization directors for obtaining novel solid forms.[7-13] It is well established that functional group interactions at the polymer-crystal interface are responsible for directing and controlling the nucleation of different crystal phases on specific polymer heteronucleants.[13-16] However, there are some instances where nucleation from the polymer surface is very slow, allowing alternative pathways to compete. In such cases, it is hypothesized that crystallization is not induced by the polymer heteronucleant because little interaction between the polymer and compound exists; this precludes efficient stabilization of nuclei and subsequent growth into macroscopic crystals. An attractive approach for solving the problem of slow nucleation from polymer heteronucleants is to generate insoluble polymers that are designed to possess complementary interactions for a given compound. To implement this strategy, inspiration was sought from the substantial body of work available on soluble additives. Tailor-made additives are typically designed to adsorb onto specific faces of a growing crystal to slow or block growth

perpendicular to that face, often affecting the morphology and the polymorphism of the target compound.[17-30] If the strong interactions between a tailor-made additive and a target compound could instead be applied at the surface of an insoluble polymer, it is hypothesized that the additive will act as a crystallization promoter. The nucleation rate should be increased because the polymer possesses functionality complementary to that of the target compound in solution thereby facilitating heteronucleation. Furthermore, the morphology of the resulting crystals should not be affected because an insoluble polymer cannot interact with multiple faces of a growing crystal.

4.2 Results and Discussion

Due to the extensive work on the effect of tailor-made additives on the morphology of acetaminophen (ACM) crystals, this compound was used as an initial target in order to determine if polymers could be tailored to accelerate nucleation.[31-33] A *polymerizable* additive, *N*-hydroxyphenyl methacrylamide, was designed and synthesized[34] to mimic ACM (Figure 4.1).[35-38] Whenever designing an inhibitor for a specific compound, the possibility exists that the particular substitution pattern chosen will preclude efficient interaction with the target crystal. Therefore, to verify that *N*-hydroxyphenyl methacrylamide would act *in solution* to modify the morphology of the acetaminophen crystals, crystallizations in the presence of the additive were performed. As the concentration of the tailor-made additive was increased, the acetaminophen crystals became more elongated (Figure 4.2). In spite of this dramatic change in the morphology of the crystals, all were confirmed to be the monoclinic polymorph of acetaminophen by Raman spectroscopy (see Section 4.4.4). Having

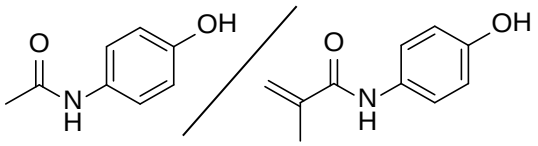

Figure 4.1. Comparison of the structure of acetaminophen to the tailor-made additive, *N*-hydroxyphenyl methacrylamide.

determined that *N*-hydroxyphenyl methacrylamide face-selectively interacts with acetaminophen crystals in solution, the additive was subsequently incorporated into polymers to determine if it possessed the ability to promote crystallization when immobilized. To explore the effect of the concentration of the tailor-made additive present in the polymer heteronucleant on the crystallization rate of the pharmaceutical, binary copolymers were prepared. The requisite properties for the second monomeric component are poor water solubility, a lack of hydrogen-bonding functionality, and a reactivity ratio similar to the additive such that random copolymers would be generated. Thus, three copolymers with styrene and increasing ratios of the tailor-made additive (1 mol%, 5 mol%, and 10 mol% of additive to total polymer) were synthesized in addition to pure polystyrene (see Section 4.4.5). In each case the pure polymer was found to be insoluble in water by UV-vis absorbance spectroscopy implicating a heterogeneous mechanism[39, 40] for influencing crystallization (see Section 4.4.7). Crystallizations of acetaminophen in the presence of the three tailor-made additive copolymers and polystyrene as well as in the absence of polymer were carried out in aqueous solution with each

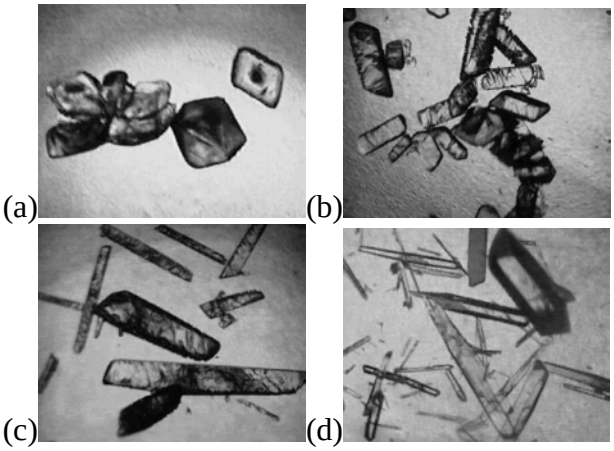

Figure 4.2. Morphology of acetaminophen crystals grown in the presence of *N*-hydroxyphenyl methacrylamide. (a) no additive, (b) 1 mM additive, (c) 3 mM additive, and (d) 6 mM additive.

crystallization condition performed eight times in triplicate (see Section 4.4.6). In order to determine the induction time for crystal appearance the crystallizations were checked by optical microscopy every fifteen minutes. On average, the induction time for crystal appearance of acetaminophen in the absence of the synthesized polymers occurred in >6000 minutes, whereas in the presence of polystyrene this time decreased to 1100 min. These observations are consistent with a decreased induction period resulting from heterogeneous nucleation. More substantial though was the decrease in the induction time for the appearance of crystals in the presence of polymers with incorporated *N*-hydroxyphenyl methacrylamide. On average crystallizations in the presence of the 1, 5, and 10 mol% *N*-hydroxyphenyl methacrylamide/styrene copolymers occurred in 243 ± 7 minutes, 189 ± 10 minutes, and 151 ± 8 minutes, respectively (times are shown with the standard error) (Figure 4.3). These results are consistent with the proposition that a soluble tailor-made additive that modifies morphology in solution acts as a crystallization promoter when incorporated into an insoluble polymer.

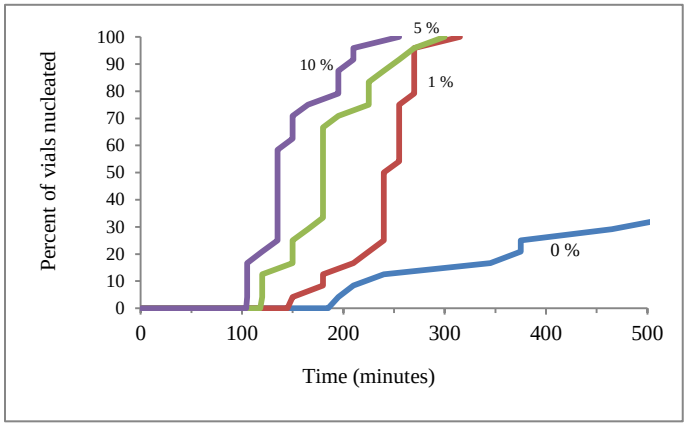

Figure 4.3. Induction time for crystal appearance for acetaminophen crystallized in the presence of N-hydroxyphenyl methacrylamide/styrene copolymers. The percentages indicated next to each line represent the molar percent of the tailor-made additive in the polymer.

If the strategy of immobilizing a tailor-made additive in a polymer to create a crystallization promoter is generally applicable, then other acetaminophen mimics should yield similar results. To explore this hypothesis, another tailor-made additive, *p*-acetamidostyrene, was synthesized.[34] This tailor-made additive possesses similar amide functionality to that of acetaminophen but also

bears a vinyl group for integration into a polymer. Acetaminophen was initially crystallized with *p*-acetamidostyrene in solution to determine if the additive could affect the morphology of the resulting crystals. Crystals of the monoclinic form of acetaminophen became increasingly elongated as the concentration of the additive was raised from 1 mM to 6 mM (see Section 4.4.3). With successful demonstration of face-selective growth inhibition, *p*-acetamidostyrene was subsequently incorporated into polymers to yield three copolymers with increasing ratios of the tailor-made additive to styrene (1 mol%, 5 mol%, and 10 mol% of tailor-made additive relative to the total polymer). The crystallizations were conducted and monitored in the same manner as the *N*-hydroxyphenyl methacrylamide/styrene copolymer system described above. The induction time for crystal appearance was significantly decreased in the presence of the *p*-acetamidostyrene/styrene copolymers. For crystallizations in the presence of the 10 mol% *p*-acetamidostyrene/styrene copolymer, crystals appear on average within an hour, one hundredth of the time needed for crystallization to occur in the absence of polymer (Figure 4.4). Despite this drastic change in the induction time for the appearance of crystals, the morphology of the ACM crystals

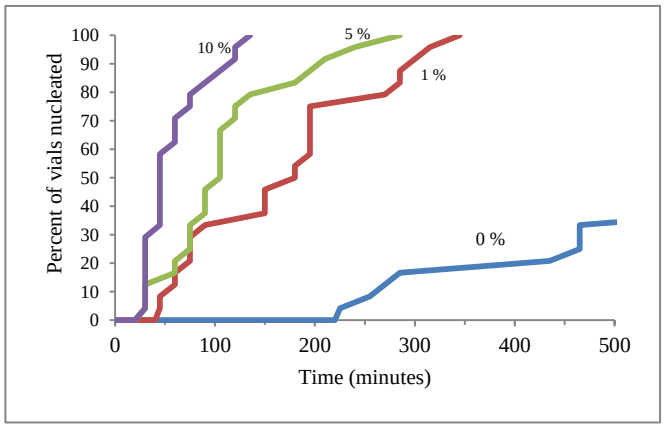

Figure 4.4. Induction time for crystal appearance for acetaminophen crystallized in the presence of p-acetamidostyrene/styrene copolymers. The percentages indicated next to each line represent the molar percent of the tailor-made additive in the polymer.

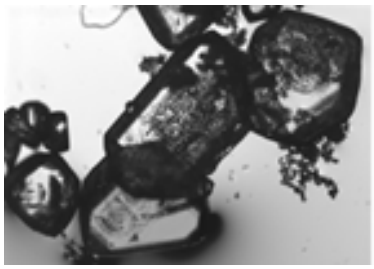

Figure 4.5. Morphology of acetaminophen crystals grown in the presence of 10 mol% *p*-acetamidostyrene/styrene.

was not affected by the presence of the tailor-made copolymers (Figure 4.5). This trend of decreasing induction times can be attributed to an increase in the incorporation of the tailor-made monomer in the copolymers, leading to more efficient organization of molecules on the polymer surface and thus faster heteronucleation.

In order to expand the capabilities of this method to crystallizations in organic solvents and eliminate any issues due to polymer solubility, cross-linked tailor-made polymers were also explored as crystallization promoters. The anti-inflammatory compound mefenamic acid was utilized as an initial target compound. A tailor-made additive: 2-((4-vinylphenyl)amino)benzoic acid was synthesized, which is structurally similar to mefenamic acid but bears a vinyl group to enable polymerization (Figure 4.6, see Section 4.4.8).[41] Mefenamic acid was initially crystallized with 2-((4-vinylphenyl)amino)benzoic acid in solution to determine if the additive would affect the morphology of the resulting crystals (1, 5, and 10 mol% relative to the total amount of mefenamic acid). As the concentration of the tailor-made additive was increased, the mefenamic acid crystals became increasingly elongated and the induction time for crystal appearance was significantly increased (see Section 4.4.9). However, with the highest amount of the tailor-made additive the crystal growth was inhibited so strongly that the crystals, although still blade-like, lacked a distinct morphology. Despite this drastic change in the morphology, all of the crystals were confirmed to be form I of mefenamic acid by Raman spectroscopy (see Section 4.4.9). Having determined that 2-((4-vinylphenyl)amino)benzoic acid face-selectively interacts with mefenamic acid crystals in solution, the tailor-made additive was copolymerized with

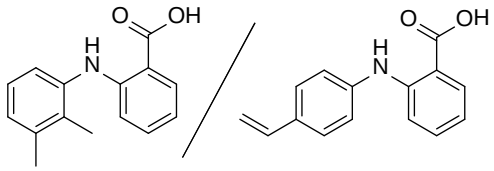

Figure 4.6. Comparison of the structure of mefenamic acid to the tailor-made additive: 2-((4-vinylphenyl)amino)benzoic acid.

divinylbenzene (DVB), in increasing molar ratios, to create cross-linked copolymers (see Section 4.4.10). Similar to the acetaminophen studies each crystallization condition was performed eight times in triplicate. In order to determine the induction time for crystal appearance, the crystallizations were monitored by time-lapse photography (photos were taken every sixty seconds). The induction time for the appearance of crystals was considerably decreased for crystallizations in the presence of the 2-((4-vinylphenyl)amino)benzoic acid/DVB copolymers, and the copolymer with the highest incorporation of the tailor-made additive yielded a ten-fold decrease in induction time for crystal appearance (see Section 4.4.11).

Although the molecular-level events leading to the induction of crystal growth from polymer surfaces cannot be directly observed, rate acceleration can arise either from the polymer stabilizing subcritically sized nuclei of the target compound in solution or through organization of molecules on the polymer surface leading to aggregates of critical dimensions. In either case, it is hypothesized that the face-selectivity of crystal growth results from preferential interaction with the surface of pre-nuclear aggregates mediated by intermolecular interactions between the polymer and the forming nucleus.[14, 15] In order to determine if there was any preferential interaction between the functionality on the tailor-made copolymer surface and the mefenamic acid molecules in solution, mefenamic acid was crystallized on polymer films comprised of the 10 mol% 2-((4-vinylphenyl)amino)benzoic acid/divinylbenzene copolymer. Powder X-ray diffraction (PXRD) analysis of the crystals present on the tailor-made copolymer films revealed that there are two reflections at 6.3° (100) and 12.7° (200); these correspond to mefenamic acid form I crystals oriented along {100} (see Section 4.4.12). In form I, carboxylic acid groups are oriented perpendicular to the (100) face,[42] suggesting that the tailor-made copolymer is preferentially interacting with these groups through hydrogen bonding.[14, 15] An intriguing

question that can test the proposed mechanism of interaction is if adsorption occurs in the same orientation when an additive is in solution as when it is anchored to a polymer. In order to test this, mefenamic acid crystals grown in the presence of 2-((4-vinylphenyl)amino)benzoic acid in solution were indexed. It was found that the additive in solution was in fact adsorbing onto the (100) face, showing that the mechanism of interaction is not changed when the additive is incorporated into a polymer (see Section 4.4.13).

4.3 Conclusion

The studies outlined here demonstrate that tailor-made additives, which alter crystal morphology in solution, can be incorporated into insoluble polymers to promote crystallization. This approach has the potential to impact a problem of considerable importance in the pharmaceutical industry: the emergence of compounds which, for purely kinetic reasons, under all growth conditions are resistant to crystallization.[43] This can severely complicate purification and form identification. In these cases, tailoring substrates to decrease the time needed for crystals to appear is an attractive approach for creating appropriate seed crystals; studies examining this approach are currently underway.

4.4 Experimental

4.4.1 Materials

Acetaminophen (ACM) was obtained from Sigma-Aldrich (MO). Mefenamic acid was obtained from Alfa Aesar (MA). The tailor-made additive *p*-acetamidostyrene was synthesized by the known literature procedure.[34] *N*-hydroxyphenyl methacrylamide was synthesized by the literature procedure.[44] 2-((4-vinylphenyl)amino)benzoic acid was synthesized by a procedure similar to that described by Wolf and coworkers (see Section 4.4.8).[41]

4.4.2 Raman Spectroscopy

For acetaminophen Raman spectra were obtained using a Renishaw inVia Raman microscope equipped with a RenCam CCD detector, 785 nm diode laser, a 1200 lines/mm grating, and 50 μm slit. Spectra were collected and analyzed using the Wire 2.0 software package. Spectra were collected in extended scan mode with a range of 100-3200 cm^{-1}. For mefenamic acid a Renishaw inVia Raman Microscope equipped with a RenCam CCD detector, 633 nm laser, 1800 lines/mm grating, and 50 μm slit was utilized for collecting data. Spectra were collected in extended scan mode in the range of 100-3500 cm^{-1} and then analyzed using the Wire 3.4 software package. Calibration was performed using a silicon standard for all experiments.

4.4.3 Crystallization of acetaminophen in the presence of the additives

The additive (*p*-acetamidostyrene or *N*-hydroxyphenyl methacrylamide) was dissolved in a 200 mM aqueous acetaminophen solution at 70 °C in a 20 mL glass vial. Three solutions with different concentrations of additive, 1 mM, 3 mM, and 6 mM, were prepared in addition to a control: a 200 mM aqueous acetaminophen solution.

Figure 4.7. Morphology of acetaminophen crystals grown in the presence of *p*-acetamidostyrene. Clockwise from top left: no additive, 1 mM additive, 3 mM additive, and 6 mM additive.

4.4.4 Raman spectra of acetaminophen crystallized in the presence of the additives

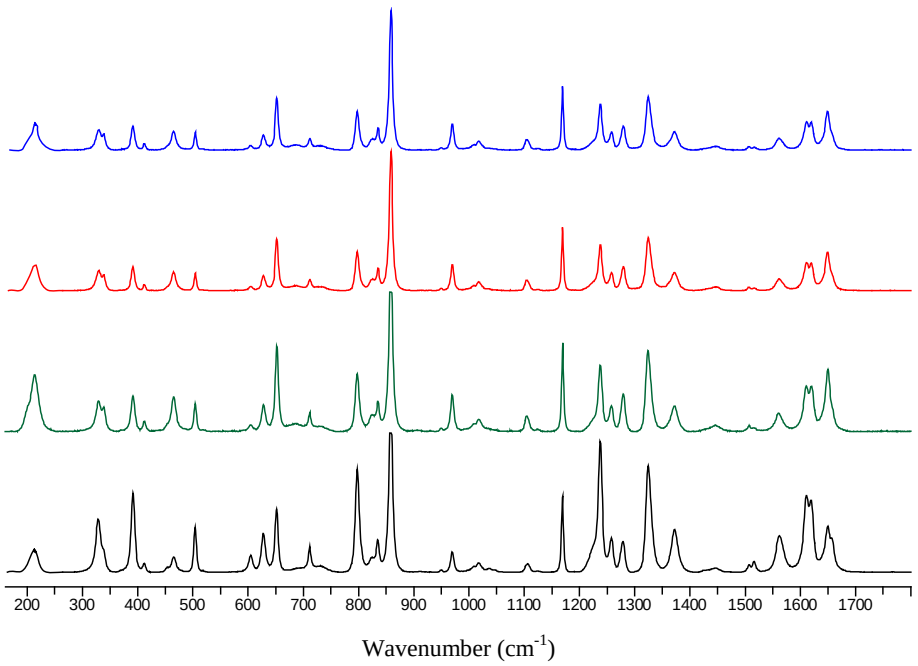

Figure 4.8. Raman spectra of acetaminophen crystals obtained from crystallizations in the presence of no additive, 1 mol% *N*-hydroxyphenyl methacrylamide, 5 mol% *N*-hydroxyphenyl methacrylamide, and 10 mol% *N*-hydroxyphenyl methacrylamide (from the bottom to the top spectrum).

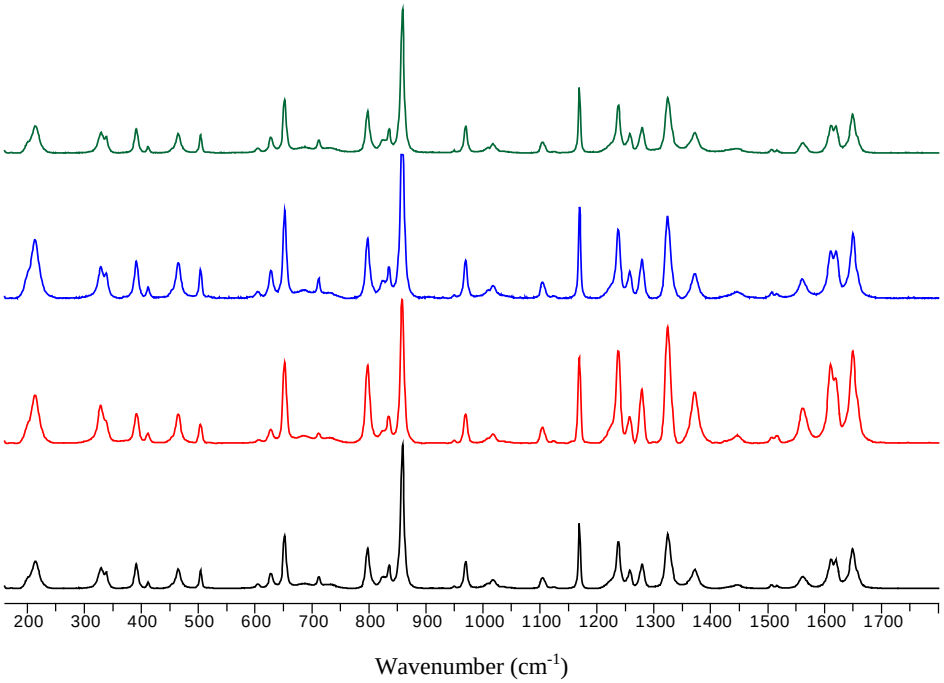

Figure 4.9. Raman spectra of acetaminophen crystals obtained from crystallizations in the presence of no additive, 1 mol% *p*-acetamidostyrene, 5 mol% *p*-acetamidostyrene, and 10 mol% *p*-acetamidostyrene (from the bottom to the top spectrum).

4.4.5 Polymerization of *p*-acetamidostyrene/styrene and *N*-hydroxyphenyl methacrylamide/styrene

Copolymers of *p*-acetamidostyrene/styrene and *N*-hydroxyphenyl methacrylamide/styrene with 1 mol%, 5 mol%, and 10 mol% of additive relative to total polymer as well as pure polystyrene were synthesized by free radical polymerization. In all cases 1 mol% of 2,2′-Azobis(2-methylpropionitrile) (AIBN) with respect to monomer was used as the initiator. Solutions of monomer and initiator dissolved in acetone (2:1 v/v acetone to monomer) were heated in glass vials under a nitrogen atmosphere for 24 hours at 75 °C to induce polymerization. Afterwards the polymers were fractionally precipitated once from CH_2Cl_2 with methanol. The polymer was then ground with a mortar and pestle. This yielded 185 mg of the 1 mol% *p*-acetamidostyrene/styrene copolymer as a white powder. GPC: M_n = 45,410, M_w = 73,546. FT-IR (KBr): 3419 (w), 3024 (m), 2921 (m), 1699 (w), 1600 (m), 1514 (w), 1492 (s), 1452 (s), 756 (s), 696 (vs) cm^{-1}. This reaction with 5 mol% *p*-acetamidostyrene relative to the total monomer used yielded 202 mg of the 5 mol% *p*-acetamidostyrene/styrene copolymer as a white powder. GPC: M_n = 31,882, M_w = 146,111. FT-IR (KBr): 3406 (w), 3024 (m), 2920 (m), 1695 (m), 1600 (m), 1514 (m), 1492 (s), 1451 (s), 756 (s), 696 (vs) cm^{-1}. This reaction with 10 mol% *p*-acetamidostyrene relative to the total monomer used yielded 168 mg of the 10 mol% *p*-acetamidostyrene/styrene copolymer as a white powder. GPC: M_n = 14,982, M_w = 35,187. FT-IR (KBr): 3426 (w), 3023 (m), 2920 (m), 1652 (w), 1600 (m), 1512 (m), 1492 (s), 1451 (s), 756 (s), 697 (vs) cm^{-1}. This reaction with 1 mol% *N*-hydroxyphenyl methacrylamide relative to the total monomer utilized yielded 197 mg of the 1 mol% *N*-hydroxyphenyl methacrylamide/styrene copolymer as a white powder. GPC: M_n = 26,725, M_w = 74,412. FT-IR (KBr): 3447 (w), 3024 (m), 2921 (m), 1600 (m), 1511 (w), 1492 (s), 1451 (s), 756 (s), 696 cm^{-1}. This reaction with 5 mol% *N*-hydroxyphenyl

methacrylamide relative to the total monomer utilized yielded 178 mg of the 5 mol% *N*-hydroxyphenyl methacrylamide/styrene copolymer as a white powder. GPC: M_n = 16,271, M_w = 67,001. FT-IR (KBr): 3435 (w), 3024 (m), 2921 (m), 1652 (w), 1600 (m), 1512 (m), 1492 (s), 1452 (s), 756 (s), 696 (vs) cm^{-1}.This reaction with 10 mol% *N*-hydroxyphenyl methacrylamide relative to the total monomer utilized yielded 151 mg of the 10 mol% *N*-hydroxyphenyl methacrylamide/styrene copolymer as a white powder. GPC: M_n = 17,474, M_w = 110,897. FT-IR (KBr): 3431 (w), 3024 (m), 2921 (m), 1652 (w), 1600 (m), 1512 (m), 1492 (s), 1451 (s), 756 (s), 697 (vs) cm^{-1}. This reaction with styrene yielded 214 mg of polystyrene as a white powder. GPC: M_n = 32,698, M_w = 67,297. FT-IR (KBr): 3024 (m), 2921 (m), 1600 (m), 1492 (s), 1451 (s), 756 (s), 696 (vs) cm^{-1}.

4.4.6 Crystallization of acetaminophen in the presence of additive-containing polymers

Acetaminophen was dissolved in water at 70 °C to produce a 200 mM solution which was subsequently added to the wells of a polypropylene plate containing the ground polymers. The plate was sealed with a Costar 3080 mat and heated for 30 min at 70 °C. The sealed polypropylene plate was removed from the heat source and all crystallizations were monitored by checking each well by optical microscopy every fifteen minutes. Three trials consisting of eight crystallizations in the presence of each type of polymer (1 mol% *p*-acetamidostyrene/styrene copolymer, 5 mol% *p*-acetamidostyrene/styrene copolymer, 10 mol% *p*-acetamidostyrene/styrene copolymer, 1 mol% *N*-hydroxyphenyl methacrylamide/styrene copolymer, the 5 mol% *N*-hydroxyphenyl methacrylamide/styrene copolymer, the 10 mol% *N*-hydroxyphenyl methacrylamide/styrene copolymer, and polystyrene) were performed as well as in the absence of the polymers. The induction time for crystallization was determined to be the moment a crystal appeared in the well.

4.4.7 Solubility of *p*-Acetamidostyrene/styrene copolymers, *N*-hydroxyphenyl methacrylamide/styrene copolymers, and polystyrene in water

p-Acetamidostyrene/styrene copolymers, *N*-hydroxyphenyl methacrylamide/styrene copolymers, and polystyrene were added to separate 4 mL vials, ~3 mg of each polymer, along with 3 mL of water and sealed. These vials were heated at 70 °C for 30 min and cooled to room temperature. The resulting aqueous solutions were filtered and the UV-vis absorbance spectrum of the each was measured. No absorbance was observed from any of the solutions above 220 nm.

4.4.8 Synthesis of 2-((4-vinylphenyl)amino)benzoic acid

The procedure used to synthesize 2-((4-vinylphenyl)amino)benzoic acid was similar to that described by Wolf and coworkers.[41] Specifically, a mixture of 4-aminostyrene (9.3 mmol), 2-bromobenzoic acid (8.8 mmol), K_2CO_3 (13.2 mmol), Cu powder (0.2-0.3 μm, 0.8 mmol), Cu_2O (<5 μm, 0.4 mmol), and 3 mL of 2-ethoxyethanol was refluxed at 130 °C for 24 hours under nitrogen. The cooled reaction mixture was poured into 30 mL of water to which decolorizing charcoal was added. The mixture was then filtered to remove the charcoal. The crude product was obtained by precipitation upon acidification of the filtrate with 1M HCl. The residue was dissolved in dichloromethane and then purified by column chromatography using a solvent system of 20:1 dichloromethane to ethyl acetate with 0.5 % acetic acid by volume. The resulting yellow needle-like crystals were obtained in 60% yield. mp= 225 °C ^{1}H NMR (500 MHz, DMSO-d_6, ppm): δ 13.10 (*s*, 1H), 9.68 (*s*, 1H), 7.91 (*dd*, J = 1.6 Hz, J = 8.0 Hz, 1H), 7.45 (*dt*, J_d = 8.4 Hz, J_t = 2.1 Hz, 2H), 7.41 (*ddd*, J = 1.7 Hz, J = 7.1 Hz, J = 8.6 Hz, 1H), 7.27 (*dd*, J = 0.8, J = 8.5, 1H), 7.22 (*dt*, J_d = 8.5 Hz, J_t =2.3 Hz, 2H), 6.80 (*ddd*, J = 1.1 Hz, J = 7.1 Hz, J = 8.0 Hz, 1H), 6.70 (*dd*, J = 10.9 Hz, J = 17.6 Hz, 1H), 5.73 (*dd*, J = 1.0 Hz, J = 17.6 Hz, 1H), 5.17 (*dd*, J = 1.0 Hz, J = 10.9 Hz, 1H); ^{13}C NMR (125 MHz, DMSO-d_6, ppm): δ 169.9, 146.4, 140.3, 136.1,

134.1, 131.9, 131.7, 127.2, 120.8, 117.4, 114.2, 113.1, and 112.5; HRMS (EI) (*m*/*z*) calcd (found) for $C_{15}H_{13}NO_2$: 239.0946 (239.0948).

4.4.9 Crystallization of mefenamic acid in the presence of 2-((4-vinylphenyl)amino)benzoic acid

The additive, 2-((4-vinylphenyl)amino)benzoic acid, was dissolved in a 8.1 mg/mL ethanol solution of mefenamic acid at 65 °C in 4 mL vials. Three trials consisting of eight crystallizations with different concentrations of the additive, 1 mol%, 5 mol%, and 10 mol% (relative to the total amount of mefenamic acid), were prepared in addition to a control: a 8.1 mg/mL ethanol solution of mefenamic acid.

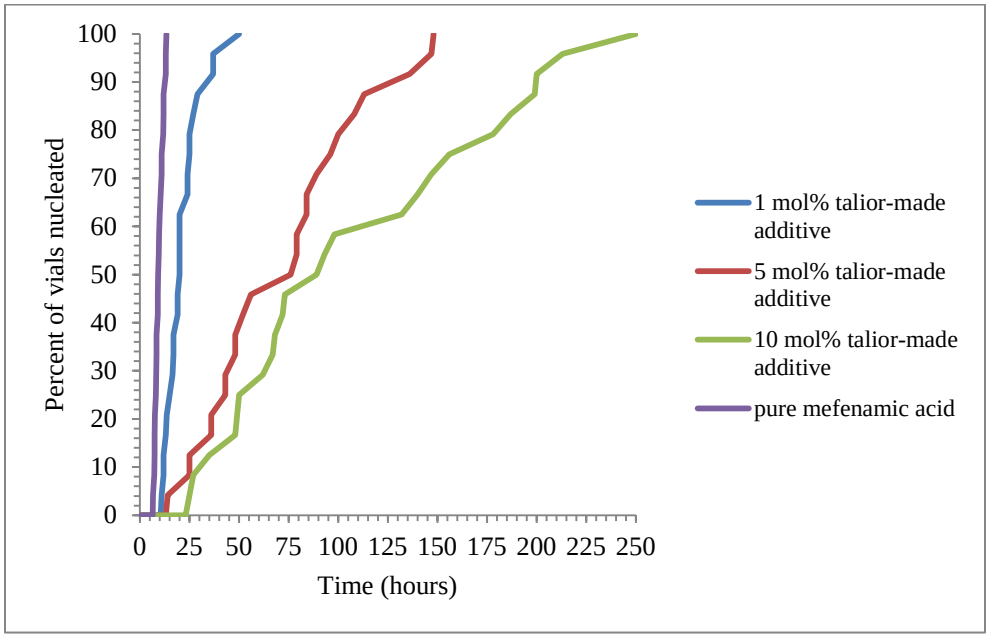

Figure 4.10. Induction time for crystal appearance for mefenamic acid crystallized in the presence of 2-((4-vinylphenyl)amino)benzoic acid in solution.

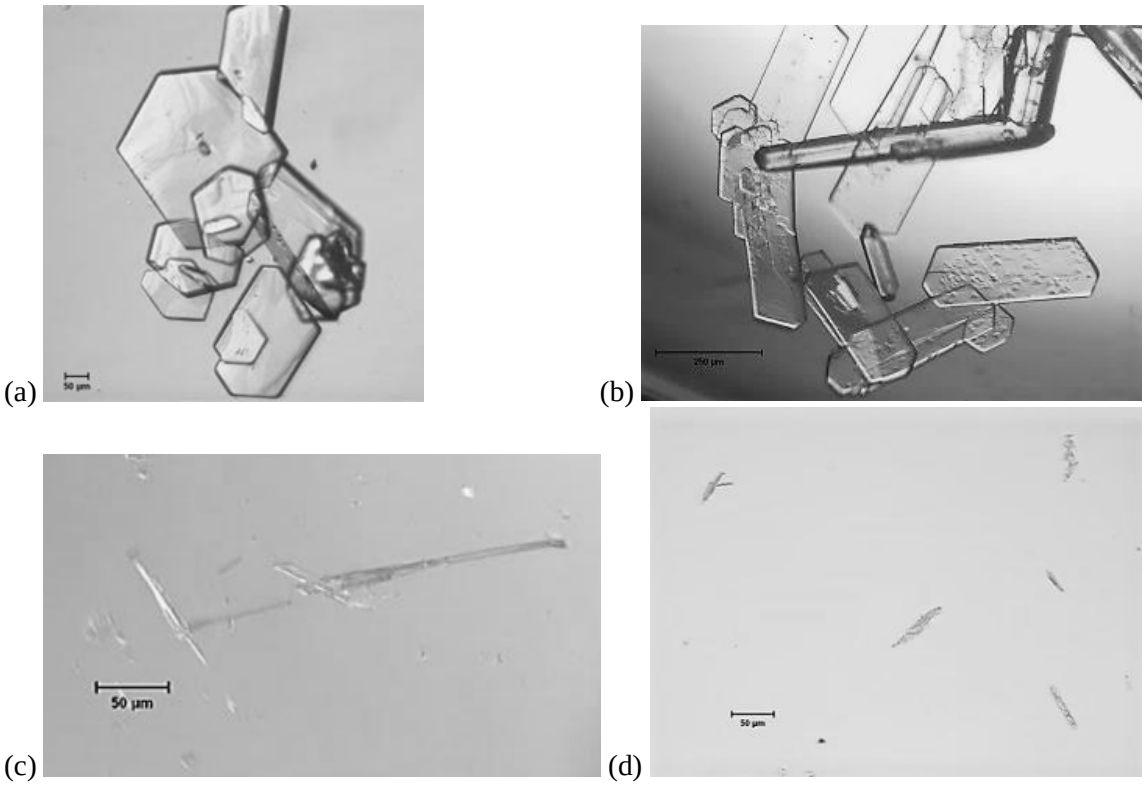

Figure 4.11. Morphology of mefenamic acid crystals grown in the presence of 2-((4-vinylphenyl)amino)benzoic acid. (a) no additive, (b) 1 mol% additive, (c) 5 mol% additive, and (d) 10 mol% additive.

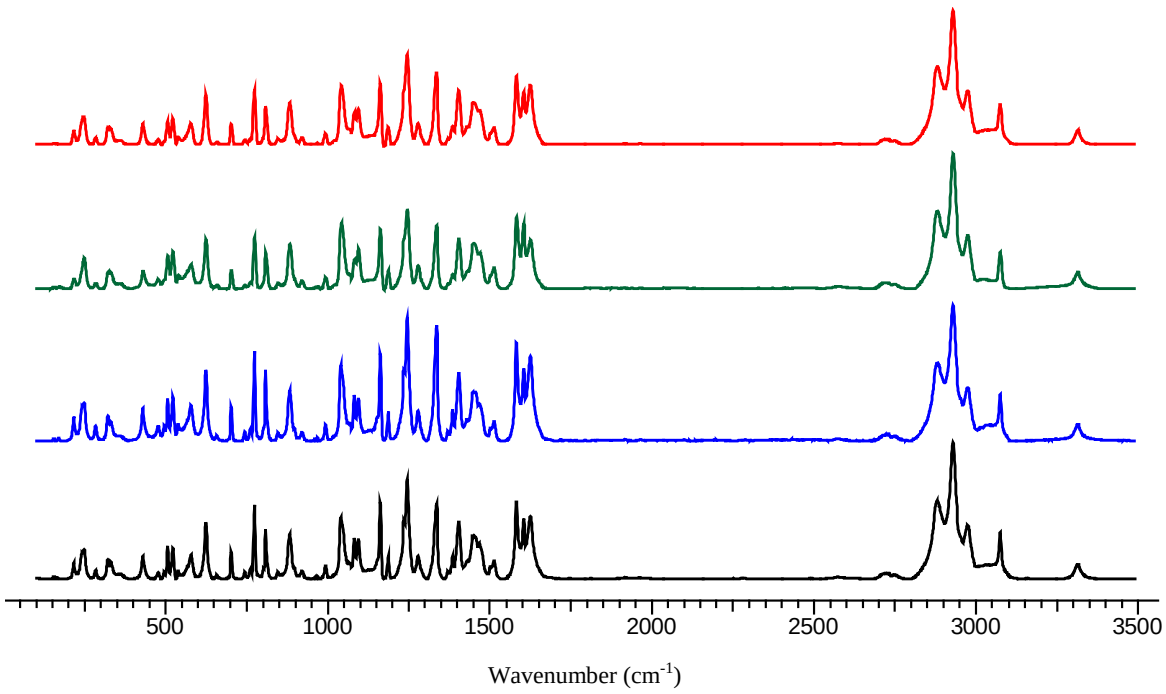

Figure 4.12. Raman spectra of mefenamic acid crystals obtained from crystallizations in the presence of no additive, 1 mol% additive, 5 mol% additive, and 10 mol% additive (from the bottom to the top spectrum).

4.4.10 Polymerization of 2-((4-vinylphenyl)amino)benzoic acid/divinylbenzene and divinylbenzene

Copolymers of 2-((4-vinylphenyl)amino)benzoic acid/divinylbenzene (DVB) with 1 mol%, 5 mol% and 10 mol% of additive to total polymer as well as pure divinylbenzene were synthesized. In all cases 2 mol% of 2,2′-Azobis(2-methylpropionitrile) (AIBN), with respect to the amount of divinylbenzene utilized, was used as the initiator. Solutions of monomer and initiator dissolved in ethanol (1:1 v/v ethanol to monomer) were heated in glass vials under a nitrogen atmosphere for 12 hours at 75 °C to induce polymerization. After polymerization was complete, each of the polymers was ground with a mortar and pestle into a fine powder (~ 1 µm as measured by optical microscopy). The ground polymers were sonicated in hot ethanol, then in hot acetone, and washed several times with hot ethanol and hot acetone. The polymers were then dried in a vacuum oven at 85 °C for two hours. Additionally, copolymer films comprised of 10

mol% 2-((4-vinylphenyl)amino)benzoic acid/divinylbenzene were synthesized by dip coating glass slides into a 10 mol% 2-((4-vinylphenyl)amino)benzoic acid/divinylbenzene monomer solution with 2 mol% of AIBN relative to the amount of DVB. The monomer coated slides were then photopolymerized with four 15 W UVA blubs in an N_2 atmosphere, to yield thin polymer films. The polymer films were then washed with ethanol and acetone. The polymer coated slides were then placed in a vacuum oven at 85 °C for two hours.

4.4.11 Crystallization of mefenamic acid in the presence of 2-((4-vinylphenyl)amino)benzoic acid/divinylbenzene copolymers and divinylbenzene

Solutions of mefenamic acid (8.1 mg/mL) in ethanol were heated at 65 °C for ten minutes in the presence of 1 mg of the 1 mol%, 5 mol%, 10 mol% 2-((4-vinylphenyl)amino)benzoic acid/divinylbenzene copolymers, and divinylbenzene. Three trials consisting of eight crystallizations in the presence of each polymer type were performed as well as a control: a 8.1 mg/mL ethanol solution of mefenamic acid. The crystallizations were monitored by time-lapse photography (photos were taken every 60 seconds) with a Canon EOS Rebel SL1 camera with a EF-S 18-55mm f/3.5-5.6 IS STM lens controlled by DSLR Remote Pro for Windows. The induction period for the appearance of crystals was determined by the first moment that a crystal appeared in the vial. The smallest crystal size that was observed using the camera was ~10 μm. In order to determine how the additive copolymer was interacting with the mefenamic acid molecules in solution, mefenamic acid was also crystallized in the presence of 10 mol% 2-((4-vinylphenyl)amino)benzoic acid/divinylbenzene copolymer films. A solution of mefenamic acid was prepared by dissolving 1 mg of mefenamic acid in 1 mL of ethanol. The solution was dispensed onto ten distinct 10 mol% 2-((4-vinylphenyl)amino)benzoic acid/divinylbenzene copolymer films and allowed to evaporate. The resulting crystals were analyzed by powder X-ray diffraction.

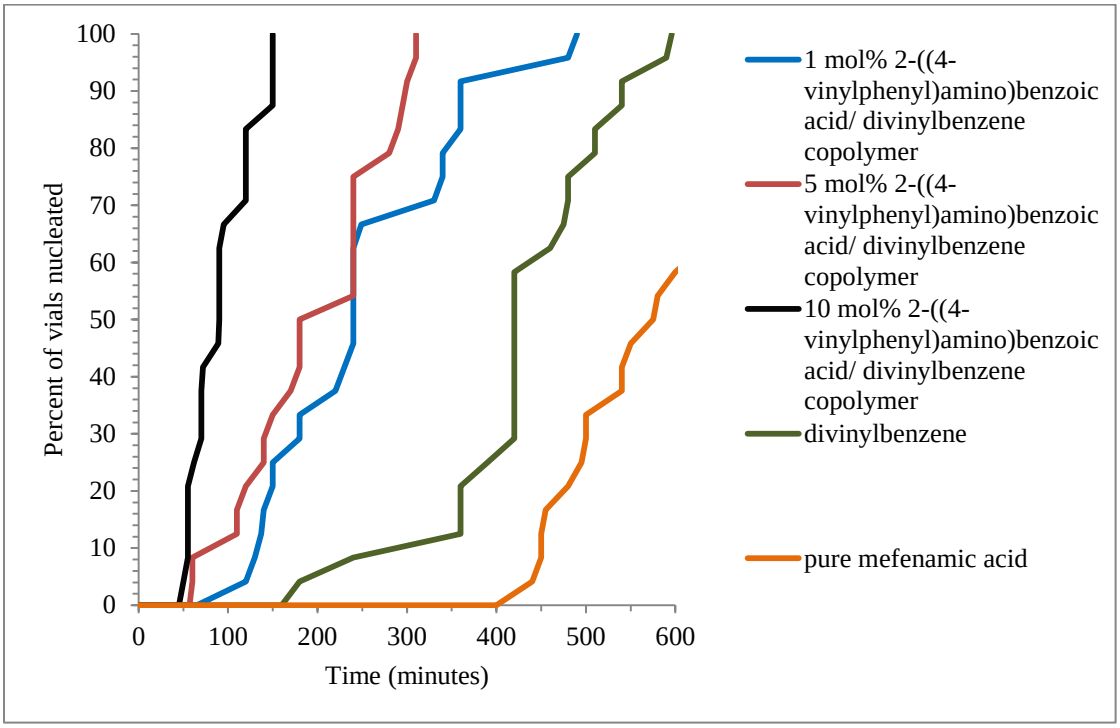

Figure 4.13. Induction time for crystal appearance for mefenamic acid crystallized in the presence of the 2-((4-vinylphenyl)amino)benzoic acid/divinylbenzene copolymers and divinylbenzene.

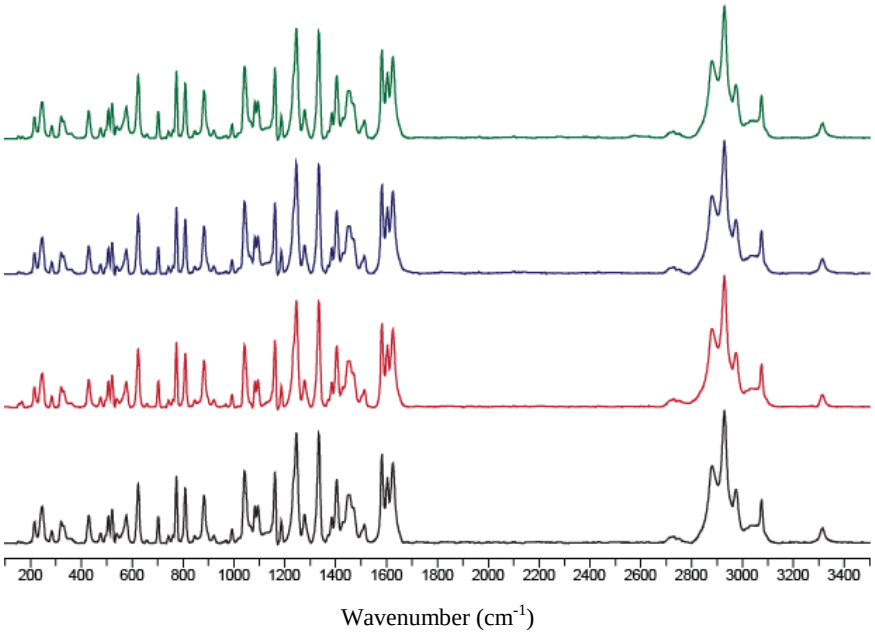

Figure 4.14. Raman spectra of mefenamic acid crystals obtained from crystallizations in the presence of no polymer, 1 mol% 2-((4-vinylphenyl)amino)benzoic acid/divinylbenzene copolymer, 5 mol% 2-((4-vinylphenyl)amino)benzoic acid/divinylbenzene, and 10 mol% 2-((4-vinylphenyl)amino)benzoic acid/divinylbenzene (from the bottom to the top spectrum).

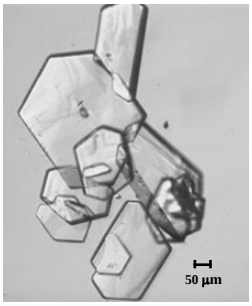

pure mefenamic

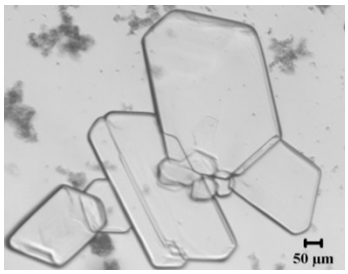

1 mol% tailor-made additive copolymerized with DVB

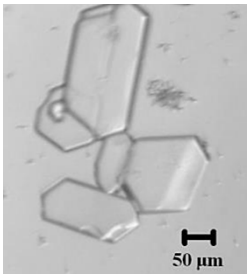

5 mol% tailor-made additive copolymerized with DVB

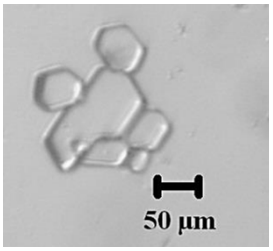

10 mol% tailor-made additive copolymerized with DVB

Figure 4.15. Morphology of mefenamic acid crystals obtained in the presence of the tailor-made additive copolymers.

4.4.12 Powder X-Ray Diffraction (PXRD)

Powder X-ray diffraction was conducted at room temperature using a Bruker D8 Advance diffractometer operating at 40 kV and 40 mA with Cu-Kα radiation (1.5406 Å). The powder patterns were collected by scanning from 5° to 45° in 2θ using a step size of 0.02° and time of 1.5 seconds/step. Powder patterns were processed using Jade Plus v9.5. The crystals on copolymer films were preferentially oriented along the (100) face.

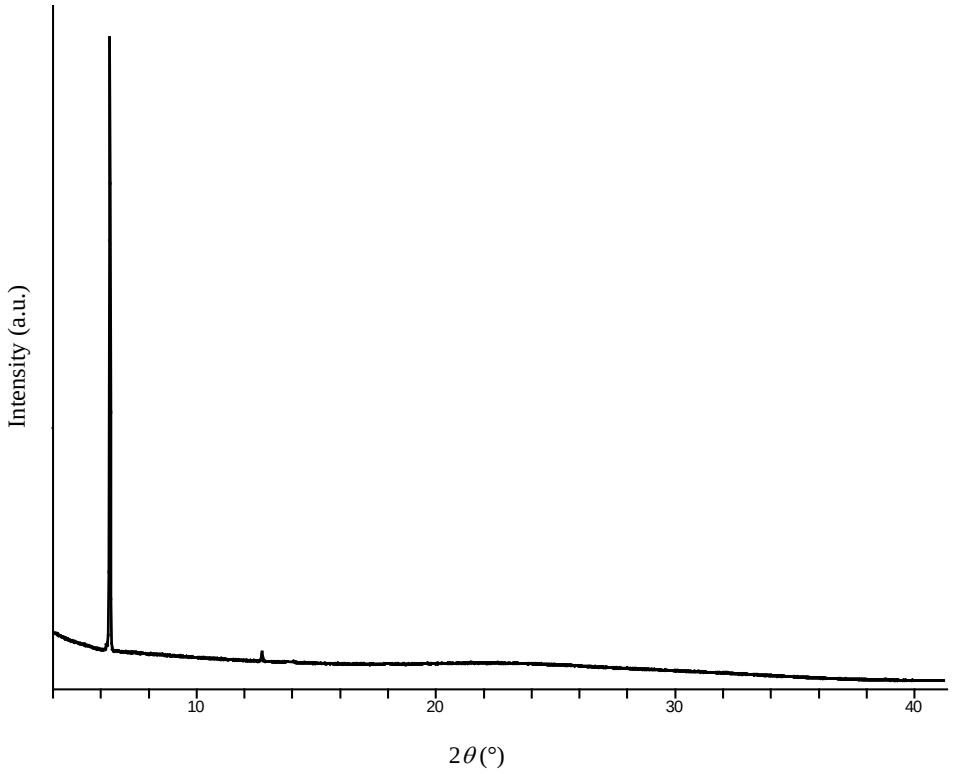

Figure 4.16. Representative PXRD pattern of mefenamic acid crystallized on a 10 mol% 2-((4-vinylphenyl) amino)benzoic acid/divinylbenzene copolymer film.

4.4.13 Indexing mefenamic acid crystals formed in the presence of 2-((4 vinylphenyl)amino)benzoic acid and pure mefenamic acid

Pure mefenamic acid and mefenamic acid crystals grown in the presence of 2-((4-vinylphenyl)amino)benzoic acid were indexed (Figures 4.17, 4.18) using a Rigaku R-Axis Spider diffractometer with an image plate area detector using graphite monochromated Cu-Kα radiation (λ = 1.54187 Å) operated at 2.0 kW power (40 kV, 44 mA). Both types of crystals were mounted on MiTeGen MicroMounts™, indexed, and then axial images were acquired. It was found that the tailor-made additive was in fact adsorbing onto the (100) face.

(a)  (b) 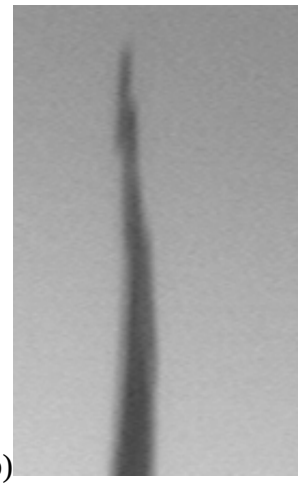

Figure 4.17. (a) View along the a axis of blade-like crystal of mefenamic acid (additive present). (b) View along the c axis of blade-like mefenamic acid crystal.

(a)  (b) 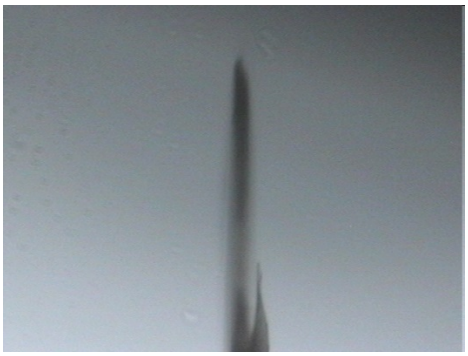

Figure 4.18. (a) View along the a axis of native mefenamic acid crystal. (b) View along the c axis of native mefenamic acid crystal.

4.4.14 Examining the effect of unground polymer on the induction time for crystal appearance

A copolymer of 10 mol% 2-((4-vinylphenyl)amino)benzoic acid/divinylbenzene was synthesized and purified identical to the procedure described in section 4.4.10. However, the polymer was not ground into a fine powder but rather left in large pieces (~ 1 mm) in order to determine how the size of the polymer heteronucleant affected the induction time for crystal appearance. The crystallizations were performed identically to those described in section 4.4.11. The induction time for crystallizations in the presence of the unground 10 mol% 2-((4-vinylphenyl)amino)benzoic acid/divinylbenzene copolymer was found to be roughly between

that of the ground 10 mol% 2-((4-vinylphenyl)amino)benzoic acid/divinylbenzene copolymer and 5 mol% 2-((4-vinylphenyl)amino)benzoic acid/divinylbenzene.

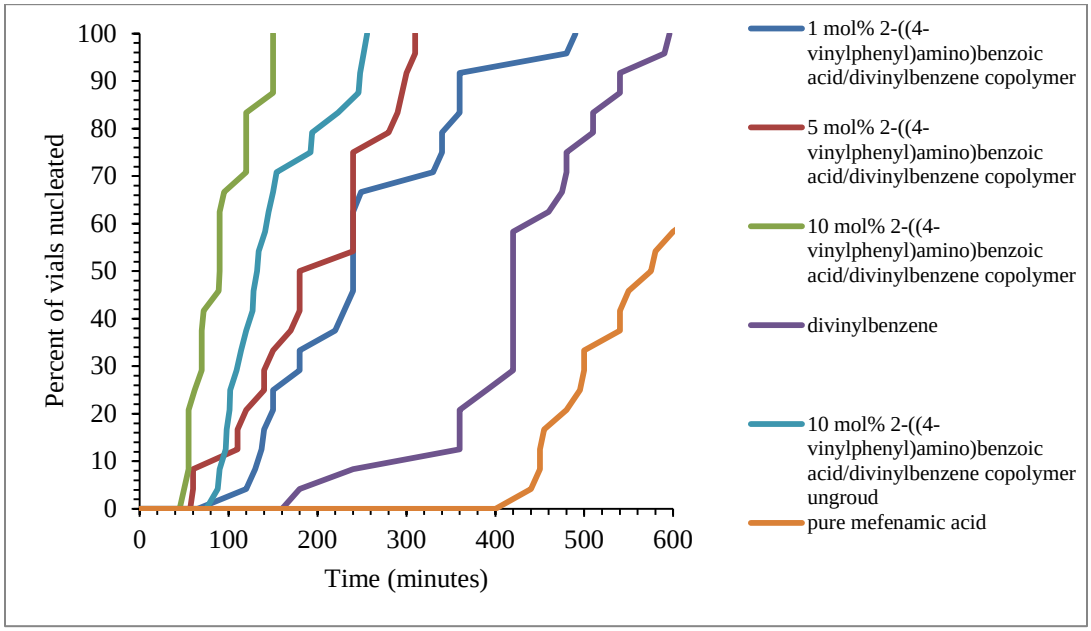

Figure 4.18. Crystallization of mefenamic acid in the presence of that 2-((4-vinylphenyl)amino)benzoic acid/divinylbenzene copolymers, unground 10 mol% 2-((4-vinylphenyl)amino)benzoic acid/divinylbenzene copolymer, divinylbenzene, and pure mefenamic acid.

4.5 References

1. Liu, X. Y., Generic progressive heterogeneous processes in nucleation. *Langmuir* **2000,** 16, (18), 7337-7345.
2. Capacci-Daniel, C.; Gaskell, K. J.; Swift, J. A., Nucleation and Growth of Metastable Polymorphs on Siloxane Monolayer Templates. *Cryst. Growth Des.* **2010,** 10, (2), 952-962.
3. Mitchell, C. A.; Yu, L.; Ward, M. D., Selective nucleation and discovery of organic polymorphs through epitaxy with single crystal substrates. *J. Am. Chem. Soc.* **2001,** 123, (44), 10830-10839.
4. Kang, J. F.; Zaccaro, J.; Ulman, A.; Myerson, A., Nucleation and growth of glycine crystals on self-assembled monolayers on gold. *Langmuir* **2000,** 16, (8), 3791-3796.
5. Lee, A. Y.; Ulman, A.; Myerson, A. S., Crystallization of amino acids on self-assembled monolayers of rigid thiols on gold. *Langmuir* **2002,** 18, (15), 5886-5898.
6. Ulman, A.; Kang, J. F.; Shnidman, Y.; Liao, S.; Jordan, R.; Choi, G. Y.; Zaccaro, J.; Myerson, A. S.; Rafailovich, M.; Sokolov, J.; Fleischer, C., Self-assembled monolayers of rigid thiols. *Journal of biotechnology* **2000,** 74, (3), 175-88.
7. Price, C. P.; Grzesiak, A. L.; Matzger, A. J., Crystalline polymorph selection and discovery with polymer heteronuclei. *J. Am. Chem. Soc.* **2005,** 127, (15), 5512-5517.
8. Lopez-Mejias, V.; Kampf, J. W.; Matzger, A. J., Polymer-Induced Heteronucleation of Tolfenamic Acid: Structural Investigation of a Pentamorph. *J. Am. Chem. Soc.* **2009,** 131, (13), 4554-4555.
9. Lopez-Mejias, V.; Kampf, J. W.; Matzger, A. J., Nonamorphism in Flufenamic Acid and a New Record for a Polymorphic Compound with Solved Structures. *J. Am. Chem. Soc.* **2012,** 134, (24), 9872-9875.
10. Sudha, C.; Nandhini, R.; Srinivasan, K., Polymer-Induced Selective Nucleation of Mono or Ortho Polymorphs of Paracetamol through Swift Cooling of Boiled Aqueous Solution. *Cryst. Growth Des.* **2014,** 14, (2), 705-715.
11. Chen, J. H.; Shao, M.; Xiao, K.; He, Z. R.; Li, D. W.; Lokitz, B. S.; Hensley, D. K.; Kilbey, S. M.; Anthony, J. E.; Keum, J. K.; Rondinone, A. J.; Lee, W. Y.; Hong, S. Y.; Bao, Z. A., Conjugated Polymer-Mediated Polymorphism of a High Performance, Small-Molecule Organic Semiconductor with Tuned Intermolecular Interactions, Enhanced Long-Range Order, and Charge Transport. *Chem. Mat.* **2013,** 25, (21), 4378-4386.
12. Lee, M. K.; Lee, H.; Kim, I. W.; Lee, J., Novel polymorphic form of adefovir dipivoxil derived from polymer-directed crystallization. *Pharmazie* **2011,** 66, (10), 766-770.
13. Diao, Y.; Helgeson, M. E.; Myerson, A. S.; Hatton, T. A.; Doyle, P. S.; Trout, B. L., Controlled Nucleation from Solution Using Polymer Microgels. *J. Am. Chem. Soc.* **2011,** 133, (11), 3756-3759.
14. Lopez-Mejias, V.; Knight, J. L.; Brooks, C. L.; Matzger, A. J., On the Mechanism of Crystalline Polymorph Selection by Polymer Heteronuclei. *Langmuir* **2011,** 27, (12), 7575-7579.
15. McClelland, A. A.; Lopez-Mejias, V.; Matzger, A. J.; Chen, Z., Peering at a Buried Polymer-Crystal Interface: Probing Heterogeneous Nucleation by Sum Frequency Generation Vibrational Spectroscopy. *Langmuir* **2011,** 27, (6), 2162-2165.
16. Curcio, E.; López-Mejías, V.; Di Profio, G.; Fontananova, E.; Drioli, E.; Trout, B. L.; Myerson, A. S., Regulating Nucleation Kinetics through Molecular Interactions at the Polymer–Solute Interface. *Cryst. Growth Des.* **2013,** 14, (2), 678-686.

17. Weissbuch, I.; Leisorowitz, L.; Lahav, M., Tailor-Made and Charge-Transfer Auxiliaries for the Control of the Crystal Polymorphism of Glycine. *Adv. Mater.* **1994,** 6, (12), 952-956.

18. Davey, R. J.; Blagden, N.; Potts, G. D.; Docherty, R., Polymorphism in molecular crystals: Stabilization of a metastable form by conformational mimicry. *J. Am. Chem. Soc.* **1997,** 119, (7), 1767-1772.

19. Staab, E.; Addadi, L.; Leiserowitz, L.; Lahav, M., Control of polymorphism by 'tailor-made' polymeric crystallization auxiliaries. Preferential precipitation of a metastable polar form for second harmonic generation. *Adv. Mater.* **1990,** 2, (1), 40-43.

20. Kitamura, M.; Ishizu, T., Kinetic effect of L-phenylalanine on growth process of L-glutamic acid polymorph. *J. Cryst. Growth* **1998,** 192, (1-2), 225-235.

21. Blagden, N., Crystal engineering of polymorph appearance: the case of sulphathiazole. *Powder Technol.* **2001,** 121, (1), 46-52.

22. He, X. R.; Stowell, J. G.; Morris, K. R.; Pfeiffer, R. R.; Li, H.; Stahly, G. P.; Byrn, S. R., Stabilization of a metastable polymorph of 4-methyl-2-nitroacetanilide by isomorphic additives. *Cryst. Growth Des.* **2001,** 1, (4), 305-312.

23. Thallapally, P. K.; Jetti, R. K. R.; Katz, A. K.; Carrell, H. L.; Singh, K.; Lahiri, K.; Kotha, S.; Boese, R.; Desiraju, G. R., Polymorphism of 1,3,5-Trinitrobenzene Induced by a Trisindane Additive. *Angew. Chem., Int. Ed.* **2004,** 43, (9), 1149-1155.

24. Cashell, C.; Corcoran, D.; Hodnett, B. K., Effect of amino acid additives on the crystallization of L-glutamic acid. *Cryst. Growth Des.* **2005,** 5, (2), 593-597.

25. Ward, M. D., Bulk crystals to surfaces: Combining X-ray diffraction and atomic force microscopy to probe the structure and formation of crystal interfaces. *Chem. Rev.* **2001,** 101, (6), 1697-1725.

26. Shtukenberg, A. G.; Lee, S. S.; Kahr, B.; Ward, M. D., Manipulating Crystallization with Molecular Additives. *Annu. Rev. Chem. Biomol. Eng.* **2014,** 5, 77-96.

27. van Enckevort, W. J. P.; Los, J. H., "Tailor-Made" inhibitors in crystal growth: a Monte Carlo simulation study. *J. Phys. Chem. C* **2008,** 112, (16), 6380-6389.

28. Farmanesh, S.; Ramamoorthy, S.; Chung, J. H.; Asplin, J. R.; Karande, P.; Rimer, J. D., Specificity of Growth Inhibitors and their Cooperative Effects in Calcium Oxalate Monohydrate Crystallization. *J. Am. Chem. Soc.* **2014,** 136, (1), 367-376.

29. Rimer, J. D.; An, Z. H.; Zhu, Z. N.; Lee, M. H.; Goldfarb, D. S.; Wesson, J. A.; Ward, M. D., Crystal Growth Inhibitors for the Prevention of L-Cystine Kidney Stones Through Molecular Design. *Science* **2010,** 330, (6002), 337-341.

30. Weissbuch, I.; Lahav, M.; Leiserowitz, L., Toward stereochentical control, monitoring, and understanding of crystal nucleation. *Cryst. Growth Des.* **2003,** 3, (2), 125-150.

31. Li, T. L.; Wen, H.; Park, K.; Morris, K. R., How specific interactions between acetaminophen and its additive 4-methylacetanilide affect growth morphology: Elucidation using etching patterns. *Cryst. Growth Des.* **2002,** 2, (3), 185-189.

32. Li, T.; Morris, K.; Park, K., Influence of Tailor-Made Additives on Etching Patterns of Acetaminophen Single Crystals. *Pharm Res* **2001,** 18, (3), 398-402.

33. Li, T.; Park, K.; Morris, K. R., Understanding the Formation of Etching Patterns Using a Refined Monte Carlo Simulation Model. *Cryst. Growth Des.* **2002,** 2, (3), 177-184.

34. Tessier, T. G. F., J. M. J.; Willson, C. G.; Ito, H., *Materials for Microlithography*. American Chemical Society: Washington, DC, 1984; p 269-292.

35. Haisa, M.; Kashino, S.; Kawai, R.; Maeda, H., The Monoclinic Form of p-Hydroxyacetanilide. *Acta Crystallogr., Sect. B.* **1976,** 32, (4), 1283-1285.

36. Haisa, M.; Kashino, S.; Maeda, H., The orthorhombic form of p-hydroxyacetanilide. *Acta Crystallogr., Sect. B.* **1974,** 30, (10), 2510-2512.

37. DiMartino, P.; Conflant, P.; Drache, M.; Huvenne, J. P.; GuyotHermann, A. M., Preparation and physical characterization of forms II and III of paracetamol. *J. of Therm. Anal.* **1997,** 48, (3), 447-458.

38. Peterson, M. L.; Morissette, S. L.; McNulty, C.; Goldsweig, A.; Shaw, P.; LeQuesne, M.; Monagle, J.; Encina, N.; Marchionna, J.; Johnson, A.; Gonzalez-Zugasti, J.; Lemmo, A. V.; Ellis, S. J.; Cima, M. J.; Almarsson, O., Iterative high-throughput polymorphism studies on acetaminophen and an experimentally derived structure for form III. *J. Am. Chem. Soc.* **2002,** 124, (37), 10958-10959.

39. Bernstein, J., *Polymorphism in Molecular Crystals*. Oxford University Press: New York, 2002.

40. Davey, R.; Garside, J., *From Molecules to Crystallizers*. Oxford University Press: New York, 2000.

41. Wolf, C.; Liu, S. L.; Mei, X. F.; August, A. T.; Casimir, M. D., Regioselective copper-catalyzed amination of bromobenzoic acids using aliphatic and aromatic amines. *J. Org. Chem.* **2006,** 71, (8), 3270-3273.

42. McConnell, J. F., N-(2,3-Xylyl)anthranilic acid, C15H15NO2. Mefenamic acid. *Cryst. Struct. Commun.* **1976,** 5, 861-864.

43. Dunitz, J. D.; Bernstein, J., Disappearing Polymorphs. *Accounts Chem. Res.* **1995,** 28, (4), 193-200.

44. Sokolova, T. A.; Ovsyannikova, L. A.; Tikhodeeva, II, Synthesis of N-Substituted Methacrylamides. *Journal of General Chemistry Ussr* **1963,** 33, (5), 1466.

Chapter 5 Conclusion

5.1 Summary of Work and Future Directions

It is important to study the potential polymorphism of a compound due to the significant differences in the kinetic and thermodynamic stabilities between polymorphic forms. However, solid form screening, as currently practiced, requires substantial sample quantities and it has thus far not been feasible to perform solid form screening as an early-stage selection criterion for choosing which bioactive compounds to advance in the pipeline. Hence, the process by which a drug candidate is chosen neglects solid form considerations until a rather late stage where the cost of failure is greater.[1, 2] The importance of form screening was supported by the discovery of two novel polymorphs of the low solubility bioenhancer piperine with PIHn as described in Chapter 2. The polymorphs were found to exhibit an enhanced solubility relative to the commercial form, allowing these novel forms to improve the efficacy of piperine as a bioenhancer.

Despite the success of PIHn in discovering novel polymorphs, it suffers from slow analysis times and large sample requirements. Now with µPIHn, a novel high throughput screening platform, one can study the potential polymorphism of a compound using only ~1 mg of material.[7] As discussed in Chapter 3, µPIHn allows for high throughput analysis of the results of hundreds of crystallizations by Raman microspectroscopy and X-ray microdiffraction, saving a considerable amount of analysis time as well as material. With µPIHn only a small amount of

material is needed in order to study the potential polymorphism of a newly synthesized compound.[7] It was found that the efficacy of PIHn was maintained despite the drastic differences in many aspects of the crystallizations including the substrate on which the crystallizations are conducted, amount of polymer heteronucleant, and the rate of evaporation. However, it has been found that mechanism by which PIHn is able to control the formation of a particular polymorph is through preferential interactions at the polymer-crystal interface. Thus, even though many of the aspects of the crystallizations have been changed with μPIHn the strong intermolecular interactions at the polymer-crystal interface are maintained, preserving the efficacy of PIHn. Despite the success of PIHn in discovering novel polymorphs, only commercial monomers have been utilized to create the polymer heteronucleants. However, by synthesizing monomers which are structurally similar to the target compound one may be able to promote crystallization by taking advantage of the strong intermolecular interactions between the polymer heteronucleant and the target compound. This could be of particular importance for compounds that are resistant to crystallization.[8] This can complicate the formulation process by inhibiting one from purifying and determining the structure of a compound. Now, tailor-made additives, which alter crystal morphology in solution, can be incorporated into insoluble polymers to promote crystallization. As described in Chapter 4, by tailoring substrates to decrease the time needed for crystals to appear it can allow researchers to create appropriate seed crystals for compounds which are resistant to or very slow to crystallize.[9]

5.2 References

1. Almarsson, O.; Zaworotko, M. J., Crystal Engineering of the Composition of Pharmaceutical Phases. Do Pharmaceutical Co-crystals Represent a New Path to Improved Medicines? *Chem. Commun.* **2004**, (17), 1889-1896.
2. Sun, Y.; Xi, H. M.; Ediger, M. D.; Richert, R.; Yu, L., Diffusion-controlled and "diffusionless" crystal growth near the glass transition temperature: Relation between liquid dynamics and growth kinetics of seven ROY polymorphs. *J. Chem. Phys.* **2009,** 131, (7).
3. Lopez-Mejias, V.; Kampf, J. W.; Matzger, A. J., Polymer-Induced Heteronucleation of Tolfenamic Acid: Structural Investigation of a Pentamorph. *J. Am. Chem. Soc.* **2009,** 131, (13), 4554-4555.
4. Lopez-Mejias, V.; Kampf, J. W.; Matzger, A. J., Nonamorphism in Flufenamic Acid and a New Record for a Polymorphic Compound with Solved Structures. *J. Am. Chem. Soc.* **2012,** 134, (24), 9872-9875.
5. Price, C. P.; Grzesiak, A. L.; Matzger, A. J., Crystalline polymorph selection and discovery with polymer heteronuclei. *J. Am. Chem. Soc.* **2005,** 127, (15), 5512-5517.
6. Roy, S.; Quiñones, R.; Matzger, A. J., Structural and Physicochemical Aspects of Dasatinib Hydrate and Anhydrate Phases. *Cryst. Growth Des.* **2012,** 12, (4), 2122-2126.
7. Pfund, L. Y.; Matzger, A. J., Towards Exhaustive and Automated High-Throughput Screening for Crystalline Polymorphs. *ACS Combinatorial Science* **2014,** 16, (7), 309-313.
8. Dunitz, J. D.; Bernstein, J., Disappearing Polymorphs. *Accounts Chem. Res.* **1995,** 28, (4), 193-200.
9. Pfund, L. Y.; Price, C. P.; Frick, J. J.; Matzger, A. J., Controlling Pharmaceutical Crystallization with Designed Polymeric Heteronuclei. *J. Am. Chem. Soc.* **2014**.